Università degli Studi di Cagliari

DOTTORATO DI RICERCA
INGEGNERIA DEL TERRITORIO

Ciclo XXV

Evaluation of climate change impacts on the hydrologic response of a sparsely-monitored basin in Sardinia, Italy, through distributed hydrologic simulations and hydrometeorological downscaling

Settore scientifico disciplinare di afferenza

ICAR/02 Costruzioni idrauliche e marittime e idrologia

Presentata da:	Dott.ssa Monica Piras
Coordinatore Dottorato	Prof. Roberto Deidda
Tutors/Relatori	Prof. Roberto Deidda Dott. Giuseppe Mascaro

Esame finale anno accademico 2012 – 2013

Abstract

The water resources and hydrologic extremes in Mediterranean basins are heavily influenced by climate variability. Modeling these watersheds is difficult due to the complex nature of the hydrologic response as well as the sparseness of hydrometeorological observations. In this work, we first present a strategy to calibrate a distributed hydrologic model, known as TIN-based Real-time Integrated Basin Simulator (tRIBS), in the Rio Mannu basin, a medium-sized watershed (472.5 km^2) located in an agricultural area in Sardinia, Italy. In the basin, precipitation, streamflow and meteorological data were collected within different historical periods and at diverse temporal resolutions. We designed two statistical tools for downscaling precipitation and potential evapotranspiration data to create the hourly, high-resolution forcing for the hydrologic model from daily records. Despite the presence of several sources of uncertainty in the observations and model parameterization, the use of the disaggregated forcing led to good calibration and validation performances for the tRIBS model, when daily discharge observations were available.

Future climate projections based on global and regional climate models (GCMs and RCMs) indicate that the Mediterranean basins will most likely suffer a decrease in water availability and an intensification of hydrologic extremes. Process-based distributed hydrologic models (DHMs), like tRIBS, have the potential to simulate the complex hydrologic response of Mediterranean watersheds. Thus, when used in combination with RCMs, DHMs can reduce the uncertainty in the quantification of the local impacts of climate change on water resources. In this study, we apply the calibrated tRIBS model in the Rio Mannu basin to evaluate the effects of climate changes reducing related uncertainties. The two downscaling algorithms and the DHM were used to simulate the watershed response to a set of bias-corrected outputs from four RCMs for two simulation extents: a reference (1971 to 2000) and a future (2041 to 2070) period. The time series and spatial maps simulated by the DHM were then post-processed by computing several metrics to quantify the changes on water resource availability and hydrologic extremes in the future climate scenarios as compared to historical conditions.

The research was carried out within the CLIMB project, founded by the 7th Framework Programme of the European Commission.

Acknowledgements

I would like to express my sincere gratidute to my supervisors, Prof. Roberto Deidda for giving me the opportunity of this doctoral research and his support toward a more critical approach in hydrologic science, Ing. Giuseppe Mascaro, for his strong contribution on founding the basis for this work and his encouraging support throughout all the activities during the PhD course.

I would like to thank Enrique Vivoni for his kind and helpful suggestions and guidelines.

The thesis was developed within the CLIMB project, founded by the 7th Framework Programme of the European Commission. Hence, my graditude goes to all the people involved in the project.

Last, but not least I would like to thank my family, my boyfriend and closest friends for their continuous support.

Table of Contents

List of figures

List of tables

1 Introduction

Natural climate variability has always characterized the Earth system. However in the last decades, human factors have added changes to natural variability creating the issue of climate change. The Mediterranean area is particularly affected by climate variability. In the last few decades, Mediterranean basins have suffered flash floods and severe droughts which have caused socio-economic problems, affecting mainly the agricultural and touristic sectors. Future climate projections suggest an even worse situation predicting, with high probability, contemporaneous temperature warming and precipitation decreasing which will cause water resources reduction and an increased frequency of hydrological extreme events.

1.1 Problem definition

Climate studies agree on the prevision that Mediterranean area appears to be particularly affected by changes under global warming (Giorgi, 2006; Intergovernmental Panel on Climate Change (IPCC), 2007). According to the A1B scenario, indeed, the mean annual warming from 2080 to 2099 compared with the period 1980-1999 is expected to be between 2.2°C and 5.1°C with higher increases in summer; at the same time mean annual precipitations are expected to decrease between 4 and 27% (Christensen et al., 2007, IPCC). Projected declines in water availability will particularly affect the agriculture sector in an area where water for production is already a scarce commodity (IPCC technical report, 2008). It is, therefore, important evaluate the effects of climate change, CC, at the local scale of hydrologic basin in order to provide possible scenarios to water managers and interested stakeholders (Cudennec et al., 2007).

Climate models work at scales too wide to allow a suitable assessment of the local impacts of CC on hydrological cycle and water resources availability. Hence, these effects could be evaluated by coupling global and regional climate models with distributed hydrological

models using downscaling techniques to bridge the scale mismatch between climate and hydrological models. The study of climate change effects on hydrological regimes, indeed, is usually conducted through a three step procedure (Xu et al., 2005) consisting of (i) select General Circulation Models (GCMs) and Regional Climate Models (RCMs) to provide future global climate scenarios under the effect of increasing greenhouse gases, (ii) develop and apply downscaling techniques to suit the scale of GCM and RCM outputs to the scales of hydrological models, and (iii) use the downscaled outputs to force hydrologic models to simulate the effects of climate change on hydrological regimes at various scales. All these phases are affected by uncertainties: choice of emission scenario, climate forcing, downscaling technique, hydrologic tool used to assess the local impacts and observed data used to calibrate it (Wilby, 2005; Proudhomme and Davies, 2009a and 2009b) which propagates from one step to the subsequent, known as *cascade of uncertainty* (Mearns at al., 2001).

1.2 Motivation and research objectives

This thesis had the main objective of developing a modeling approach which allowed evaluating local hydrological impacts of climate change in a Mediterranean medium sized basin, located in an agricultural area of southern Sardinia, Italy. Outputs were post processed in order to provide probabilistic predictions to reduce the uncertainties in the possible hydrologic response. Climate models and a physically based distributed hydrologic model had been applied in cascade. Different future climate scenarios were used as driving inputs of hydrological simulations in the future period; hence, the uncertainty was characterized using multi-model ensemble techniques.

The specific methodologies and steps were the following:

- selection of a modeling approach to assess hydrologic effects of CC in a specific study

area;

- setup and application of a hydrologic model to simulate land-surface water and energy fluxes at high spatial and temporal resolution using all available data;
- calibration and validation of the hydrologic model in the period during which observed historical data were available, to find a set of parameters which minimized the distance between observed and simulated data;
- use selected RCMs as forcing of hydrologic simulations during a reference and a future period;
- evaluation of climatic trends in the study area comparing meteorological data in future and reference periods;
- assessment of climate change impacts on water resources budget in the study area with probabilistic outputs taking into account different sources of uncertainty;
- provision of high resolution spatio-temporal information which could be used to support management water resources at local scale (e.g. soil moisture and actual evapotranspiration).

This work was conducted within the framework of the CLIMB (CLimate Induced changes on the hydrology of Mediterranean Basins) project, founded by European 7th FP, with the main aim of reducing uncertainties and quantifying risk through an integrated monitoring and modeling system (Ludwig et al., 2010). In particular, it was developed within the work package, WP, 5 related to the hydro(geo)logical modeling. This thesis focused on one of the seven CLIMB case studies, the Rio Mannu basin located in southern Sardinia, which could be considered a representative example of Mediterranean catchments. It was, indeed, heavily influenced by climate variability and characterized by the sparseness of hydrometeorological

observations, as many other basins in this area (Moussa et al., 2007, Cudennec et al., 2007).

The Rio Mannu basin was selected for two main reasons. First, it included within its boundary the Azienda S. Michele, an agricultural experimental farm managed by the Agency for Research in Agriculture of Sardinian Region (AGRIS), one of the project partners. Hence, this basin gave the possibility to perform the analyses at basin scale and field scale (not considered in this study). Second, during the last 30 years, the Rio Mannu basin had been affected by prolonged drought periods that caused water restrictions for the agricultural and touristic sectors, with consequent significant financial losses and social conflicts. As a result, despite the lack of historical observations of hydrometeorological data, this watershed was a representative study case in the island of Sardinia for conducting a multidisciplinary analysis of the local impacts of climate changes, ranging from the quantification of the future availability of water resources, to the evaluation of the social and economical consequences for the population.

This research concentrated on the basin scale using the distributed hydrologic model tRIBS, TIN based Real time Integrated Basin Simulator, (Ivanov et al., 2004a and 2004b) to simulate the hydrologic processes at high spatial and temporal resolution notwithstanding the scarcity of available data. The model was calibrated and validated in the period during which the limited observed streamflow data were found to be less uncertain. Two downscaling procedures, one for precipitation and the other for reference evapotranspiration, were performed, calibrated and validated in order to provide the model with suitable meteorological data in that calibration-validation period. Despite the presence of several sources of uncertainty in the observations and model parameterization, the use of the disaggregated forcing led to good calibration and validation performances for the tRIBS model, when daily discharge observations were available. The same methodology was used to disaggregate outputs of climate models, selected and

provided by WP 4 of the same project, and to conduct high-resolution hydrologic simulations with the goal of quantifying the impacts of climate change on water resources and the frequency of hydrologic extremes within the medium-sized basin.

1.3 Thesis outline

The thesis consists of three chapters after the introductory part (**Chapter 1**).

Chapter 2 contains the description of the Rio Mannu basin and related data set, the presentation of the hydrologic model, tRIBS, and its application in the study case. It focuses on input data treatment needed for its implementation and the phases of calibration and validation. The lack and sparseness of hydrometeorological data is overcome relying on two statistical downscaling tools which allow creating the high-resolution forcing (precipitation and potential evapotranspiration) required to perform detailed hydrologic simulations at hourly time scale. The downscaling tools are calibrated using data collected at different resolutions over diverse time periods. After demonstrating the reliability of each disaggregation algorithm, these tools are used to adequately calibrate and validate the hydrologic model based on streamflow observations available over a multi-year period, encompassing a wide range of flood and low flow conditions.

Chapter 3 firstly analyses the outputs of four Regional Climate Models, RCMs, selected within the CLIMB project as the most skillful ones among a set of fourteen RCMs of the ENSEMBLES project. The main climatic forcing, precipitation and temperature, are analyzed in a control period (1971-2000) and in a future period (2041-2070), highlighting possible trends. The RCMs outputs are disaggregate using the same methodologies used in the calibration-validation period to obtain input data at the required resolution. Subsequently, the results of the tRIBS simulations forced by the RCMs outputs are shown in the two periods (multi-model ensemble) and post-processed to compute several hydrologic metrics. This allows quantifying

the impacts of climate change on water resources and the frequency of hydrologic extremes within the Rio Mannu basin.

Chapter 4 after summarizing the contents of this dissertation discusses the main results regarding the procedure used to calibrate a distributed hydrologic model in a medium size Mediterranean basin affected by poor data availability and the assessment of climate change effects on the case study, showing critical points and possible ways to continue the research.

2 Study area and hydrologic model

This chapter contains the description of the study area, the Rio Mannu basin located in Sardinia, Italy, the related data set and the reasons for its selection. The hydrologic model, tRIBS, is presented together with its application in the study case focusing on input data treatment needed for its implementation. Finally, the calibration and validation of the model are discussed. As many other Mediterranean catchments, the Rio Mannu basin is affected by poor data availability. The lack and sparseness of hydrometeorological data is overcome relying on two statistical downscaling tools which allow creating the high-resolution forcing (precipitation and potential evapotranspiration) required to perform detailed hydrologic simulations at hourly time resolution. The downscaling tools are calibrated using data collected at different resolutions over diverse time periods. After demonstrating the reliability of each disaggregation algorithm, these tools are used to adequately calibrate and validate the hydrologic model based on streamflow observations available over a multi-year period.

2.1 Introduction

Mediterranean areas are highly sensitive to climate variability and this vulnerability has significant impacts on water resources and hydrologic extremes. During the last few decades, intense flood and flash-flood events have caused relevant socioeconomic losses (Chessa et al., 2004; Delrieu et al., 2005; Silvestro et al., 2012), while persistent drought periods have limited water availability, causing restrictions that mainly affected the agricultural sector, often a pillar of the local economy. Unfortunately, future climate projections (IPCC, 2007; Schörter et al., 2005; Giorgi, 2006) depict an even worse scenario since they predict, with high probability, that Mediterranean countries will suffer a general decreasing water availability (in terms of both rainfall and runoff) and an increasing occurrence of extreme hydrological events (IPCC, 2008;

Frei et al., 2006). This may cause, in cascade, a reduction of crop production and, in the worst scenario, a decrease of their quality due to the concomitant degradation of cultivated soils and water used for irrigation (Olesen and Bindi, 2002; Schörter et al., 2005).

As most semiarid areas of the world, Mediterranean watersheds are characterized by a complex hydrologic response due to the erratic and seasonal nature of rainfall, its strong interannual variability, and the highly heterogeneous land surface properties (Moussa et al., 2007). These features lead to the possible occurrence of a large range of initial basin wetness conditions prior to a storm event, and, in turn, to strong non-linear relations between rainfall and runoff (Piñol et al., 1997; Gallart et al., 2002; Beven, 2002). Modeling such complex systems in a continuous fashion to manage and plan water resources as well as to predict hydrologic extremes is a difficult task. A possible strategy is the use of process-based hydrologic models (DHMs) that are able to quantify the vertical and lateral water fluxes in spatially distributed fashion at high (sub-daily) time resolution, and to capture the interaction between surface and subsurface processes (Van der Kwaak and Loague, 2001; Ivanov et al., 2004a; Camporese et al., 2010, among others). These models are able to: (i) reproduce the different basin states during the dry season, the wetting-up period and the wet season (Noto et al., 2008), and (ii) to simulate the diverse surface and subsurface runoff types (Vivoni et al., 2007 and 2010) that typically characterize the hydrological regime of Mediterranean basins (Piñol et al., 1997).

Distributed hydrologic models have been applied to study the hydrologic impacts of future climate change scenarios, with forcing provided by General (GCMs) or Regional (RCMs) Climate Models (e.g., Abbaspour et al., 2009; Cayan et al., 2010; Liuzzo et al. 2010; Sulis et al., 2011, 2012; Montenegro and Ragab, 2012). In Mediterranean areas, conducting studies based on this approach is challenging for two reasons. First, the basin size is relatively small in most areas

(<1000 km^2) and a spatiotemporal scale gap exists between GCM and RCM outputs and the scale of the dominant hydrological processes (Wood et al., 2004). Second, they are often affected by data sparseness, e.g. the data required to calibrate distributed hydrologic models are often characterized by limited spatial coverage and coarse time resolution, and they may have not been collected during simultaneous periods. For example, streamflow observations may be available in a period with no meteorological or rainfall data. In this thesis we proposed a possible solution to this issue (Mascaro et al., 2013b).

2.2 Study area

The study area is the Rio Mannu di San Sperate basin, located in southern Sardinia (Italy), with the outlet section at Monastir, a little town about 25 km North of Cagliari, the regional chief town. Fig. 2.1 shows the watershed, its localization and topographic aspect. Its WGS84 UTM coordinates vary between 4355115 and 4387635 m in latitude N and between 500725 and 524295 m in longitude E. The basin drains an area of 472.5 km^2 mainly characterized by gently rolling topography, belonging to the Campidano plain, except the southeastern part which reaches an height of 963 m in the "Sette Fratelli Chain". The main physiographic properties, including elevation, slope and river network features, are reported in Table 2.1. The mean, minimum and maximum elevations are 296 m, 66 m and 963 m respectively, while the mean slope is about 17%. The concentration time was computed using the Giandotti formula (Giandotti, 1934) as:

$$T_C = \frac{4\sqrt{A_b} + 1.5L}{0.8\sqrt{z_{mean} - z_{\min}}} \quad (1)$$

where A_b is the basin area, L is the length of the main reach, z_{mean} and z_{min} are the mean and minimum elevation, respectively.

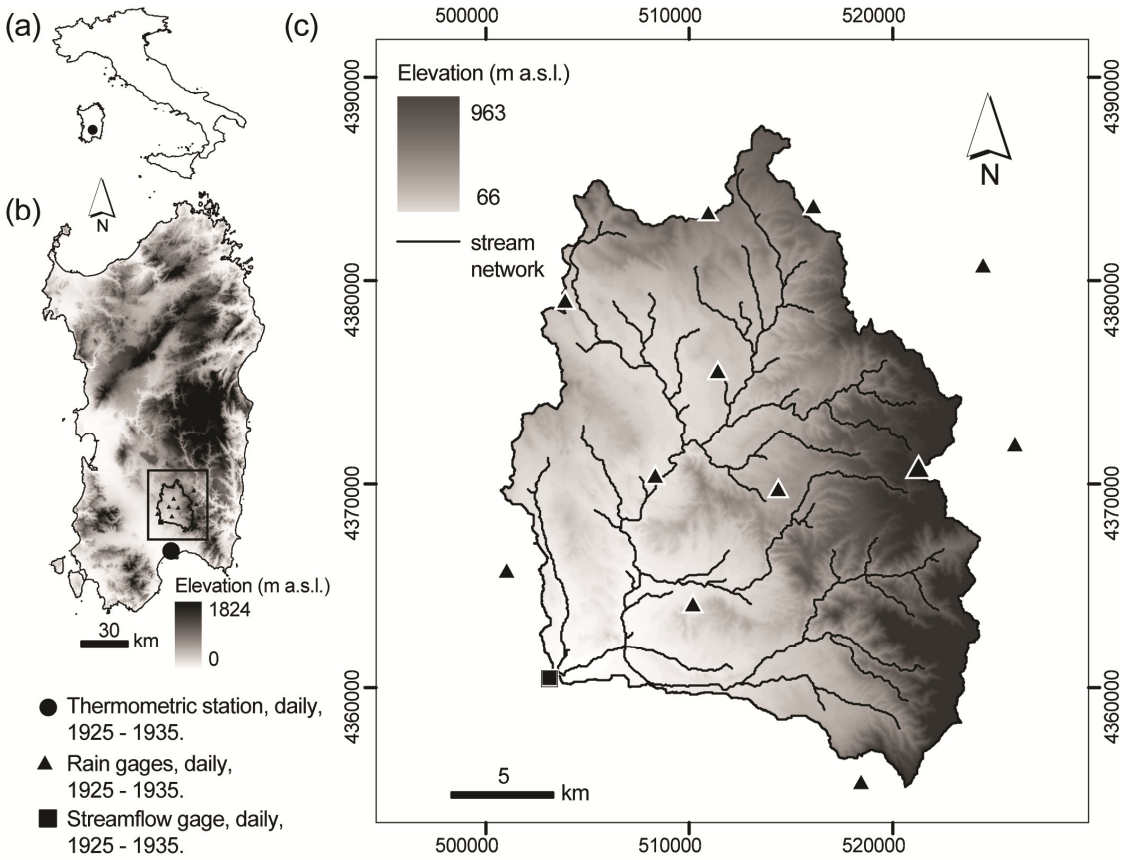

Fig. 2.1 Location of the Rio Mannu di San Sperate at Monastir basin (RMB) within (a) Italy and (b) the island of Sardinia. (c) Digital elevation model (DEM) of the RMB including UTM coordinates. Panels (b) and (c) also report the position of the thermometric station, rain gages and streamflow gage at the basin outlet with daily data observed during the years 1925-1935.

A_b (km^2)	z_{min} (m a.s.l.)	z_{max} (m a.s.l.)	z_{mean} (m a.s.l.)	β_{mean} (%)	L (km)	T_c (h)
472.5	66	963	296	17.3	39	12

Table 2.1 Physiographic characteristics of the RMB including area (A_b), minimum (z_{min}), maximum (z_{max}) and mean (z_{mean}) elevation, mean slope (β_{mean}), length of the main reach (L), and concentration time (T_c).

The Rio Mannu basin (RMB in the following) is characterized by typical Mediterranean climate with wet periods from October to April and dry periods from May to September. Fig. 2.2 shows the mean monthly values of precipitation, streamflow and temperature in the catchment.

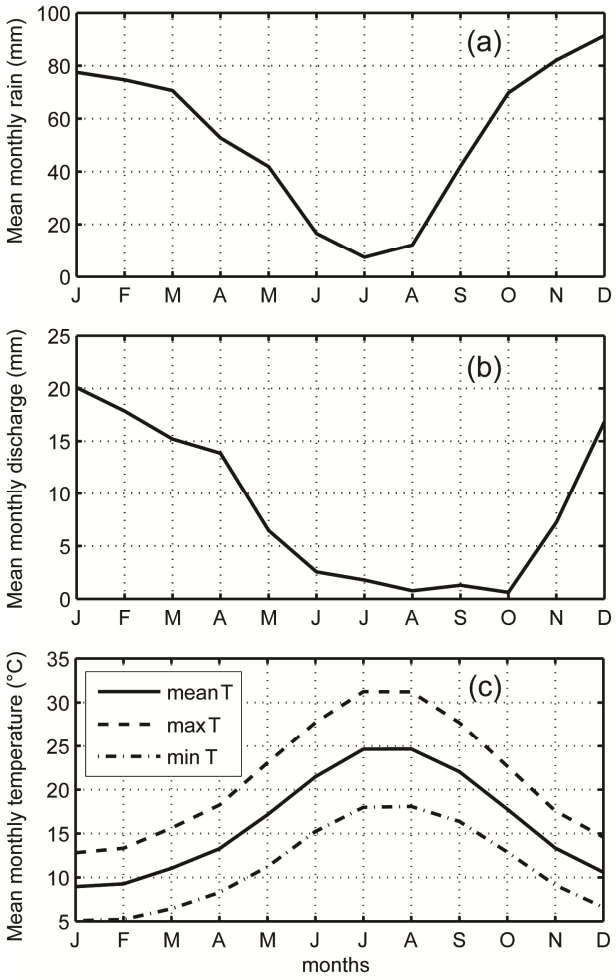

Fig. 2.2 Mean monthly (a) precipitation, (b) discharge and (c) temperature in RMB computed in different periods in which daily data were available. Refer to Table 2.2 for the period of data availability.

Given the topographic configuration (maximum elevation is 963 m a.s.l.) and geographic position (39° N) the only input in water balance is rainfall and snow melt can be neglected. As a result, the pattern of mean monthly discharge is in phase with rainfall, with highest values in winter months and lowest values from June to October (Fig. 2.2b). The streamflow regime is characterized by low flows (less than 1 m^3/s) for most of the year, with few flood events in autumn and winter, caused by frontal systems of typical duration of 1-3 days (Chessa et al., 1999; Mascaro et al., 2013a). Mean annual precipitation is about 600 mm, mainly concentrated in the rainy period (94%). Mean monthly temperature ranges from 9°C in winter and 25°C in

summer (Fig. 2.2c).

The basin is one of the seven case studies of the EU FP7 CLIMB Project, of which this work is part (Ludwig et al., 2010). It has been selected, although its poor data availability (shown subsequently), for two main reasons. First, it is representative of Mediterranean climate and issues. In particular, during the last 30 years, the RMB has been affected by prolonged drought periods that caused water restrictions for the agricultural sector, with significant financial losses and social conflicts as a consequence. Second, it includes within its boundaries an experimental agricultural farm where productivity of several typical Sardinian crops is monitored by the Sardinian Agency for Research in Agriculture, AGRIS, partner of the Project. As a result, this catchment is an emblematic study case in the island of Sardinia to carry out a multidisciplinary assessment of the local impacts of climate changes, ranging from the quantification of the future availability of water resources and occurrence of hydrologic extremes (as it is shown in chapter 3), to the evaluation of the corresponding social and economical vulnerability.

2.3 Data set

The data set consists of hydrometeorological data and geospatial data, whose availability and quality is discussed in the following.

Hydrometeorological data, including precipitation, temperature and streamflow, were collected during different and sometimes non overlapping time periods and at different time resolutions. They were mostly archived in technical reports of the Italian Hydrologic Survey (the 'Annali Idrologici'). As a result, the first step consisted of reading the data from the 'Annali Idrologici' and archiving them in electronic format. Daily discharge data at the RMB outlet section (square in Fig. 2.1c) were collected and published for 11 years, from 1925 to 1935. During the same period 12 rain gages (triangles in Fig. 2.1c) provided daily rainfall data and one thermometric station, located in Cagliari (circle in Fig. 2.1b), registered daily minimum (T_{min}) and maximum (T_{max}) temperature. This poor data availability represented a challenge for the calibration of the hydrologic model (as described in section 2.4). As a result, we took advantage of more recent high resolution meteorological data in RMB: (i) precipitation records at 1-min from automatic rain gages observed during the years 1986-1996, and (ii) hourly meteorological data from 1 station over the period 1995-2010. A summary of hydrometeorological data characteristics, including resolution, availability period, and source is reported in Table 2.2, while the stations location is shown in Fig. 2.3. As illustrated in the following, high resolution data had been exploited to develop and calibrate two downscaling tools to disaggregate the coarse dataset observed in the calibration and validation periods selected in the years 1925-1935, producing the forcing at hourly resolution required by the hydrologic model tRIBS.

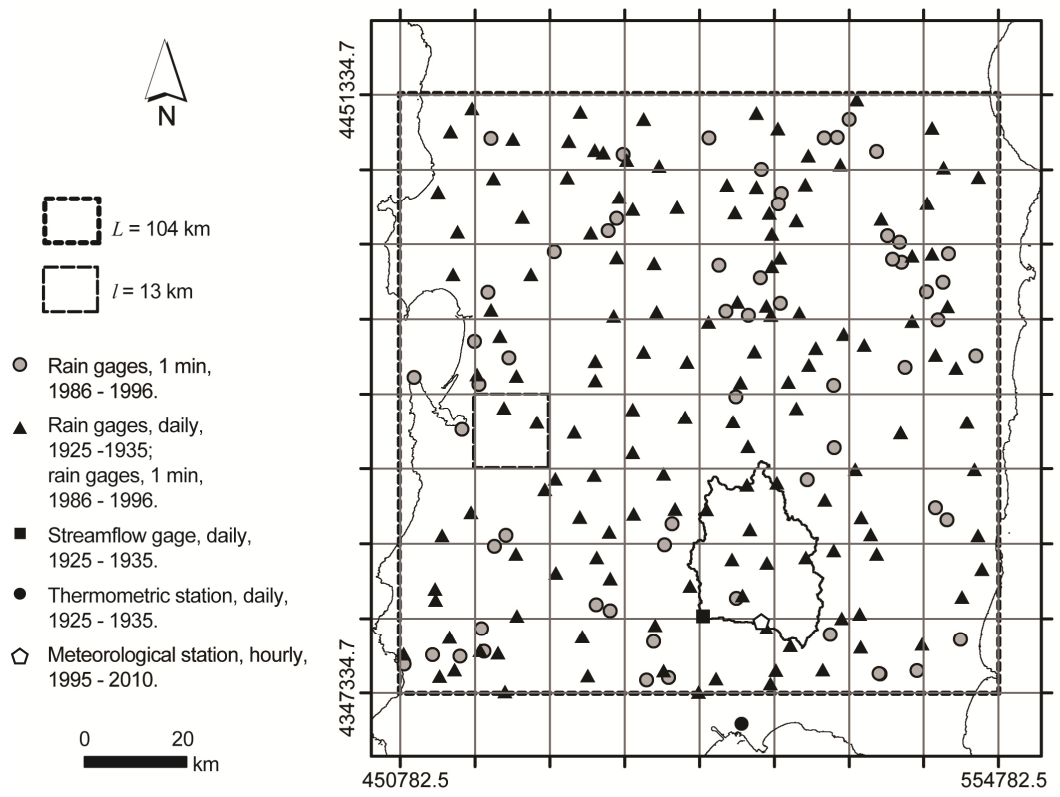

Fig. 2.3 Location of rain gages, meteorological stations and streamflow gage. The square with a dashed line is the coarse domain L x L (L = 104 km) containing the fine scale grid at resolution l x l (l = 13 km) used to calibrate the precipitation downscaling tool. See Table 2.2 for details.

Data	Period	Resolution	# of gages	Source
Streamflow	1925-1935	Daily*	1	AI
Precipitation	1925-1935	Daily*	12	AI
	1986-1996	1 min	204	IHS
Temperature	1925-1935	Daily**	1	AI
	1995-2010	1 h***	1	ARPAS

Table 2.2 . Hydrometeorological data used in the study, including the available period, the resolution, the number of gages and the source for each type of data. The sources include: AI, "Annali Idrologici"; IHS, Italian Hydrologic Survey (data provided by the branch in Sardinia); and ARPAS, the Sardinian Agency for Environmental Protection. (*) Read at 9 am; (**) Only minum and maximum temperature(T_{min} and T_{max}); (***) Air temperature, air humidity, global radiation, and wind speed at 2 m height.

Geospatial (GIS) data for the RMB included: a Digital Elevation Model (DEM) at 10-meter resolution (Fig. 2.1c); pedological map, digitized and geo-referenced from a map of Sardinia at scale 1:250'000 (Aru et al., 1992); land cover (LC) map derived from the COoRdination de l'INformation sur l'Environment (CORINE) project of the European Environment Agency (EEA) for the year 2008; orthophotos of the entire Island for years 1954 and 2006. These maps were provided by different agencies of the Sardinian Region Government. Pedological and LC data were preprocessed to be used as input for the DHM.

CODE	PROFILE	DEPTH
A2	Profiles A-R, A-Bt-R and A-Bw-R and emerging rock	from shallow to deep
B1	Emerging rock, soils with a profile A-C and secondary A-Bw-C	shallow
B2	Profiles A-C, A-Bw-C and secondary emerging rock	from shallow to average deep
C1	Emerging rock, soils with a profile A-C and secondary A-Bw-C	shallow
C2	Profiles A-C, A-Bw-C, emerging rock and secondary soils with a profile A-Bt-C	from shallow to average deep
D1	Emerging rock and soils with a profile A-C and secondary A-Bw-C	shallow
D4	Profiles A-Bw-C, A-C and secondary emerging rock	from deep to shallow
F1	Emerging rock, soils with a profile A-C and A-Bt-C	from shallow to average deep
G1	Profiles A-C, emerging rock and secondary A-Bw-C	shallow
G2	Profiles A-Bw-C, A-Bk-C and A-C	from average deep to deep
G3	Profiles A-C	deep
H1	Profiles A-C, A-Bw-C and A-Bk-C	from shallow to deep
I1	Soils with a profile A-Bt-C, A-Btg-Cg and secondary A-C	deep
I2	Soils with a profile A-Bt-Ck, A-Btk-Ckm and secondary A-C	deep
L1	Profiles A-C and secondary A-Bw-C	deep
L2	Profiles A-C	deep
O	Urban areas	-

Table 2.3 List of original Aru pedological map classes within RMB (free translation from the Italian legend).

The original pedological map presented, for each class of the map, a range of soil texture classes and a qualitative description of the soil depth, shortly summarized in Table 2.3. The RMB was characterized by a total of 17 classes. A series of field campaigns were conducted in 2011 by CLIMB partners to reduce the uncertainty on soil texture within the framework of the project described in Ludwig et al. (2010). A total of 50 soil samples of 80 cm depth were collected throughout the watershed and analyzed to characterize the texture. These data were then used as a guide to aggregate the 17 classes and reduce the range of possible soil texture types for each class. The original and the resulting maps are shown in Fig. 2.4, while the percentage distribution of the classes in the reclassified map is reported in Table 2.4.

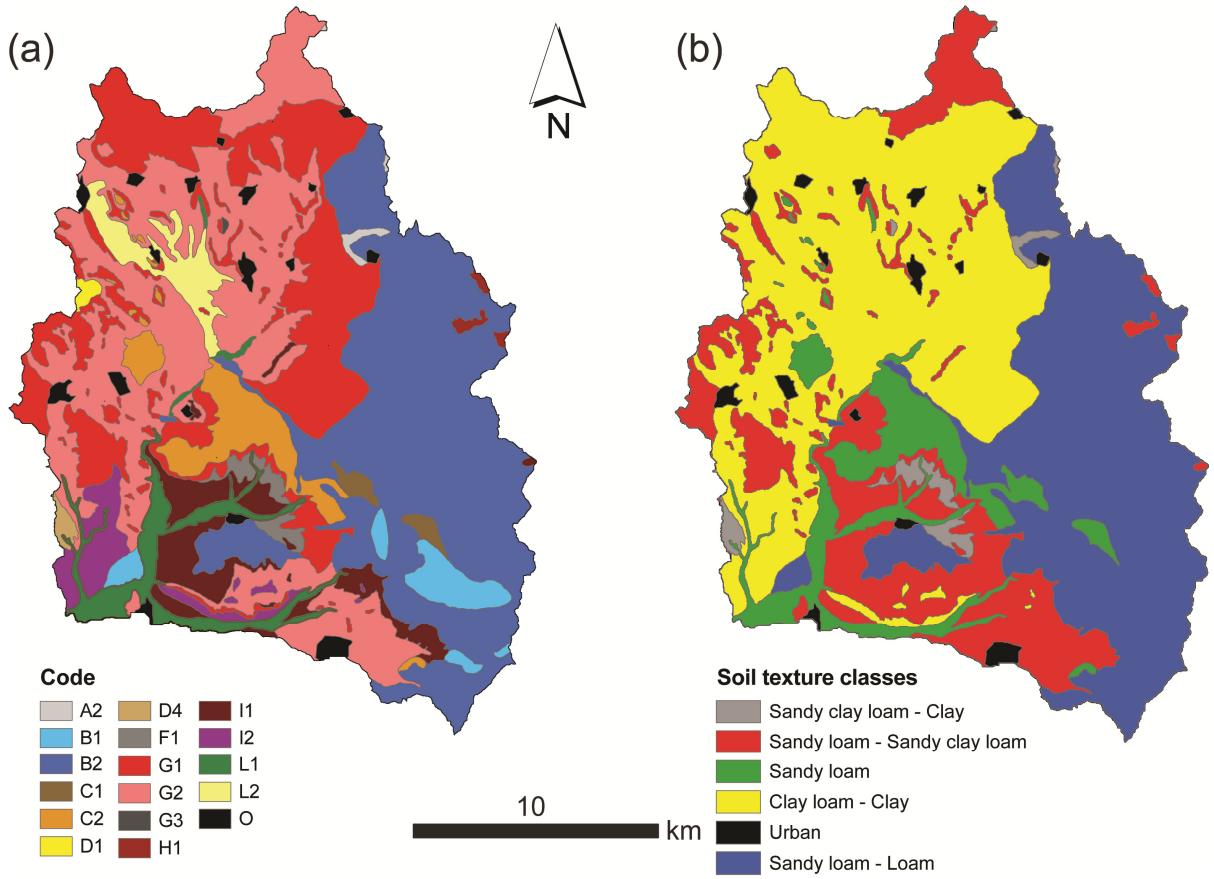

Fig. 2.4 (a) Pedological map (Aru et al., 1992) for RMB and (b) reclassified soil texture map used as input for the tRIBS model.

The original CORINE LC classes (Fig. 2.5a) were aggregated into 8 groups, obtaining the map shown in Fig. 2.5b. According to the reclassification the main classes were agriculture (comprising main crops as wheat, corn and artichoke), which occupies about 48% of the basin area, and sparse vegetation, including Mediterranean species, (about 26%). The other groups were olives, forests, pasture, vinegars and urban areas, as reported in Table 2.4. The year in which the LC map was released (2008) was quite distant from the period in which streamflow data required to calibrate the hydrologic model was available (1925-1935). As a result, in order to evaluate the stationarity of the LC conditions, the orthophotos of the years 1954 and 2006 were carefully compared. The visual comparison revealed minimal differences making us confident on the use of the LC map of the year 2008 as input for the hydrologic model.

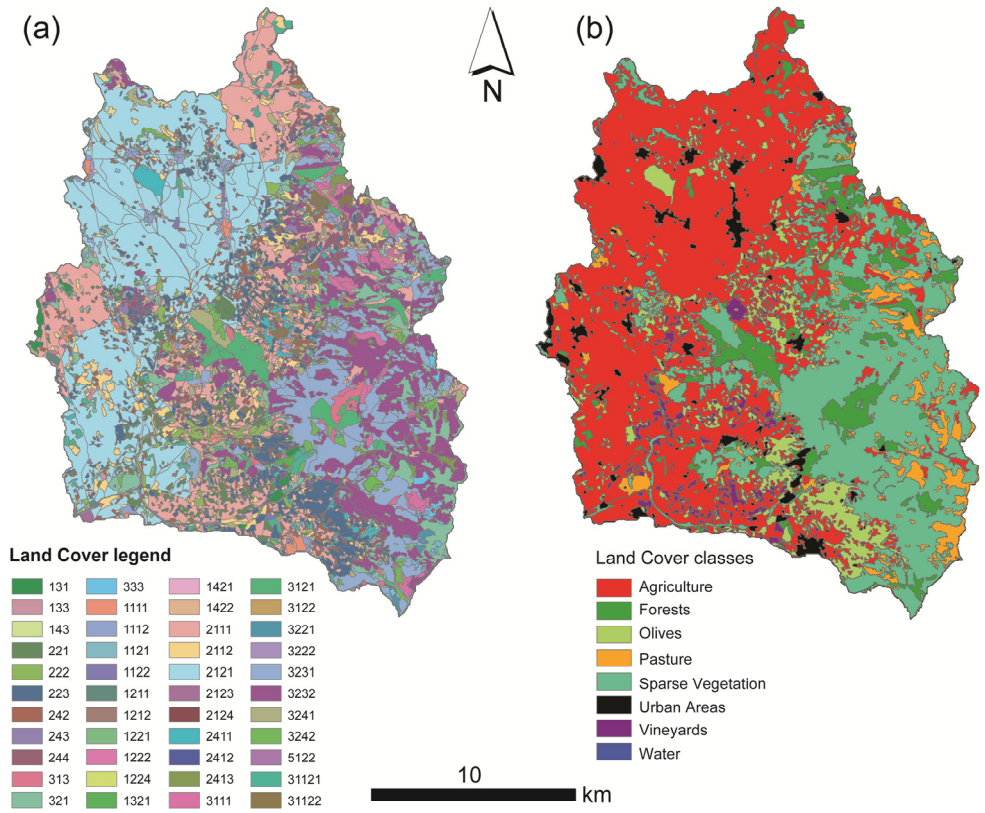

Fig. 2.5 (a) Original CORINE LC map for RMB and (b) LC map used as input for the tRIBS model.

Land Cover Class	% basin area	Range of Soil Texture Classes	% basin area
Agriculture	47.64	Sandy clay loam - clay	1.57
Forests	7.09	Sandy loam - sandy clay loam	19.59
Olives	8.07	Sandy loam	8.84
Pastures	5.43	Clay loam - clay	36.66
Sparse vegetation	26.08	Urban	1.52
Urban areas	3.25	Sandy loam - loam	31.82
Vineyards	2.44		
Water	0.02		

Table 2.4 Land cover and range of soil texture classes used as input for the tRIBS model, with the corresponding percentage of basin area.

2.4 Hydrologic model

We used the TIN based Real Time Integrated Basin Simulator, tRIBS (Ivanov et al., 2004a, 2004b) a process-based, distributed hydrologic model (DHM) which is able to continuously represent the different hydrologic processes. It was originally developed at MIT by Prof. Rafael Bras' research group as the integration and further development of two previous models, Real-time Integrated Basin Simulator, RIBS (Garrote and Bras, 1995) and TIN-based Channel-Hillslope Integrated Landscape Development model, CHILD (Tucker et al., 2001).

The model represents the topography through Triangulated Irregular Networks (TINs). This allows significant reduction of computational nodes as compared to grid-based models (Vivoni et al., 2004, 2005), by representing the domain with multiple resolutions: larger number of nodes where the topography is complex and less details in flat homogenous areas. The use of TINs has also the advantage of preserving linear features such as stream networks and terrain breaklines. Voronoi polygons are the basic computational elements, in which the domain is discretized starting from TIN. In each element the governing equations are solved using a finite-difference control-volume approach (Ivanov et al., 2004a). Considering local dynamics and lateral mass exchanges the model can reproduce the spatially distributed hydrologic response of

a catchment. In each element, the model explicitly simulates the different processes involved in the hydrological cycle (Fig. 2.6):

- Rainfall interception is computed following the canopy water balance model (Rutter at al., 1972).
- Radiation and surface balance are computed using the combination equation (Penman, 1948; Monteith, 1965), gradient method and force-restore (Lin, 1980; Hu and Islam, 1995).
- Evapotranspiration is estimated through three components (Wigmosta et al., 1994): evaporation from wet canopy, canopy transpiration and bare soil evaporation (Deardorff, 1978).
- The infiltration process is based on the assumption of gravity-dominated flow in heterogeneous, anisotropic soil (Cabral et al., 1992; Beven, 1982, 1984). Different saturation levels in the soil column are given by the evolution of moisture fronts (unsaturated zone) (Morel-Seytoux et al., 1974; Neuman, 1976) coupled with variable groundwater table depths (saturated zone). Topography and soil drive lateral fluxes in vadose zone and groundwater during storm and interstorm periods (Smith et al., 1993; Childs and Bybordi, 1969). Accounting for these detailed processes, runoff generation is possible via four mechanisms: saturation excess, infiltration excess, perched subsurface stormflow and groundwater exfiltration.
- Runoff routing is composed of two parts: non-linear hydrologic routing, governing overland flow, and kinematic wave routing, modeling water transport and dispersion in natural channels.

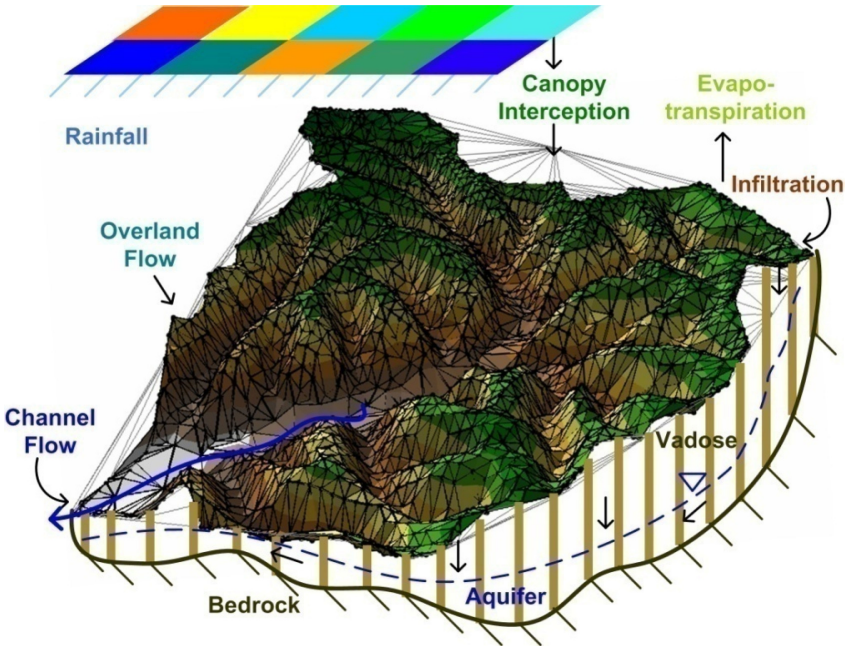

Fig. 2.6 Schematization of hydrologic processes represented in tRIBS model (Ivanov et al., 2004a, 2004b).

Model parameters can be divided into three groups: routing parameters, which are spatially uniform, soil and vegetation parameters, which vary in space and are provided through maps and look-up tables. A detailed description of the physical processes simulated by the model and its parameterization is given by Ivanov et al. (2004a, b). Applications of the selected DHM to date have ranged from multiyear, continuous simulations using NEXRAD (Ivanov et al., 2004a, 2004b), to event-based hydrograph predictions based on radar now-casting fields (Vivoni et al., 2006) or short-lead-time NWP fields. tRIBS has been used to track hydrologic response to precipitation forcing, downscaled with different techniques (Forman et al., 2008; Mascaro et al., 2010) and to assess the impact of climate change (Liuzzo et al., 2010).

Model inputs, beyond the watershed TIN, consist of spatial maps of surface properties (e.g., soil texture and land cover maps) and meteorological data. The time resolution of meteorological data must be at least hourly, it can be finer but not courser. These data are utilized to compute the surface energy fluxes and evaporation potential. Missing hourly data to compute potential evapotranspiration with the available formulas (Penman-Monteith, Deardorff

or Priestly-Taylor), the model accepts potential evapotranspiration values as input, which are converted in real evapotranspiration based on soil moisture state.

tRIBS outputs include time series of discharge at any location in the stream network and spatial maps of several hydrological variables (e.g. actual evapotranspiration, soil water content at different depths) at specified times or integrated over the simulation period. Recently, the code has been parallelized to be used in high performance computing platforms (Vivoni et al., 2011), increasing the possibility of simulating large watersheds response for long periods. These characteristics make the tRIBS model suitable to be used in studies aimed at quantifying the impact of climate change on water resources and hydrologic extremes at the basin scale, while addressing the different sources of uncertainty.

2.4.1 Hydrologic model setup

In order to setup the hydrological model tRIBS for the RMB simulations several steps were undertaken. The spatial framework was created converting the original DEM in a property TIN and, from this, the tRIBS spatial domain based on Voronoi polygons. As stated in section 2.3, some analysis was devoted to aggregate and harmonize the original land cover and soil texture maps in order to reduce the number of calibration parameters. The DHM required meteorological data at least at hourly resolution as input. In the RMB, in the period in which streamflow data for calibration-validation were available (1925-1935) the meteorological data had a daily resolution (section 2.3). As a result, two downscaling strategies, one for precipitation and the other for reference evapotranspiration (ET_0), were developed in order to provide the model with suitable data. The downscaling procedures are discussed in the following section 2.5.

The original DEM (Fig. 2.1c) was used to create the TIN network and, from this, the tRIBS spatial domain based on Voronoi polygons. Following the approach of Vivoni et al.

(2005), we created several TINs with different resolutions with the objective of identifying the best compromise between spatial aggregation and computational effort. The TINs resolution was evaluated comparing the horizontal point density, *d*, against two metrics characterizing the accuracy of terrain representation. The horizontal point density was defined as:

$$d = \frac{n_{TIN}}{n_{DEM}}, \qquad (2)$$

where n_{TIN} is the number of TIN nodes and n_{DEM} the number of DEM cells while the accuracy metrics are the vertical tolerance, z_r, (maximum vertical error) and the root mean square error (RMSE) between TIN and DEM elevations. The relationship *d* versus z_r and RMSE versus z_r are shown in Fig. 2.7a while the TIN is displayed in Fig. 2.7b. For this case study the TIN with z_r = 3 m was chosen, resulting in a total of 171'078 nodes, with *d* = 0.036 (or 3.6% of the DEM nodes) and RMSE = 1.50 m. An alternative parameter to quantify the irregular sampling of elevation nodes by TINs was the equivalent cell size, r_e, defined as the average grid spacing of points in a TIN:

$$r_e = \sqrt{\frac{A_b}{n_{TIN}}} = \frac{r}{\sqrt{d}} \qquad (3)$$

where $A_b = n_{DEM} r^2$ is the basin area and *r* is the DEM cell length.

The selected TIN was compared with the original 10-m DEM and a DEM aggregated at 50-m resolution, size chosen in order to reach a similar equivalent cell size as in the TIN (r_e = 52.7 m). The effects of terrain coarsening were illustrated in terms of the frequency distribution of topographic attributes (Vivoni et al., 2004), as shown in Fig. 2.8. While elevation (panel (a)) was not affected, slope and, in particular, curvature and topographic index (panels (b), (c) and (d)) appeared to be influenced by aggregation. The figure reveals that the selected TIN was able

to capture adequately the frequency distribution of elevation, slope, curvature and topographic index of the original DEM, performing better than the aggregated DEM with about the same equivalent resolution.

Soil depth map was obtained combining the DEM and the soil texture information, following a procedure described on the website of the Distributed Hydrology Soil Vegetation Model (http://www.hydro.washington.edu/Lettenmaier/Models/DHSVM/tools.shtml).

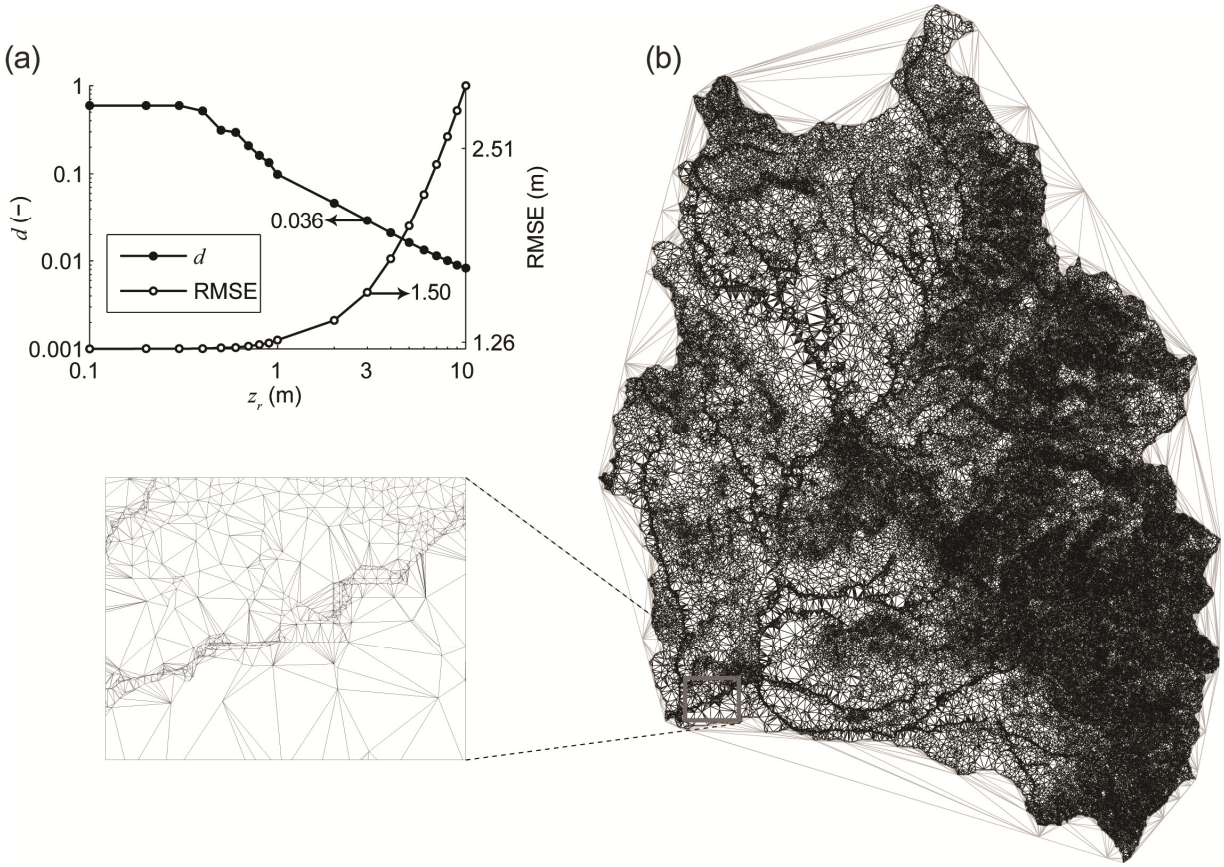

Fig. 2.7 (a) Relations between vertical accuracy z_r (maximum elevation difference between TIN and DEM) and horizontal point density d and RMSE between DEM and TIN elevations. (b) Voronoi polygons of selected TIN with z_r = 3 m corresponding to d = 0.036 and RMSE = 1.5 m.

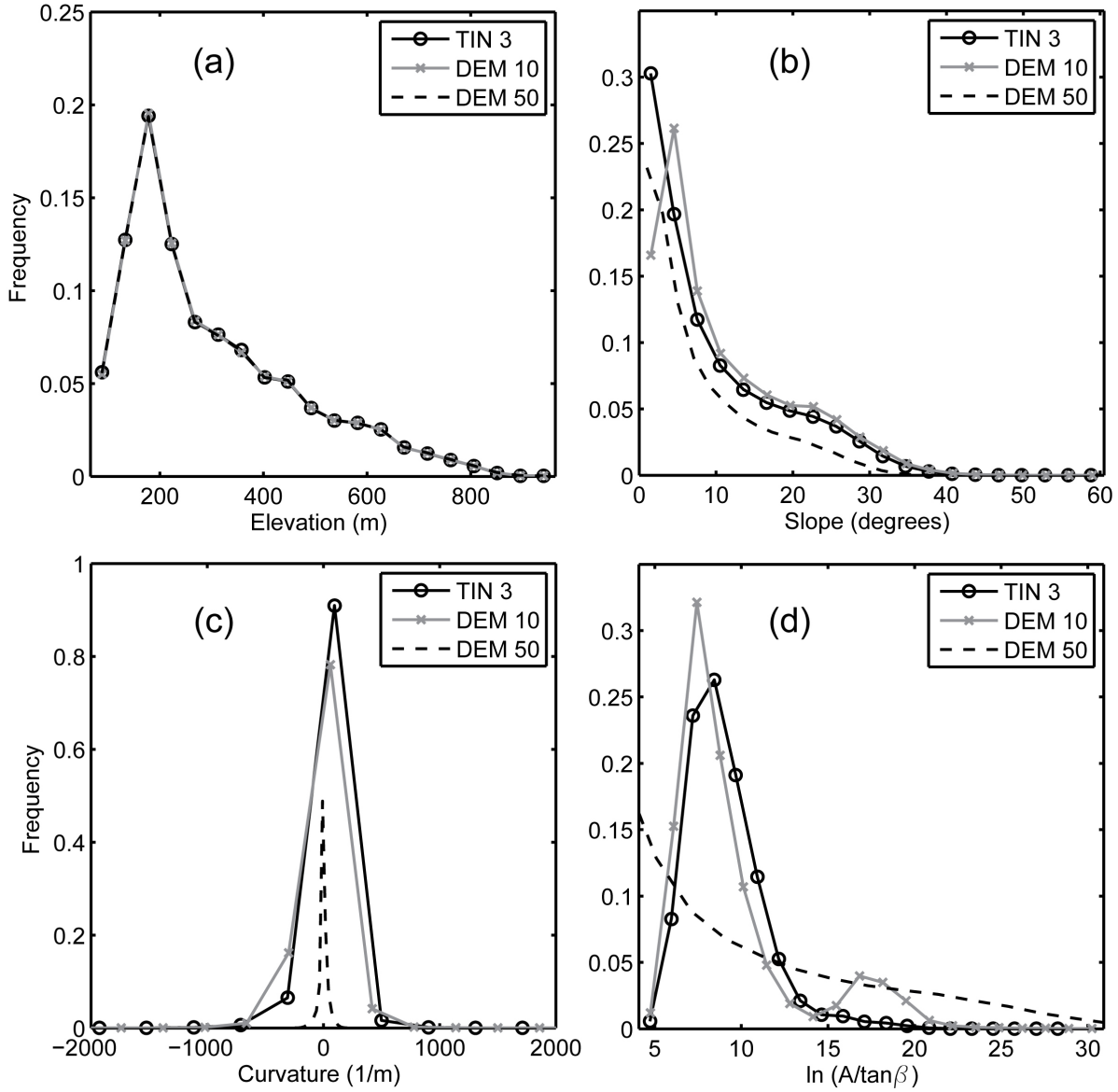

Fig. 2.8 Comparison of frequency distributions of (a) elevation, (b) slope, (c) curvature and (d) topographic index of the original 10-m digital elevation model (DEM 10), selected trianguleted irregular network (TIN 3) and a DEM aggregated at 50-m resolution (DEM 50).

The model tRIBS is able to ingest different types of precipitation inputs and it makes available more methods to estimate the evapotranspiration losses. Among those possibilities the ones which allowed overcoming the data sparseness and coarse resolution in the calibration validation period were chosen. Precipitation fields can be given as point observations of rain gages which are interpolated through the Thiessen polygon method. Alternatively, they can be spatial grids, as those produced by climate models, weather radars (Ivanov et al., 2004b; Vivoni

et al., 2006; Nikolopoulus et al., 2011), numerical weather forecasting models or reanalysis products (Vivoni et al., 2009; Robles-Morua et al., 2012), and stochastic downscaling models (Forman et al., 2008; Mascaro et al., 2010). In order to capture the dynamics of the hydrologic response under different types of storm events, the physical equations implemented in the model requires precipitation inputs at least at hourly resolution. We provided the model with precipitation grids obtained through a downscaling procedure which is explained in the following section 2.5.1. The real evapotranspiration (ET_R) losses are computed as a fraction of the potential evapotranspiration (ET_0) based on the soil moisture available in the upper soil layer, using a piecewise-linear equation with different parameterization accounting for bare soils or vegetated surfaces (Mahfouf and Noilhan, 1991; Ivanov et al., 2004a). The model has the possibility to compute ET_0 solving the energy balance through the Penman-Monteith approach (Penman, 1948; Monteith, 1965) based on hourly meteorological data, observed at stations or as grids, and on soil and vegetation parameters. Otherwise it can be forced directly with time series or grids of ET_0 computed offline. Failing to provide meteorological data required by the Penman-Monteith formula, we exploited the second possibility developing a downscaling procedure for ET_0 based on daily minimum and maximum temperatures, the only meteorological data available in the period for calibration and validation. The procedure is described in the following section 2.5.2.

2.5 Downscaling tools

The hydrologic model tRIBS required meteorological data at hourly resolution as input. In the RMB, the available meteorological data in the period of calibration-validation (1925-1935) had a daily resolution (section 2.3). As a result, two downscaling strategies were developed, one for precipitation and the other for reference evapotranspiration, ET_0, in order to provide the model with suitable data.

2.5.1 Downscaling strategy for precipitation

Among the different methods which have been recently developed to disaggregate precipitation events (Wilby and Wigley, 1997; Bardossy et al., 2011), a procedure based on multifractal theory was chosen. In particular, we adopted the multifractal downscaling model known as Space Time RAINfall (STRAIN) model. This model is able to simulate the precipitation variability in temporal, spatial and spatiotemporal frameworks in a wide range of scales, through binary multifractal cascades produced by a log-Poisson stochastic generator (Deidda et al., 1999; Deidda, 2000). The objective was to downscale daily precipitation observed by a network of rain stations producing gridded maps at hourly resolution. In order to reach this goal, a disaggregation tool was developed based on a previous application of the STRAIN model in Sardinia. Badas et al. (2006), indeed, downscaled precipitation from the coarse scale L = 104 km and T_1 = 6 h up to a fine scale l = 13 km and T_2 = 45 min. In this thesis work, precipitation data were available in the coarse spatial domain at daily resolution in the period 1925-1935 and at 1-min resolution in the period 1986-1996. The location of the rain gauges used to calibrate the downscaling model, together with the coarse and the fine scale domains are displayed in Fig. 2.3.

The downscaling procedure in the RMB was achieved through two steps which are shown schematically in Fig. 2.9. In the first step, the STRAIN model was used to perform a

temporal disaggregation of the rainfall volume observed in the domain L x L (L = 104 km) from the scale T_0 = 24 h to the scale T_1 = 6 h. In the second step, the model was utilized in a spatiotemporal framework to downscale precipitation from the coarse scale L x L x T_1 to the fine scale l x l x T_2 (l = 13 km, T_2 = 45 min), as in Badas et al. (2006). In order to be used as input for the tRIBS model, the resulting downscaled precipitation grids were aggregated in time from T_2 = 45 min to 1 h. This further aggregation was undertaken to reduce computational time and to harmonize meteorological input forcing (precipitation and ET_0) time resolution.

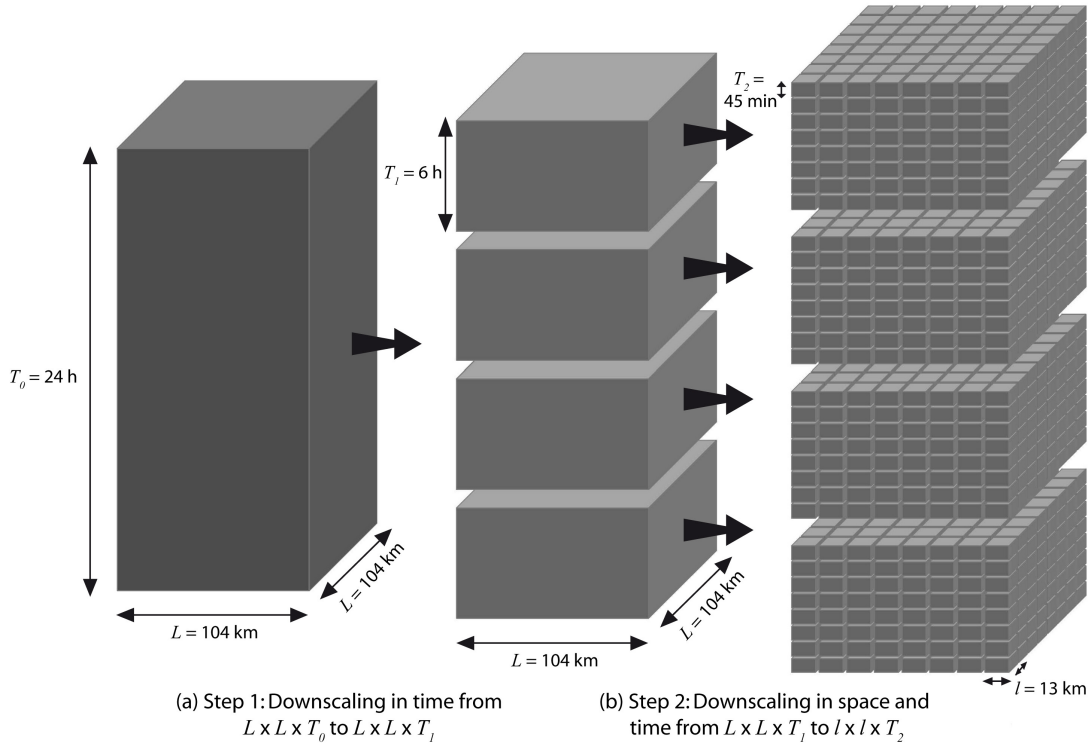

Fig. 2.9 Schematic of the precipitation downscaling tool based on STRAIN model. The procedure consisted of two steps: (a) disaggregation in the time domain from the coarse scale L x L x T_0 (L = 104 km, T_0 = 24 h) to the fine scale L x L x T_1 (T_1 = 6 h); and (b) disaggregation in the space-time domain from the coarse scale L x L x T_1 to the fine scale l x l x T_2 (l = 13 km, T_2 = 45 min).

Observed precipitation fields are characterized by multifractal properties which the STRAIN model reproduces through a log-Poisson stochastic generator dependent on two parameters, c and β. These parameters were estimated by means of invariance and multifractal

analysis between the coarse and the fine scales. A wide group of rainfall events and one or more coarse scale predictors were used to create empirical calibration relationships between the two parameters. Previous studies (Deidda et al., 1999, 2004, 2006; Badas et al., 2006), found that the parameter β was almost constant and equal to e^{-1}, while the parameter c was related to the coarse scale mean rainfall intensity R (mm/h) through the relation:

$$c = c_{\infty} + a \cdot e^{-\gamma R}, \tag{4}$$

with parameters c_{∞}, a and γ. Once the coarse predictors were used to derive values of c and β from the calibration relations, an ensemble of small-scale rainfall fields was generated, each representing a possible scenario statistically consistent with the same coarse scale condition. Details on the scale invariance and multifractal analysis can be found in Deidda (2000) and in Deidda et al. (1999, 2004). In the following, the model calibration in the time and in the space-time frameworks is briefly described. Finally, the performances of the downscaling procedure are evaluated in section 2.5.3.

Precipitation downscaling in the time domain

The spatial grid, shown in Fig. 2.3 with a cell size l = 13 km and an extension L = 104 km, was created in such a way that each cell contains at least one gage, as in Badas et al. (2006). The data observed by the gages in each pixel were averaged for a given time step, obtaining for the period 1986-1996 a dataset of gridded precipitation fields at resolution of 13 km and 45 min over the coarse domain of 104 x 104 km^2.

A group of 300 precipitation events at the coarse scale of L x L x T_0 were selected to perform the scale invariance and multifractal analysis from T_0 = 24 h to T_1 = 6 h and estimate the parameters c and β. For this purpose, the events were ordered according to the coarse scale rain intensity R and grouped in 20 classes of 15 events on which the values of c, β and R were averaged. The

relation between c and R, shown in Fig. 2.10a with the c estimates in the 20 classes, followed equation 4 and β was equal to e^{-1}, as found in the previous cited works. The values of the parameters c_∞, a and γ are reported in Table 2.5.

	c_∞	a	γ
Time domain	0.43	0.93	1.94
Space-time domain	1.49	2.23	3.04

Table 2.5 Parameter values of the calibration relation (4) of the STRAIN model for applications in the time and space-time domains, which are valid when expressing R in mm h-1.

Precipitation downscaling in the space-time domain

The application of the STRAIN model in three dimensions (space and time) requires the identification of a velocity parameter U (km h^{-1}) that transfers the statistical properties observed in the space scale to the time scale. Following the approach of Badas et al. (2006), we adopted U = 17.33 km h^{-1}; hence, downscaling was carried out from L = 104 km to l = 13 km in space and from $T_1 = L/U$ = 6 h to $T_2 = l/U$ = 45 min in time. To perform the scale invariance analysis, the precipitation fields were aggregated from the coarse scale L x L x T_1 to the fine scale l x l x T_2. The model was calibrated using a total of 800 precipitation events. As for the application in the time domain, events were grouped in 40 classes of 20 events and a single set of averaged parameters c and β was computed for each class, finding, again, $\beta = e^{-1}$ across the classes and c (estimated with $\beta = e^{-1}$) linked to R according to equation (4). The resulting calibration relation is shown in Fig. 2.10b while parameters c_∞, a and γ are reported in Table 2.5. In the previous study, the spatial distribution of precipitation in the Sardinian island appeared to be a non-homogeneous field, mainly due to the terrain aspects. Since the STRAIN model reproduces homogeneous fields, we followed the procedure suggested by Badas et al. (2006) to apply the model while accounting for the effect of orography.

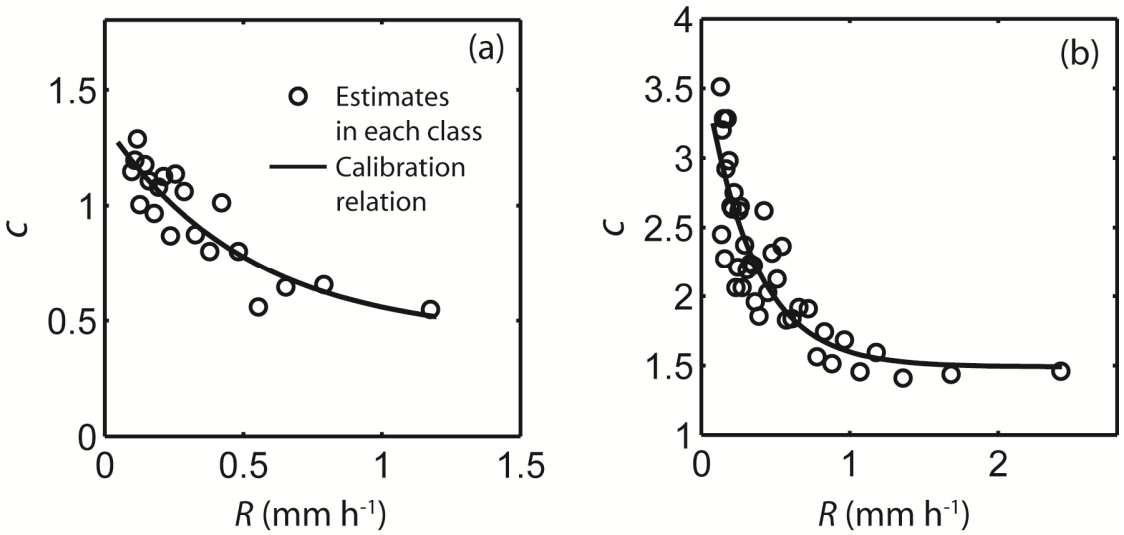

Fig. 2.10 Calibration relations (4) between the STRAIN model parameter *c* and the coarse-scale mean precipitation intensity *R* for application in the (a) time and (b) space-time domains.

2.5.2 Downscaling strategy for potential evapotranspiration

When hourly meteorological data, required for internal ET_0 computation, are missing the tRIBS hydrologic model can be forced by time series or grids of hourly potential evapotranspiration, ET_0, computed offline with alternative approaches (see section 2.4.1). In our case study, in the period in which data for calibration was available (1925-1935, section 2.3), the presence of daily T_{min} and T_{max} only permitted estimating ET_0 at daily resolution using, e.g., the Hargreaves equation (Hargreaves, 1994; Hargreaves and Allen, 2003). To circumvent this scale discrepancy, we designed a procedure to disaggregate ET_0 from daily to hourly scale, using the hourly dataset of meteorological variables available from 1995 to 2010 (Fig. 2.3, table 2.2). The strategy was based on the computation of dimensionless functions $\varphi_m(h)$, representing the diurnal cycle of the process averaged for each month and computed as:

$$\varphi_m(h) = \frac{\left\langle ET_0(h,m)\big|_H \right\rangle}{\left\langle ET_0(m)\big|_D \right\rangle}, \tag{5}$$

the ratio between the monthly climatological averages of ET_0 at hourly scale $\left\langle ET_0(h,m)\big|_H \right\rangle$ (subscript H), and at daily scale, $\left\langle ET_0(m)\big|_D \right\rangle$ (subscript D). These terms were given by the following equations:

$$\left\langle ET_0(h,m)\big|_H \right\rangle = \frac{1}{N_y}\frac{1}{N_m}\sum_{y=1}^{N_y}\sum_{d=1}^{N_m} ET_0(h,d,m,y)\big|_H \tag{6}$$

$$\left\langle ET_0(m)\big|_D \right\rangle = \frac{1}{N_y}\frac{1}{N_m}\sum_{y=1}^{N_y}\sum_{d=1}^{N_m} ET_0(d,m,y)\big|_D \quad . \tag{7}$$

where N_m is the number of days in month m, N_y is the number of years considered for the climatological mean (in our case, $N_y = 16$), while $ET_0(h,d,m,y)\big|_H$ and $ET_0(d,m,y)\big|_D$ are the hourly and daily potential evapotranspiration computed for hour h in day d, month m and year y. The dimensionless functions $\varphi_m(h)$ could be used to disaggregate ET_0 from daily to hourly resolution as:

$$ET_0(h,d,m,y)\big|_H = \varphi_m(h)\cdot ET_0(d,m,y)\big|_D \quad . \tag{8}$$

In our case study, the procedure was calibrated and validated in the period in which high resolution meteorological data were available (1995-2010) and applied in the period of hydrologic model calibration (1925-1935) when only temperature data were recorded. Calibration and application of the ET_0 downscaling tool are described in the following.

In the period 1995-2010, we computed $ET_0(h,d,m,y)\big|_H$ using the Penman-Monteith (PM) equation (Allen at al., 1989, 2006), using equation:

$$ET_0(h,d,m,y)\big|_H = \frac{0.408\Delta(R_n - G) + \gamma\dfrac{37}{T_h+273}u_2\left(e^0(T_h) - e_a\right)}{\Delta + \gamma\left(1 + 0.34\dfrac{r_s}{r_a}\right)} \tag{9}$$

The formula is reported for the sake of completeness but the reader is referred to Allen et al. (1989, 2006) for the meaning and computation of single terms. Values of stomatal resistance (r_s) and albedo (a), required in equation (9), were taken from a study of Montaldo et al. (2008) in Sardinia. Daily estimates were derived by summing hourly values over the 24 hours of each day. Hence, having hourly and daily ET_0 values for the entire period, it was possible the implementation of equations (6) and (7) and, from those, the computation of the monthly dimensionless functions (5). Fig. 2.11a shows examples of $\varphi_m(h)$ for the months of January, April, July and October. It can be noticed that, as expected, fall and winter months presented a more pronounced peak in the central hours of the day due to the shorter daylight period. In the same period (1995-2010) we investigated the relationship between daily ET_0 computed with PM formula, $ET_0(d,m,y)\big|_{D,PM}$, and daily ET_0 computed with Hargreaves (HG) equation (Hargreaves, 1994; Hargreaves and Allen, 2003) starting from daily T_{min} and T_{max}, $ET_0(d,m,y)\big|_{D,HG}$, having equation:

$$ET_0(d,m,y)\big|_{D,HG} = 0.0023 \cdot RA \cdot (T + 17.8) \cdot TD^{0.5} \qquad (10)$$

Again, the reader can find in Hargreaves (1994) further information and symbols meaning. The analysis was carried out for each of the four seasons, with the aim of accounting for the variability of climate. We found that a simple linear relation:

$$ET_0(d,m,y)\big|_{D,PM} = p_0 + p_1 \cdot ET_0(d,m,y)\big|_{D,HG} \qquad (11)$$

could be used to link the two types of estimates. The values of p_0 and p_1 estimated for each season are reported in Table 2.6, along with the linear correlation coefficient (CC) and the root mean square error (RMSE) between $ET_0(d,m,y)\big|_{D,PM}$, and $ET_0(d,m,y)\big|_{D,HG}$. Fig. 2.11b shows an example for the spring season.

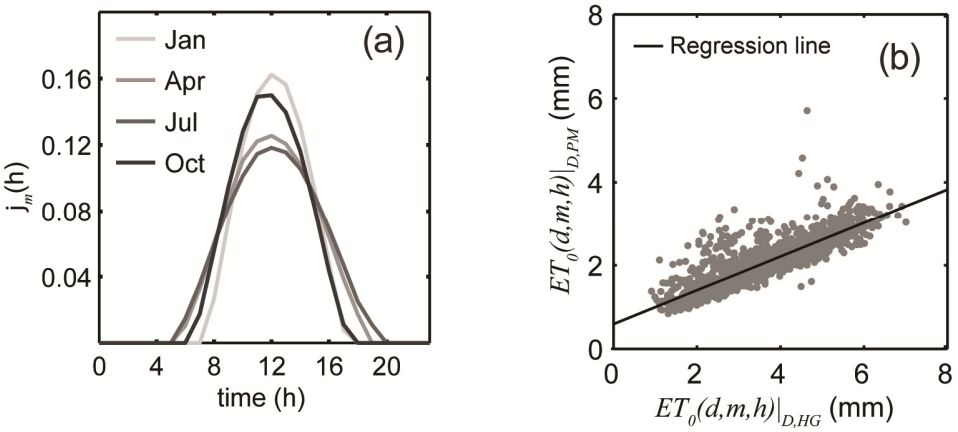

Fig. 2.11 (a) Dimensionless function $\varphi_m(h)$ for the months January, April, July and October, and (b) scatterplot between the daily ET_0 computed with the PM and HG formula during the spring season (MAM), along with the regression lines.

Season	p_0	p_1	CC	RMSE
DJF	0.409	0.367	0.608	0.165
MAM	0.593	0.404	0.835	0.322
JJA	1.486	0.269	0.538	0.361
SON	0.405	0.429	0.875	0.248

Table 2.6 Parameters p_0 and p_1 of the linear regression (11) between daily ET_0 expressed in mm and computed with the PM and HG formulas for each season (DJF: December, January and February; MAM: March, April and May; JJA: June, July and August; SON: September, October and November). The linear correlation coefficient (CC) and the root mean square error (RMSE) are also reported.

The procedure was applied in the period of hydrologic model calibration - validation (1925-1935), starting from daily temperature data (T_{min} and T_{max}). The computation of hourly time series of ET_0 was achieved by (i) calculating $ET_0(d,m,y)|_{D,HG}$ for a given day d in month m and year y; (ii) using the linear relation (11) to derive an estimate of $ET_0(d,m,y)|_{D,PM}$, with the values of p_0 and p_1 chosen depending on the season (Table 2.6); (iii) using equation (8) with the specific monthly dimensionless function, $\varphi_m(h)$, to obtain the evapotranspiration at hourly scale $ET_0(h,d,m,y)|_H$ for h = 0, 1, ..., 23. A schematization of the entire downscaling procedure for ET_0 is reported in Fig. 2.12.

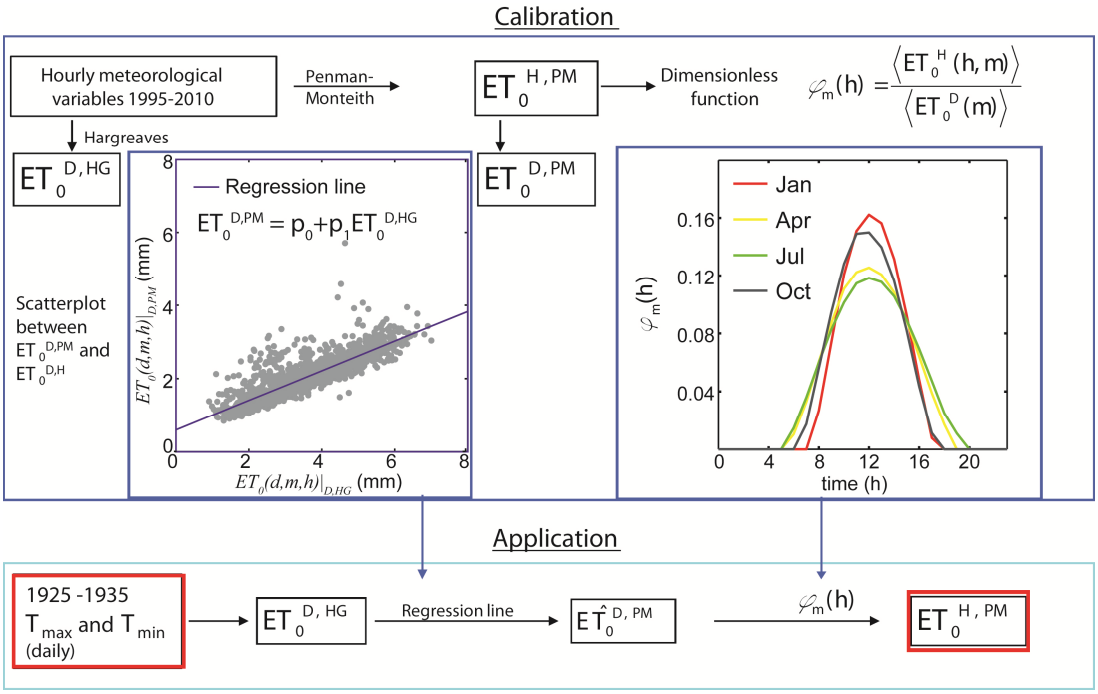

Fig. 2.12 Schematizzazion of the downscaling procedure for reference evapotranspiration.

2.5.3 Validation of the downscaling strategies

The performances of the downscaling strategy for precipitation were evaluated comparing empirical cumulative density functions (ECDFs) of observed and synthetic rainfall series. We considered separately the time and the space - time frameworks and, at the end, the entire downscaling procedure. We randomly selected 10 observed rainfall events at the coarse scale in each group used in the scale invariance multifractal analyses. For each event, the STRAIN model generated 100 disaggregated series using the parameters values found in the calibration phase (Fig. 2.10 and Table 2.5). The observed and the synthetic high-resolution rainfall series were divided by corresponding R to have unitary coarse scale mean. We compared the ECDFs of the 10 observed standardized rainfall series at high resolution (i^*) with the ECDFs of the 90% confidence intervals derived from the 10 x 100 standardized synthetic series. Results are shown in Fig. 2.13, where panels (a) - (d) refer to the time domain while panels (e) - (h) refer to the space - time domain. The STRAIN model seemed able to well reproduce the statistical

variability in time over a large range of standardized rainfall intensities and to have the capacity to capture the small-scale spatiotemporal precipitation distribution with reasonable accuracy.

The entire downscaling procedure was evaluated considering the same daily rainfall events used to verify the application in the time domain. The mean daily rainfall intensities in the coarse domain of 104 x 104 km were first disaggregated in time, producing an ensemble of 10 disaggregated series at time resolution T_1 = 6 h (Fig. 2.9a). For each event of these series, the STRAIN model performed the disaggregation in space and time generating an ensemble of 10 fields at the fine scale l x l x T_2 (Fig. 2.9b), for a total of 100 (10 by 10) disaggregated grids. Fig. 2.13 panels (i) - (l) presents the comparison between the ECDFs of the observed standardized rainfall series against the 90% confidence intervals of the generated series for four intensities. The model shows a relative good skill in reproducing the rainfall distribution at the fine scale.

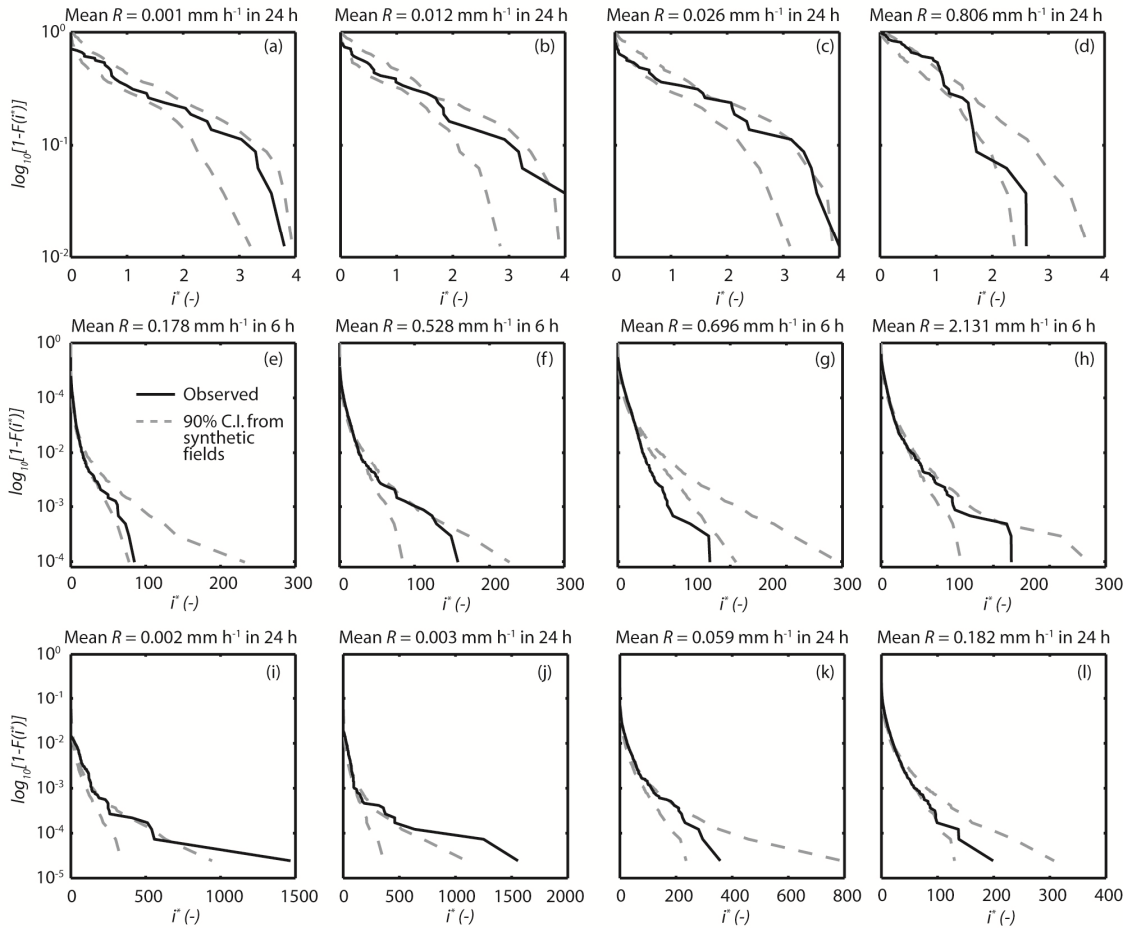

Fig. 2.13 Comparison between the empirical cumulative density functions (ECDFs) of the small-scale observed precipitation fields and the 90% confidence intervals derived from an ensemble of 100 synthetic fields generated with the downscaling tool. The small-scale precipitation intensities were standardized and indicated as i* (see text for details). Panels (a)-(d) and (e)-(h) show results for the applications in the time and space-time domains, respectively, while panels (i)-(l) report results for the entire disaggregation procedure.

The downscaling strategy for ET_0 was evaluated in the period during which high resolution meteorological data were available (1995 - 2010). We compared the inter annual mean RMSE and the percent bias, between (i) the hourly ET_0 obtained with the disaggregation method starting from daily T_{min} and T_{max}, and (ii) the hourly ET_0 estimated with the PM formula using the meteorological data. Table 2.7 reports the results for each season of the period 1995-2010. The RMSE was quite low in each season and characterized by little inter annual variability; hence the downscaling procedure did not introduce a relevant error. The percent bias is always negative but small confirming that we obtained a quite good estimation of the hourly ET_0, even if slightly

underestimated especially in winter.

Season	RMSE (mmh^{-1})	Bias (mmh^{-1})
DJF	0.019	-0.004
MAM	0.031	-0.009
JJA	0.039	-0.015
SON	0.029	-0.011

Table 2.7 RMSE and Bias between (i) the hourly ET_0 obtained with the disaggregation method starting from T_{min} and T_{max}, and (ii) the hourly ET_0 estimated with the PM formula using the meteorological data for each season of the years 1995-2010.

2.6 Calibration and validation

2.6.1 Selection of calibration and validation periods

The discharge data in the RMB outlet were published in annual technical reports of the Italian Hydrologic Survey (called "Annali Idrologici") for the years 1925-1935. Streamflow was estimated through a rating curve by reading the water stage every day at 9 a.m. (Table 2.2). The information published in each annual report included: the time series of daily water stage and discharge; the rating curve, provided as a set of stage and discharge points (linear interpolation is performed between each point); the stage and discharge values that were measured during the year to update the rating curve; and a description of the possible problems encountered during the year that affected the current or the past discharge estimates.

To select the periods for model calibration and validation, we carefully inspected the information and the data contained in the technical reports, finding that: (i) the rating curves exhibited significant variation across the 11 years; and (ii) a number of significant problems were reported for some years that affected the quality of the discharge estimates (e.g., in 1929, an eddy close to the measurement device caused a consistent bias). To minimize data uncertainty, we identified three consecutive years (1930-1932), during which the published rating curves did not

vary significantly and problems were not reported. Next, we fitted a rating curve using the stage and discharge measurements over the three years and used this to derive a discharge time series from the stage records. Klemes (1986) and other authors suggest to use a wet period for calibration and a drier period for validation, especially when the hydrologic model is used to evaluate the effects of climate change. Among those three years, the year 1930 presented the major number of flood events and was then selected for calibration, while 1931 and 1932 were used to validate the model performance.

2.6.2 tRIBS calibration and validation

The hydrologic model tRIBS depends on a high number of parameters that can be divided into three groups according to the simulated processes: (i) channel and hillslope routing parameters, (ii) soils hydraulic and thermal properties parameters and (iii) vegetation properties parameters. Following Ivanov et al. (2004b) and results of a sensitivity analysis, the most influential parameters were found to be the saturated hydraulic conductivity at the surface (K_s) and the conductivity decay parameter (f), used to model the variation of K_s with the soil depth (Cabral et al., 1992). The values of K_s and f were modified within the ranges typical for the corresponding soil texture classes (Fig. 2.4), while, for the other parameters, we adopted literature values for similar soil and vegetation properties (Rawls et al., 1983; Noto et al., 2008; Montaldo et al., 2008; Vivoni et al., 2010)

Using the downscaling model STRAIN (Deidda et al., 1999; Deidda, 2000 and Badas et al., 2006) as explained in Section 2.5.1, we created an ensemble of 50 disaggregated rainfall fields at the scale l x l x T_2 for the time slice 1930-1932, starting from the daily mean rainfall intensities measured in the large grid L x L (Fig. 2.3). The resulting disaggregated precipitation grids were subsequently aggregated in time from T_2 = 45 min to 1 h. No downscaling was

performed in those days without rain and grids with zero rainfall were created. The ability of the downscaling tool to represent observed precipitation was further checked comparing the observed and simulated series of daily mean areal precipitation (MAP) in the RMB. The simulated MAP series was obtained aggregating the synthetic grid at daily resolution and computing the spatial basin average. Observed series, on the other hand, was derived applying the Thiessen polygon method to the observations of the 12 gages represented by triangles on Fig. 2.1c. The RMSE and bias between observed (MAP_O) and downscaled (MAP_D) values computed on rainy days are reported in Table 2.8 for the period 1925 – 1935. The RMSE has little interannual variability (average value of 4.38 mm) while the bias is negative (mean of – 0.89 mm) indicating a tendency of the downscaling process to slightly underestimate the observed MAP (less than 10%). The hourly basin averaged ET_0 series was computed applying the disaggregation strategy (Section 2.5.2) in each Voronoi polygon of the RMB and calculating the weighted mean across the basin. The values of T_{min} and T_{max} in each Voronoi element were determined by correcting the temperature observed at the station of Cagliari (circle in Fig. 2.1b) as a function of the element elevation, using an adiabatic lapse rate of -6.5°Ckm^{-1}.

The simulations with tRIBS model were performed using the parallelized code (Vivoni et al., 2011) in the Saguaro super computer at Arizona State University. Following the approach of Vivoni et al. (2005) we utilized a spin-up interval of two years prior to the start of the calibration period. The most influencing parameters were manually adjusted within the ranges typical for the corresponding soil texture classes (Fig. 2.4b) until a good estimation of the observed monthly streamflow volumes was reached. Table 2.9 shows the parameters values in the main classes, reporting the calibrated ones in italics.

Year	RMSE (mm)	Bias (mm)
1925	4.34	-1.06
1926	4.28	-0.78
1927	4.18	-1.49
1928	3.95	-0.60
1929	4.19	-1.31
1930	*5.63*	*-0.64*
1931	*4.27*	*-0.76*
1932	*3.15*	*-0.74*
1933	4.86	-1.35
1934	3.97	-0.29
1935	4.48	-1.03
All	4.37	-0.89

Table 2.8 RMSE and Bias between the daily observed mean areal precipitation (MAP_O) and the ensemble average from the downscaling tool and aggregated at daily scale (MAP_D) for rainy days. Italic font is used for years selected to calibrate and validate the hydrologic model.

Fig. 2.14a shows the time series of the observed discharge compared against the 90% confidence intervals derived from the ensemble streamflow simulations. In the two insets we can better visualize the comparison over two time periods with significant flood events, and appreciate the different resolution between the observations (daily) and model outputs (sub-hourly). For each inset, we also plotted the difference between the downscaled ensemble average (MAP_D) and observed (MAP_O) mean areal precipitation at the daily scale. Despite the uncertainty in hydrometeorological inputs, the model reproduced, with reasonably accuracy, the shape and timing of the major flood events. In some cases, the mismatch between observed and simulated precipitation inputs led to underestimation or overestimation of flood peaks. For example, the model was not able to reproduce the peaks labeled as M (missed), due to a previous period of underestimated precipitation (negative MAP_D-MAP_O). Similarly, the timing of flood peaks could be also affected, as illustrated by the label D (delayed). These discrepancies could not be entirely ascribed to a failure of the proposed procedure. First, the coarse (daily) sampling of

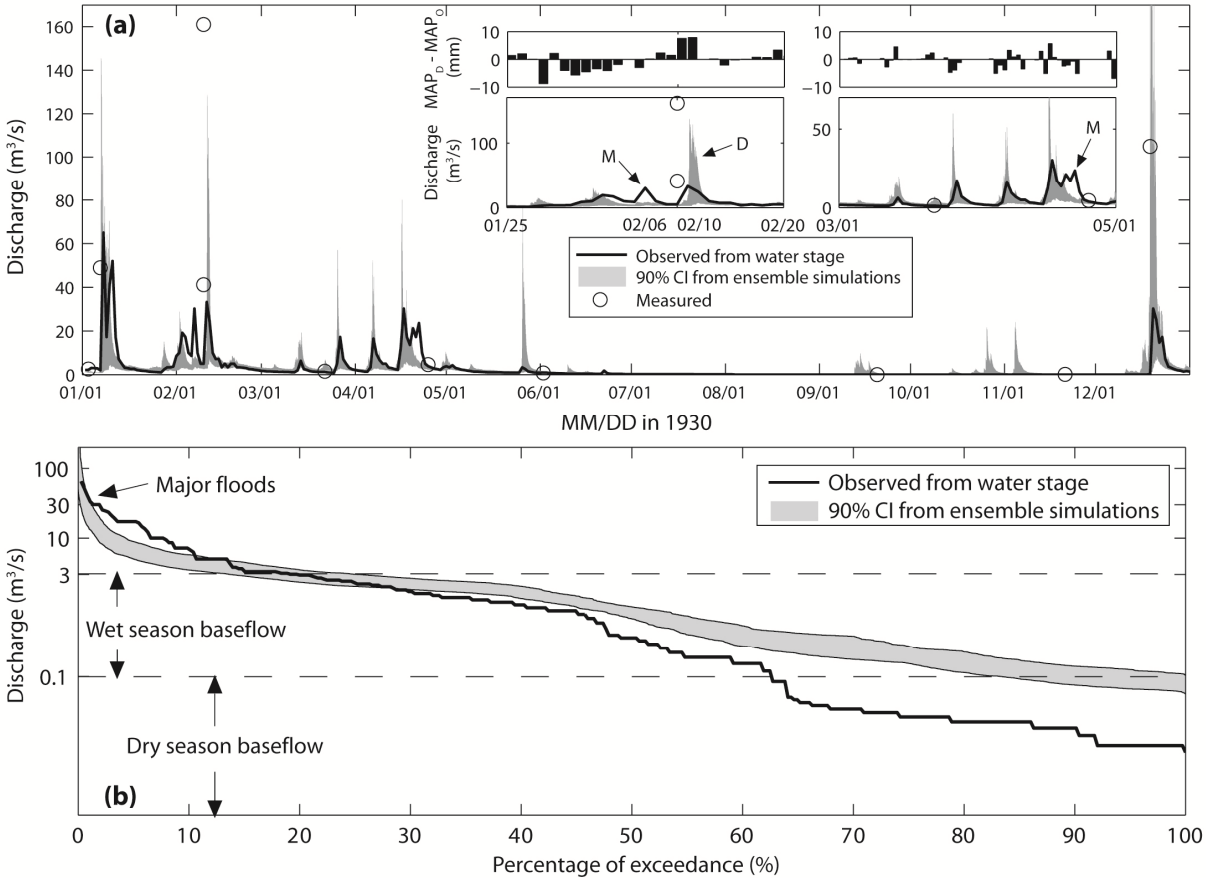

Fig. 2.14 Result of the tRIBS model calibration (year 1930). (a) Comparison between the observed discharge against the 90% confidence intervals (CI) derived from the 50 ensemble simulations of the tRIBS model. In the insets, a zoom on two periods with significant flood events is reported to better visualize the comparison, along with the difference between the daily MAP_D and MAP_O (see text for the definition). The circles represent the discharge values measured by the Italian Hydrologic Survey to update the rating curve. (b) Comparison between the observed flow duration curve and the 90% confidence intervals derived from the 50 ensemble simulations.

stage levels was not sufficient to capture the high frequency of the discharge variability and the magnitude of the flood peaks properly, whereas the sub-hourly resolution of tRIBS outputs allowed better representing the system dynamics, as it is discussed below. Second, since the downscaling tool redistributed in stochastic fashion the daily rainfall volumes from a large domain (104 km x 104 km grid shown in Fig. 2.3) to smaller areas and times, it could be possible that, in some days, the multifractal model failed to capture the exact spatial localization of the storms. As a consequence, cases where MAP_D and MAP_O differed should be somehow expected,

as they are part of the uncertainty associated with the disaggregation approach.

Land Cover Properties	Variable (unit)	Major Land Cover Types: Agriculture	Sparse vegetation	Olives	Forests	Pasture
Area	A (%)	47.64	26.08	8.07	7.09	5.43
Vegetation fraction	v (-)	0.5	0.5	0.5	0.5	0.4
Albedo	a (-)	0.2	0.2	0.2	0.18	0.2
Vegetation height	h (m)	1.0	1.0	3.0	10.0	0.7
Vegetation transmission	K_t(-)	0.5	0.5	0.5	0.5	0.5
Minimum stomatal resistance	r_{min} (sm^{-1})	100	100	100	100	100

Soil Properties	Variable (unit)	Major Soil Types: Clay loam –Clay	Sandy loam – Loam	Sandy loam – Sandy clay loam
Area	A (%)	36.66	31.82	19.59
Saturated hydraulic conductivity	K_s (mmh^{-1})	0.60	13.20	3.00
Conductivity decay	f (mm^{-1})	0.00051	0.00096	0.00096
Porosity	n (-)	0.475	0.463	0.398
Saturated soil moisture	θ_s (-)	0.385	0.434	0.330
Residual soil moisture	θ_r (-)	0.090	0.027	0.068
Stress soil moisture	θ^* (-)	0.308	0.347	0.264
Pore size distribution index	m (-)	0.165	0.252	0.319

Table 2.9 Parameters of tRIBS model for the main land cover and soil texture classes in the RMB.

Time scale	Calibration NSC Min, Mean, Max	Validation NSC Min, Mean, Max
Daily	-3.53, 0.07, 0.61	-0.99, 0.02, 0.42
Weekly	-5.50, 0.46, 0.83	-0.72, 0.13, 0.47
Monthly	-0.06, 0.55, 0.89	0.30, 0.25, 0.74

Table 2.10 Nash-Sutcliffe coefficients (NSC) between observed and simulated water volume at daily, weekly, and monthly time scales. The minimum, mean and maximum values across the 50 ensemble members are reported for the calibration and validation periods.

The circles in Fig. 2.14a are the streamflow measurements made by the Italian Hydrologic Survey during campaigns aimed at updating the rating curve. Some of these observations were collected during three major flood events. One can note how the model was able to capture fairly well the magnitude of the high values observed between two daily

discharge readings. This was an important and promising result that built confidence on the model utility for analyses of flood frequency under climate change. Table 2.10 reports the Nash-Sutcliffe coefficient (NSC) (Nash and Sutcliffe, 1970) computed for the water volume derived from the observed streamflow and the ensemble streamflow simulations. Specifically, the minimum, mean and maximum values of the 50 ensemble members are reported for different aggregation times (daily, weekly and monthly). Linear variability between discharge observations was assumed to calculate the volume. Clearly, the lowest values of NSC (poor performances) were obtained at daily resolution, because at this scale the direct correspondence between observation and simulations was more affected by the different sampling time step and by mismatching in the disaggregated forcing. When larger time scales were considered, NSC increased and reached a mean value of 0.55 at monthly resolution. In terms of total runoff volume, the ensemble mean was 170 mm (standard deviation, STD, of 70 mm across the 50 members) and the observation was 183 mm. This underestimation (~10%) could be explained by the lower simulated MAP (mean and STD of 848 and 118 mm) as compared to the observation (902 mm). In both the observed streamflow and the ensemble mean, the runoff coefficient was found to be~0.20 for this period.

To further illustrate the model performance, Fig. 2.14b shows the comparison between the observed flow duration curve (FDC) and the 90% confidence intervals from the ensemble simulations. The shape of the observed FDC was well reproduced within the range of wet season baseflow and for the major flood events. The model underestimated the streamflow values corresponding to the percentage of exceedance of 2 to 10%, due to a tendency to simulate steeper recession limbs. The shapes of simulated and observed FDCs diverged in the interval of dry season baseflow. However, in that range of discharge values, the absolute error between the

observations and simulations was very low, and the observed data were quite uncertain, as they were affected by releases from urban and irrigation activities.

Results for the validation period (years 1931 and 1932) are shown in Fig. 2.15. It can be noted the good performances in reproducing the discharge time series (Fig. 2.15a) over year 1931 and most of 1932. In the period from October to December 1932, the model simulated a number of peaks that were not observed, while sometimes underestimated the discharge, due to the same reasons discussed for the calibration period. Those peaks lowered the NSC values at the different aggregation times, as reported in Table 2.10. As in the calibration period, the total simulated runoff volume (mean of 103 mm and STD of 17 mm) was lower than the observation (147 mm), due to lower precipitation simulated by the downscaling tool (mean of 993 mm and STD of 96 mm) as compared to the observed total (1025 mm). The simulated runoff coefficient throughout the two years was on average 0.10 in the simulations, slightly smaller than the observed value of 0.14. Despite the discrepancies present in the time series and the metrics, Fig. 2.15b reveals an excellent agreement between the shapes of observed and simulated FDCs, even in the range of the dry season baseflow. Overall, these results suggest that the combined use of the downscaling algorithms and the tRIBS model allowed reproducing with reasonable accuracy the hydrologic response of the RMB within the 3 years selected for calibration and validation. This holds promising for the subsequent application of these simulation tools to evaluate the local impacts of future climate change scenarios (chapter 3).

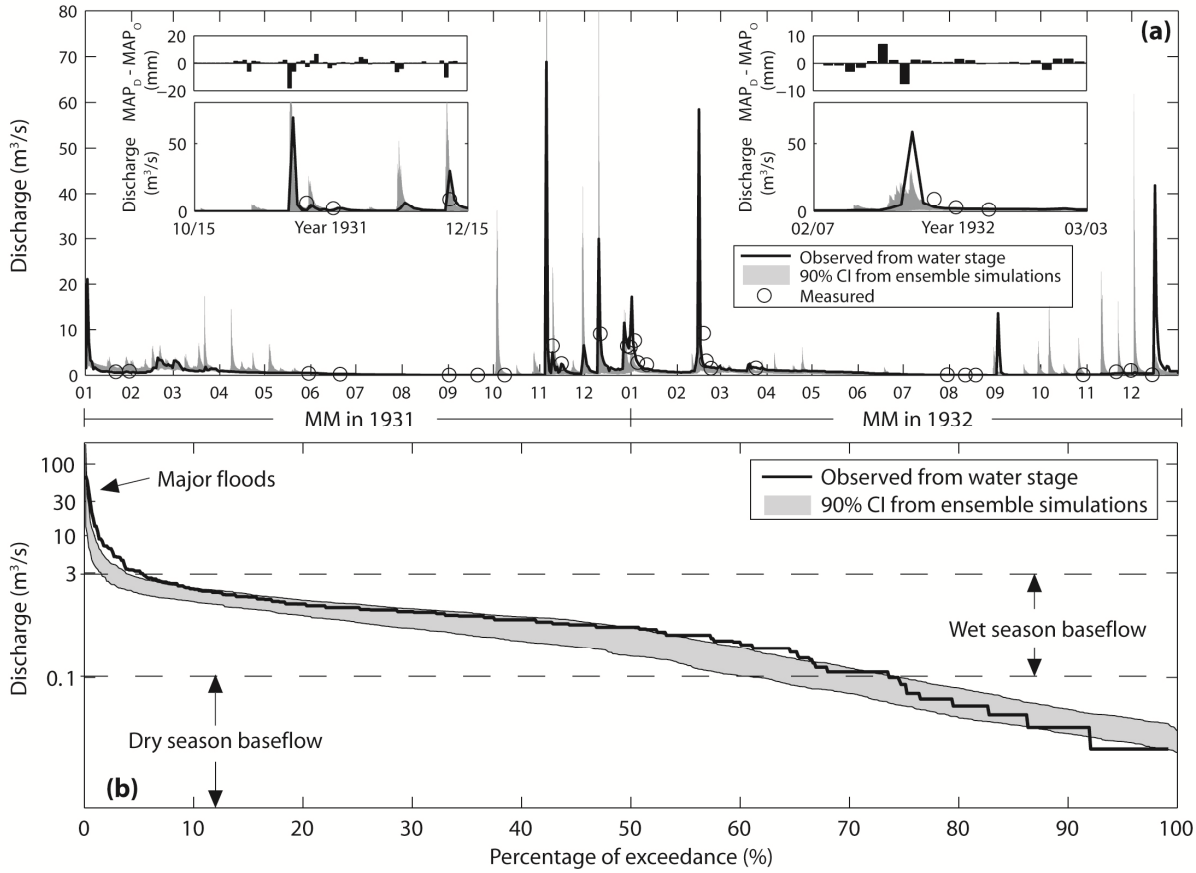

Fig. 2.15 Result of the tRIBS model validation (years 1931-1932). See Fig. 2.14 for a description of the figure content.

2.7 Summary and conclusions

We applied a process-based distributed hydrologic model in the Rio Mannu basin, a medium-size watershed (area of 472.5 km^2) in the Mediterranean island of Sardinia, Italy. In the RMB, precipitation, streamflow and meteorological data were collected in different historical periods and at diverse temporal resolutions. We showed how this sparse hydrometeorological dataset could be used to calibrate two downscaling tools that are able to create high-resolution (hourly) precipitation forcing from daily observations and estimates of the hourly potential evapotranspiration for use in the distributed hydrologic model application.

Despite the presence of several sources of uncertainty in the observations and model parameterization, the use of the downscaled forcing led to good calibration and validation

performances for the tRIBS model over the years from 1930 to 1932 with available daily discharge observations (Mascaro et al., 2013b). To our knowledge, this was the first study where a distributed hydrologic model is applied in the island of Sardinia. Different from most applications based on daily forcing, the methodology proposed here allows conducting hydrologic simulations at high time and space resolutions, thus capturing with higher detail the complex interactions between surface and subsurface processes occurring in Mediterranean watersheds. This methodology will be utilized in the subsequent chapter to disaggregate the outputs of different RCMs and simulate the hydrologic response of the RMB under different climate change scenarios, thus quantifying their local impacts on water resources and the frequency of hydrologic extremes.

3 Hydrologic impacts of climate changes

Future climate projections based on global and regional climate models (GCMs and RCMs) indicate that the Mediterranean basins will most likely suffer a decrease in water availability and an intensification of hydrologic extremes. Process-based distributed hydrologic models (DHMs), like tRIBS, have the potential to simulate the complex hydrologic response of Mediterranean watersheds. Thus, when used in combination with RCMs, DHMs can reduce the uncertainty in the quantification of the local impacts of climate change on water resources. Hence, we used the two downscaling algorithms and the DHM, whose characteristics, set up and calibration were discussed in the previous chapter, to simulate the Rio Mannu basin response to a set of bias-corrected outputs from four RCMs for two simulation extents: a reference (1971 to 2000) and a future (2041 to 2070) period. The time series and spatial maps simulated by the hydrologic model were then post-processed by computing several metrics to quantify the changes on water resource availability and hydrologic extremes in the future climate scenarios as compared to historical conditions.

The chapter is organized as follows. First the four RCMs are introduced together with a brief description of the reasons for their selection. The validation, downscaling and bias correction procedures are also presented. Next, changes in climate signals are evaluated comparing the statistics of the main meteorological forcing, precipitation and temperature, in the two different time slices. Observed data in the reference period are provided as an additional source of comparison. Finally, the results of the hydrologic simulations forced with the climate models and measured data are presented and discussed to assess the impact of climate change in the Rio Mannu watershed.

3.1 Climate data

3.1.1 Climate models description

In this study the climate projections were provided by three Regional Climate Models, RCMs (the Sweden RCA model, the Netherlands RACMO2 Model, the Germany REMO Model), and two General Circulation Models, GCMs (the HadCM3 Model (high sensitivity) and the Germany ECHAM5 / MPI OM), selected within the ENSEMBLES project. Four GCM-RCM combinations of these climate models were selected as the best performing in all the CLIMB study sites (Deidda et al., 2013). For simplicity and graphical advantage, we defined an acronym for each climate model used in this work. The list of climate models, GCM-RCM combination and acronyms is given in Tables 3.1 and 3.2.

Climate model	Climatological center and model	Acronym
GCMs	Hadley Centre for Climate Prediction, Met Office, UK HadCM3 Model (high sensitivity)	H
	Max Planck Institute for Meteorology, Germany ECHAM5 / MPI OM	E
RCMs	Swedish Meteorological and Hydrological Institute (SMHI), Sweden RCA Model	RC
	Max Planck Institute for Meteorology, Hamburg, Germany REMO Model	RE
	Koninklijk Nederlands Meteorologisch Instituut (KNMI), Netherlands RACMO2 Model	RM

Table 3.1 Climatological center and acronyms of the Global Climate Models (GCMs) used as drivers of ENSEMBLES Regional Climate Models (RCMs) considered in this study (first two rows) and acronyms of the RCMs (last three rows).

RCM acronym	RCM	GCM
ERC	RCA Model	ECHAM5 / MPI OM
ERE	REMO Model	ECHAM5 / MPI OM
ERM	RACMO2 Model	ECHAM5 / MPI OM
HRC	RCA Model	HadCM3 Model

Table 3.2 List of the GCMs-RCMs combination acronyms used in this study associated to their GCMs and RCMs (acronyms).

The combinations included two different RCMs nested in the same GCM (the Germany ECHAM5 / MPI OM, E, combination ERE and ERM) and the two different GCMs forcing the same RCM (the Sweden RCA model, RC, combination ERC and HRC), giving also the possibility to explore different sources of uncertainties. Their outputs were mostly available from 1951 to 2100 at daily scale and at the same spatial resolution of 0.22 degrees which corresponds to a grid resolution of approximately 24 km. Future climate predictions were based on greenhouse gas and aerosol concentrations from the A1B emission scenario (Nakićeović et al., 2000), which is considered the most realistic. The A1 scenarios were conceived to represent an integrated world characterized by fast economic growth, maximum population of 9 billion reached in 2050, quick spread of new and efficient technologies, and extensive social and cultural interactions. The A1B scenario, in particular, provided a balanced use of all energy sources. We defined two periods, each 30 years long, for the assessment of climate change within the CLIMB project: a reference time slice from 1971 to 2000 and a future time slice from 2041 to 2070 (respectively, REF and FUT in the following).

3.1.2 RCMs validation, bias correction and downscaling

Climate model data were validated using the same dataset for six catchments of the CLIMB project, the CRU E-OBS dataset from the ENSEMBLES EU-FP6 project, available by the ECA&D project (http://www.ecad.eu) and hosted by the Climate Research Unit (CRU) of the Hadley Centre. E-OBS data included gridded observations of daily precipitation and temperature, which had different advantages. They were based on high-quality historical measurements on a European network, available not only at the same spatial resolution of ENSEMBLES RCMs but even using the same grid of points (rotated grid of 0.22 degrees). The original data had been corrected in order to minimize the influence of local and orographic

effects. The grids had been obtained using kriging interpolation, one of the best linear unbiased estimation methods. More details on the evaluation, selection and validation procedures of climate models within the CLIMB project can be found in Deidda et al. (2013). Climate change predictions at local scale are affected by a large amount of uncertainty which arises from the considered emission scenario, from the use of different GCMs and RCMs (intermodel variability), from the different realizations of the same scenario with a given GCM (internal model variability or natural climate variability) and from the downscaling techniques (Wilby et al., 2000; Prudhomme and Davies, 2009; Todd et al., 2011). The selected set of RCMs allowed to explore the intermodel variability comparing the climate change response of different RCMs nested in a single GCM and the response of the same RCM forced by different GCMs. Even if the set of climate models was quite small, a descriptive evaluation of the uncertainties was possible.

In order to run hydrological models and assess climate change effects at the basin scale, climate models outputs need to be downscaled (Wilby and Wigley, 1997; Bardossy et al., 2011) and bias-corrected. The same downscaling procedures adopted in the calibration-validation period (Mascaro et al., 2013b) and described in the previous chapter were used in this study. They allowed to obtain high resolution precipitation and reference evapotranspiration fields required by the hydrologic model tRIBS. Precipitation grids were downscaled using the Space Time RAINfall (STRAIN) model, the multifractal method described in Deidda (1999 and 2000) and in Badas et al. (2006). This approach allowed disaggregating precipitation both in space and in time (Fig. 2.9 in chapter 2). Starting from areal averages of daily precipitation obtained by averaging rainfall values over a 4x4 matrix of ENSEMBLES grid points centered in the catchment, covering an area of about 100 x 100 km^2, the model was able to create hourly

precipitation fields at the spatial resolution of about 1 km^2 (Fig. 3.1 from Deliverable 4.3 of CLIMB project).

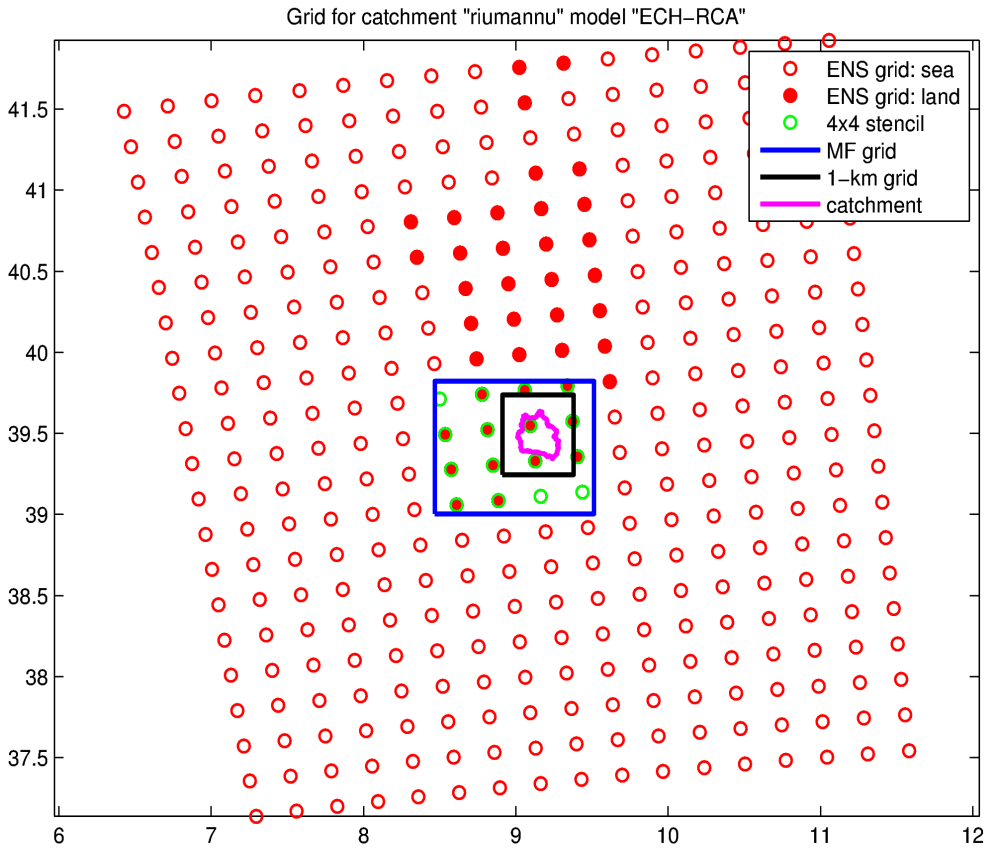

Fig. 3.1 Rio Mannu river basin, RMB, area and downscaling structure. In the map, the dots represent the grid points of the original ENSEMBLES 25 km x 25 km grid. Red dots (land) trace clearly the shape of Sardinia (and of the southernmost tip of Corsica), while white dots indicate the sea grid-points of the surrounding Mediterranean. The purple line includes the catchment area. The black line includes the area selected for 1 km x1 km downscaling. The blue line includes the 4x4 stencil points, that are surrounded by a green circle. (kindly provided by CLIMB Deliverable 4.3).

Hourly reference evapotranspiration values were obtained through its specific downscaling strategy (section 2.5.2 in previous chapter) starting from daily minimum and maximum temperatures grids. The procedure was calibrated using high resolution meteorological data, the Penman - Monteith and the Hargreaves formulas (Mascaro et al., 2013b). In the case of RCMs grids, temperature fields were previously downscaled in space following the approach of Liston and Elder (2006) which considers a spatial interpolation scheme (Barnes, 1964, 1973) and orographic corrections. Bias correction is usually necessary to adjust seasonal statistics of

climate model outputs. This was achieved by correcting the seasonal probability distribution functions using the daily translation method, which was shown to be skilful in many hydrologic impact studies (Wood et al., 2004; Maurer and Hildago, 2008). Having the same number of data, scatter plots of E-OBS and climate models simulated values were used as transfer function to correct the model value according to the corresponding observed value. The procedure assured the coincidence of the moments of the probability distribution function of the corrected modeled data with those of measured ones.

A systematic underestimation of monthly precipitation was noticed comparing climate models corrected outputs with available local observed data. Hence, it appeared necessary to further adjust precipitation fields to take into account local climatology which was not quite well represented even using the E-OBS dataset as validation counterpart. Mean areal precipitation (MAP) values in the RMB were computed based on daily data measured by rain gages in the period 1951-2008. The mean monthly MAP values were compared with those obtained in the period 1951-2010 using the 4 RCMs precipitation grids (Table 3.3). The monthly ratios between observed MAP and the mean of the climate models were used as correction multipliers.

Model	Jan	Feb	Mar	Apr	May	Jun	Jul	Aug	Sep	Oct	Nov	Dec
ERC	45.34	45.15	34.77	43.74	24.48	13.76	3.05	6.78	44.87	51.83	66.54	53.92
ERE	45.24	40.21	35.64	43.31	23.17	12.57	2.91	6.04	41.09	53.82	72.56	58.02
ERM	44.20	46.44	33.08	40.22	26.80	14.58	2.54	5.43	34.25	52.37	63.35	52.70
HRC	43.95	51.21	34.79	44.68	26.85	9.82	3.19	6.12	33.15	56.92	71.51	59.82
RCM mean	44.68	45.75	34.57	42.99	25.33	12.68	2.92	6.09	38.34	53.74	68.49	56.11
Observed	58.85	63.90	57.13	52.56	37.42	16.35	6.93	12.65	41.75	62.91	81.08	83.04
Ratio	1.32	1.40	1.65	1.22	1.48	1.29	2.38	2.08	1.09	1.17	1.18	1.48

Table 3.3 Monthly Mean Areal Precipitation (MAP) in the RMB in the period 1951-2010 (mm) simulated by the four RCMs; average of the four RCMs (RCM mean); observed by rain gages in the period 1951-2008 (mm); and ratio between RCM mean and the observation.

3.1.3 Climate change anomalies

Climate change signals were evaluated comparing mean annual and monthly values of the main meteorological forcing, precipitation and temperature, during the two periods. In the reference time slice measured data at daily resolution were available from several rain gages and from one thermometric station near the Rio Mannu watershed. We took advantage solely of observed rainfall data as a further source of comparison due to the higher uncertainty of this variable in RCMs as compared with temperature. In order to obtain hourly precipitation grids which could be next used to force the DHM, we considered 152 rain stations in the same large domain as in the calibration and application of the STRAIN model (grid with L = 104 km in Chapter 2, Fig. 2.3) and we run again the multifractal tool for the period 1971-2000. Only one of the possible disaggregated series had been considered for the computational effort required by successive hydrologic simulations. Based on RCMs and observed rainfall grids, mean areal precipitation, MAP, values in the RMB were computed and used for the parallel analysis. Figures 3.2 and 3.3 present annual and monthly results for precipitation while figures 3.4 and 3.5 refer to temperature.

All RCMs agreed on the prediction of a decreased annual precipitation amount in the FUT period ranging from 12% to 21% (HRC) (Fig.3.2). The dashed line in Fig. 3.2 represents observed mean annual MAP in the REF period. Observed MAP resulted slightly smaller than RCMs mean probably due to the different set of measured data used to correct RCMs (Table 3.3) and to the application of the downscaling tool which redistributed in stochastic fashion the daily rainfall volumes from the large domain (Mascaro et al., 2013b). Climate models were instead corrected considering daily precipitation values of stations within or quite close to the basin in the period 1951-2008.

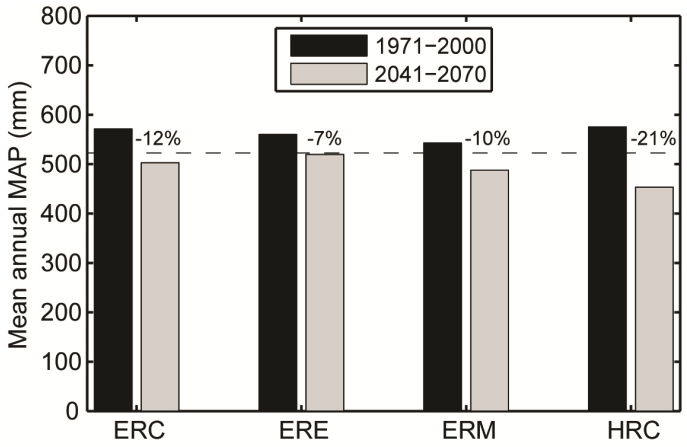

Fig. 3.2 Mean annual MAP in the RMB predicted by the RCMs in REF (black bars) and FUT (gray bars) periods; horizontal dashed line represents mean annual MAP observed by 152 rain gauges (downscaled from the coarse grid in Fig. 2.3) in REF period.

On a monthly basis the sign of variation depended on months and models (Fig. 3.3, panels (a) and (b)). In October, February and June only one model reversed the tendency of reduction predicting an increase, in December and January, instead, monthly precipitation increased according to three models (significantly for ERM in December and for HRC in January, more than 20%). A marked decrease had to be expected in April and May according to all the models. Hence, MAP was predicted to slightly increase in winter months and decrease in the other seasons. If we look at the mean monthly number of rainy days (defined as days during which MAP > 1 mm/d), presented in panels (c) and (d) of Fig. 3.3, we can note that all the RCMs agreed on a fall in all months in the FUT period except for the months of January and February (no significant change) and of July and August for HRC model (increase). The mean rain intensity in rainy days (Fig. 3.3 panels (e) and (f)) showed a less consistent trend in change. There were eight months (October, November, winter months, April, June and July) during which at least one RCM predicted a raise in rain intensity. This means that the probability of strong events was expected to enhance (increased precipitation amounts in less days), especially

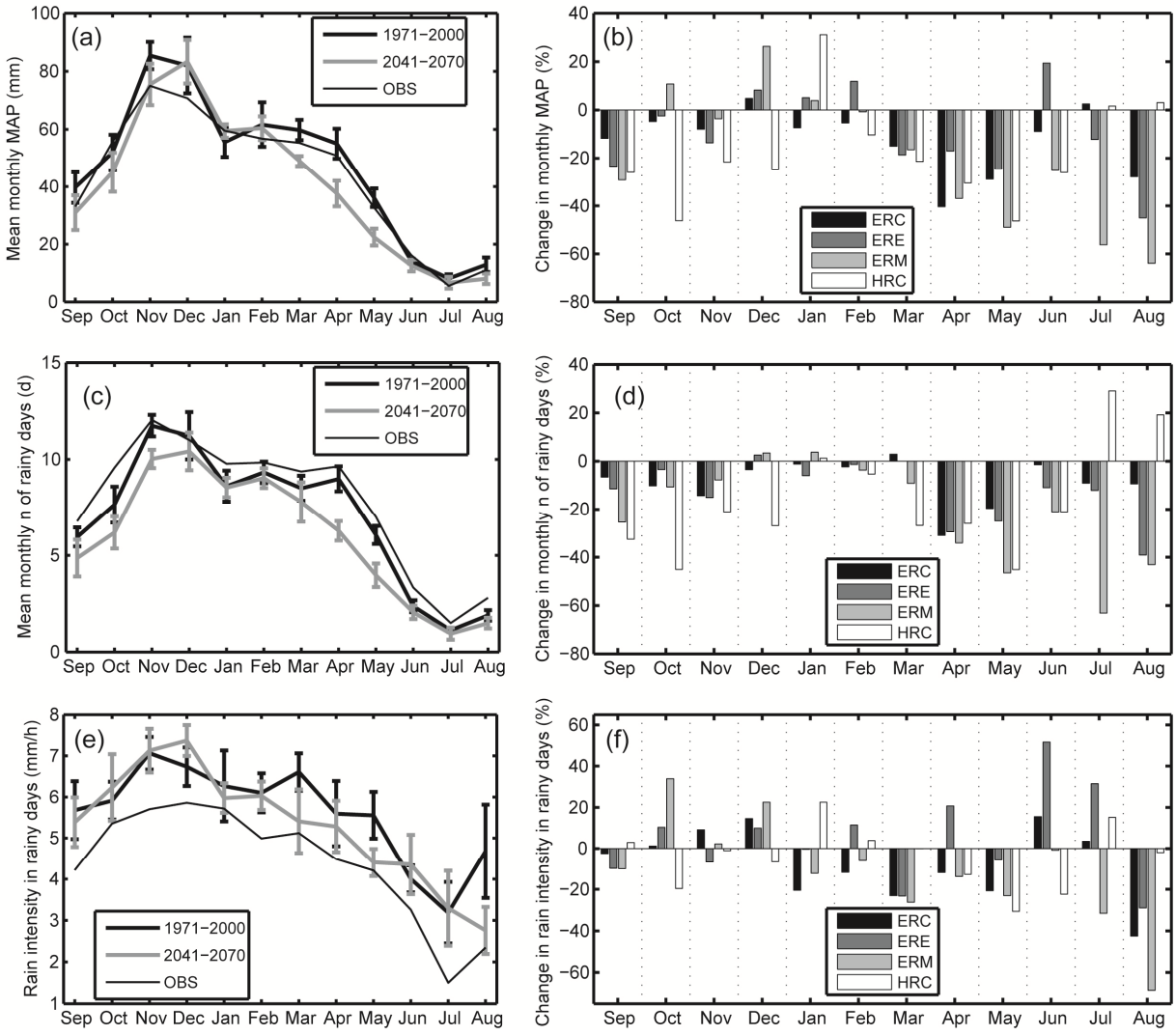

Fig. 3.3 (a) Mean monthly MAP in the RMB plotted as mean ± standard deviation of the RCMs in the REF (black line) and FUT (gray line) periods; thin black line (without standard deviation) represents mean monthly MAP observed by152 rain gauges.(b) Relative change in mean monthly MAP between FUT and REF period. (c) Same as (a), but for the number of rainy days in each month (MAP>1 mm/d). (d) Same as (b), but for the number of rainy days in each month. (e) Same as (a), but for the rain intensity in rainy days in each month. (f) Same as (b), but for the rain intensity in rainy days in each month.

in October, April, June and July. Panels (a), (c) and (e) of Fig. 3.3 allow also to compare RCMs means with observed MAP (thin black line) statistics in the REF period. Simulated mean monthly MAP is higher than observed one in some months (Fig. 3.3a). The number of rainy days tended to be slightly underestimated by RCMs (Fig. 3.3c) and, as a consequence, the rain intensity in rainy days presented larger values (Fig. 3.3e).

Temperature trends displayed less uncertainty than precipitation. All RCMs, in fact, predicted increased mean annual values (Fig. 3.4) in FUT period varying from 1.9°C to 3°C according to the HRC model. Also the monthly comparison was consistent among the 4 RCMs (Fig. 3.5) with positive changes in FUT period in all the seasons, ranging from about 7% (ERE June) to 30% (HRC March). The results presented in this thesis allowed to observe that in this study case the uncertainty due to the driving GCM (ERC and HRC combinations) is bigger than the variation caused by the two different RCMs nested in the same GCM (ERE and ERM).

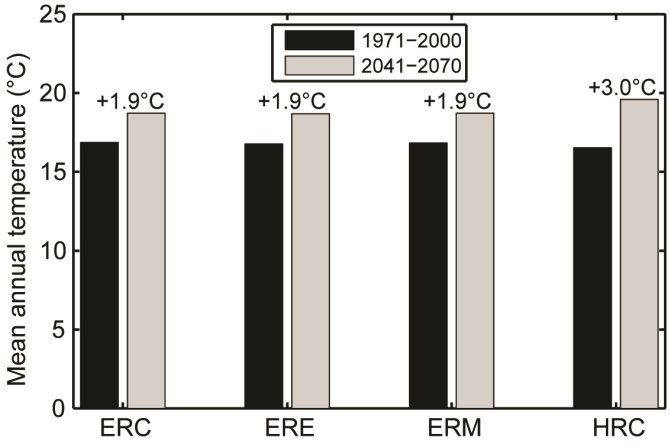

Fig. 3.4 Mean annual temperature in the RMB predicted by the RCMs in the REF (black bars) and FUT (gray bars) periods.

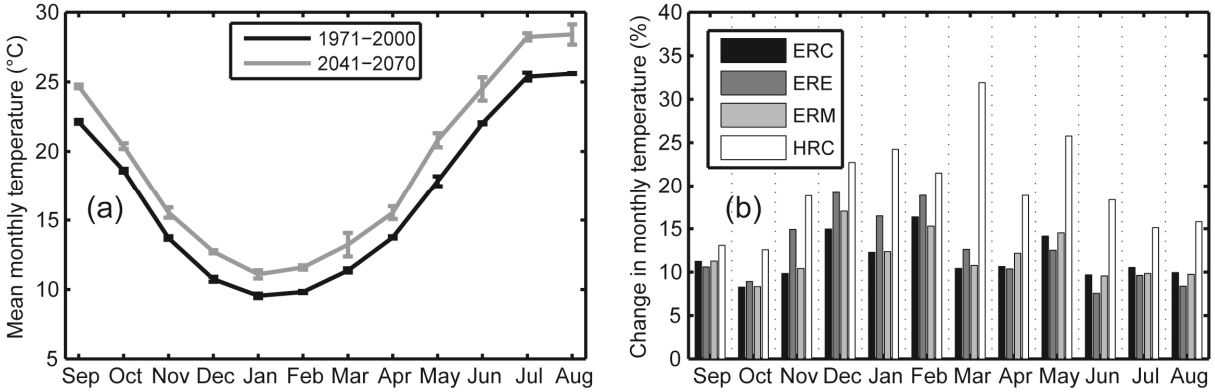

Fig. 3.5 (a) Mean monthly temperature in the RMB plotted as mean ± standard deviation of the RCMs in the REF (black line) and FUT (gray line) periods. (b) Relative change in mean monthly temperature between FUT and REF period.

3.1.4 MAP statistical properties

As further analysis, we investigated two statistical properties of precipitation, always computed as MAP in the RMB. First, we applied the Multiple Threshold Method General Pareto Distribution, MTM-GPD (Deidda, 2010) to daily MAP values predicted by the 4 RCMs and observed by rain gages (OBS). The GPD was proposed as a suitable threshold-invariant three-parameter distribution function to reliably describe the exceedances of daily rainfall records with the property of reflecting the local climate signature. Looking at the MTM-GPD parameters, reported in table 3.4 for REF and FUT periods, different aspects could be observed. In the reference period HRC model had the highest probability of extreme rainfall events (ξ) and ERE the lowest while in future period that probability was predicted to be quite similar among the climate models. The scale parameters (α) which give information on the mean were not so different among the RCMs but bigger than OBS one and the mean tended to decrease in the future except for HRC ensemble member. On the contrary, the probability of rainfall (ζ) for this latter model was scheduled to halve, meaning less events but more intense. Figures 3.6 - 3.9, panel (d), show the empirical survival functions (continuous lines) and the MTM-GPD fit (dashed lines) in REF (black) and FUT (grey) periods for each RCM compared with the case of observed daily MAPs. We can note how the fitting could reliably capture the highest records even if the maximum thresholds were low (maximum 14.5 mm). Panels (a) and (b) of the same figures report some steps of the procedure to compute the MTM-GPD parameters in REF and FUT periods, respectively; panels (c) is the same in each figure referring to OBS analyses.

RCM	ξ^M REF	ξ^M FUT	α^M REF	α^M FUT	ζ^M REF	ζ^M FUT
ERC	0.195	0.185	5.433	5.017	0.221	0.219
ERE	0.105	0.206	5.192	4.354	0.240	0.251
ERM	0.204	0.226	4.758	4.942	0.242	0.203
HRC	0.228	0.213	4.945	6.679	0.222	0.116
OBS	0.209	-	3.651	-	0.287	-

Table 3.4 Parameters of the MTM-GPD fit to daily MAP values in the RMB in REF and FUT periods and with OBS data.

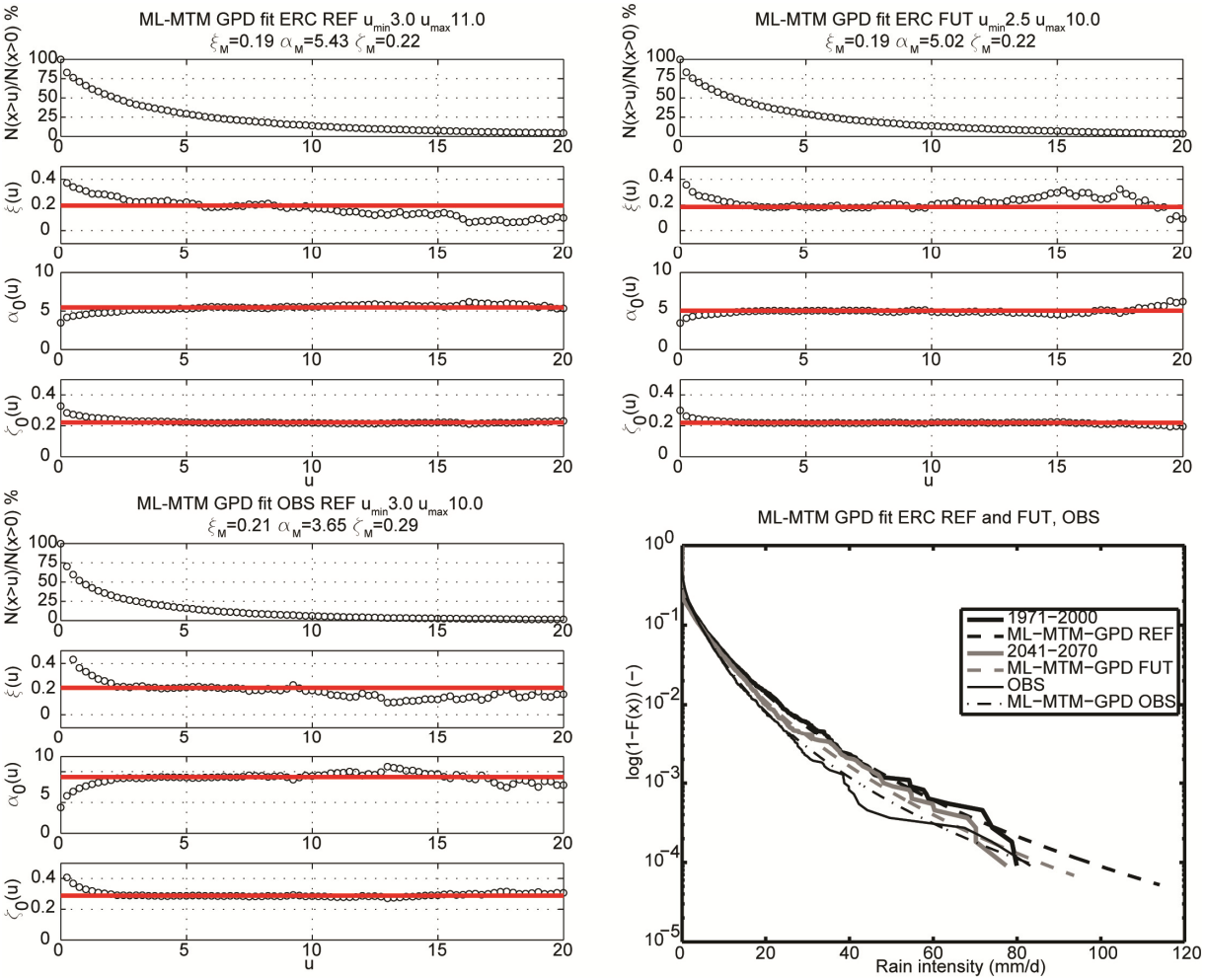

Fig. 3.6 (a) MTM application on daily MAP values predicted by ERC in REF period. First plot shows the size of the records exceeding the thresholds u. The second plot displays the ξ estimates as the theshold u range from 0 to 20 mm: the ξ_M MTM estimate is the median value (horizontal line) within the range of selected thresholds. Similarly, the third and fourth plots display the unconditioned α_0 and ζ_0 estimates provided as a function of u. (b) and (c) shows the same plots as (a) but for MAP values predicted by ERC in FUT period and for OBS MAP. (d) Empirical survival functions (continuous lines) and MTM-GPD fit (dashed lines) of ERC MAP in REF (black) and FUT (grey) periods and for OBS (thin black) MAP.

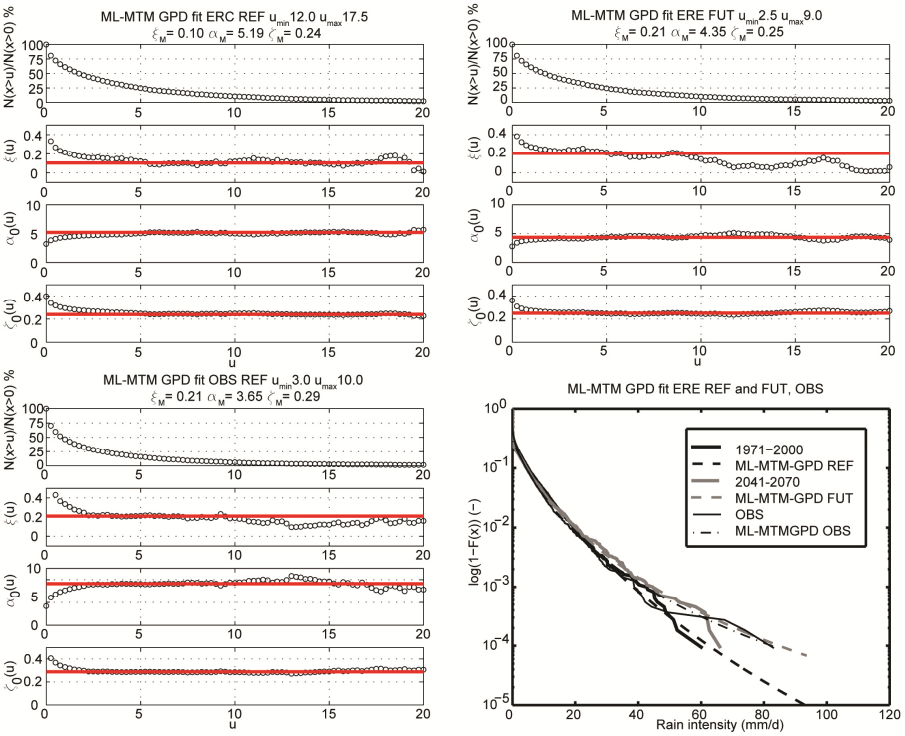

Fig. 3.7 Same as Fig. 3.6 for ERE model.

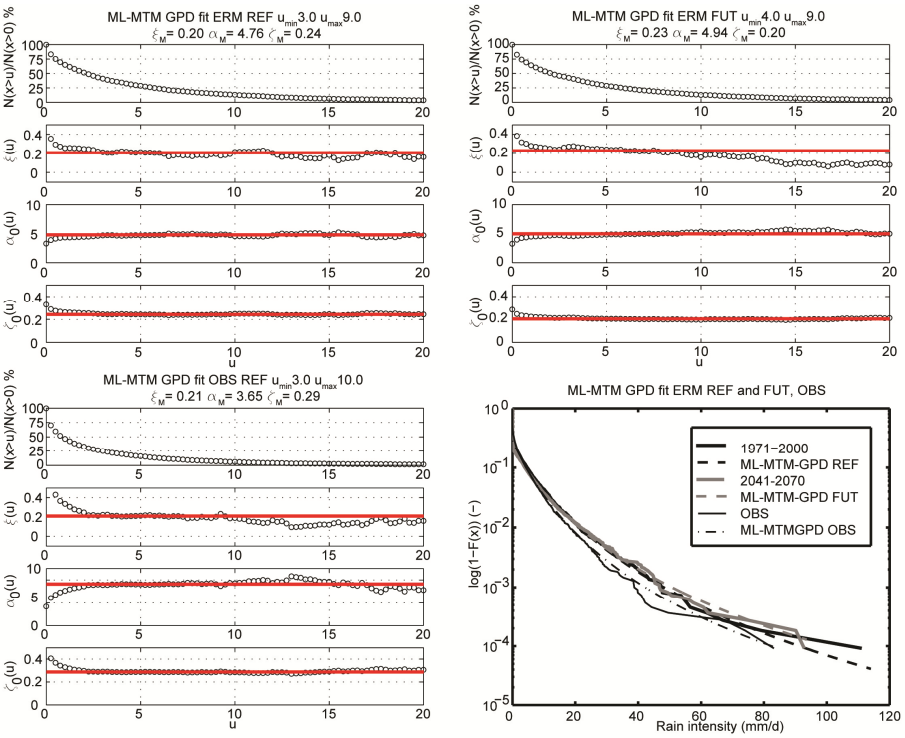

Fig. 3.8 Same as Fig. 3.6 but for ERM model.

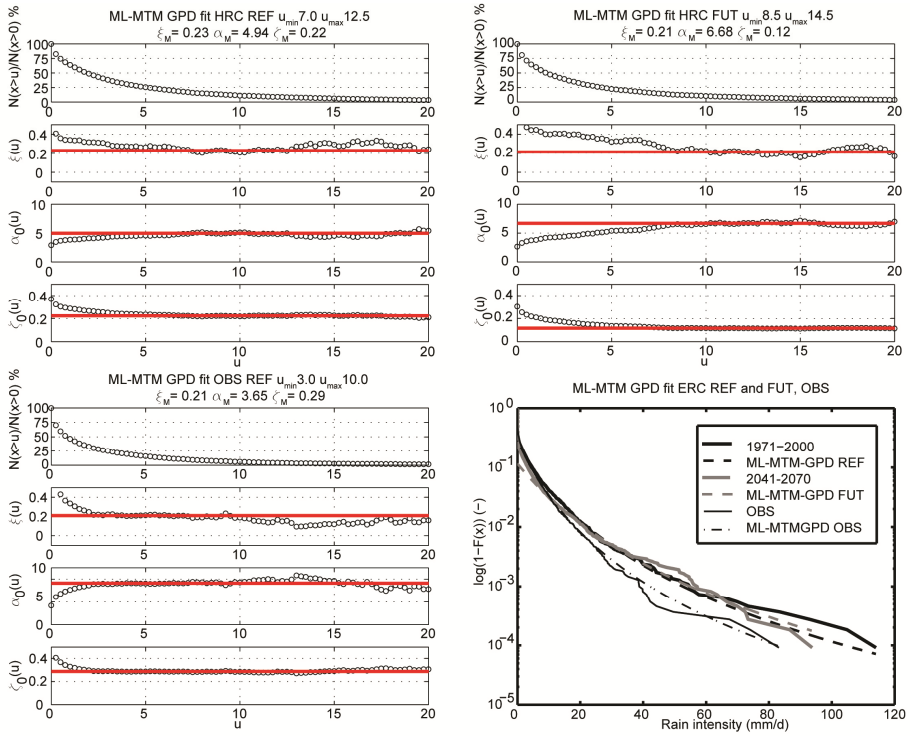

Fig. 3.9 Same as Fig. 3.6 but for HRC model.

The second statistical investigation regarded the annual maximum daily MAP values using the generalized extreme value (GEV) distribution, the expected distribution of the maxima within blocks of one year. Table 3.5 reports the GEV parameters for reference and future period while Fig. 3.10 shows the sorted values with the corresponding GEV fit using the maximum likelihood estimates. In the figure the values of each climate model in the REF period were compared with the observed ones and with the future. The measured annual maximum MAP values presented the highest shape parameter *k* indicating a major tendency towards a Fréchet distribution (bounded on the left and presenting a right tail). RCMs distributions instead could be classified as Gumbel ones (unbounded on the left and on the right). The ERM ensemble member displayed the most similar behavior comparing FUT and REF shapes and parameters. These statistical analyses put on evidence that (i) climate models precipitation were not consistent with each other; (ii) there was no coherence even between REF and FUT periods of the same model,

and (iii) RCMs rainfall was different from observed one not only in predicted values but also in the type of distribution.

	κ		σ		μ	
RCM	REF	FUT	REF	FUT	REF	FUT
ERC	0.007	-0.019	13.063	12.294	38.982	36.067
ERE	0.012	-0.082	7.717	9.912	31.566	34.721
ERM	0.06	0.032	12.613	13.253	35.432	36.095
HRC	0.191	0.008	11.775	16.251	34.259	36.104
OBS	0.331		8.443		27.002	

Table 3.5 Parameters of GEV fit with ML method to maximum annual daily MAP values for each RCM in REF and FUT period and OBS data.

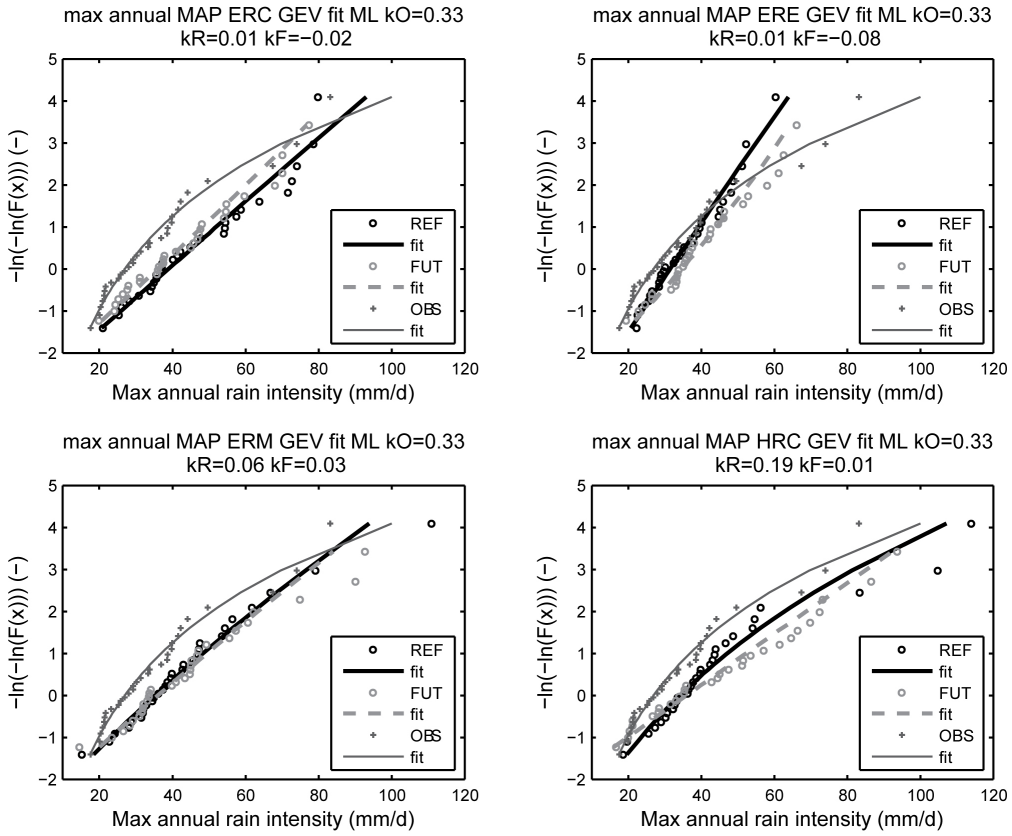

Fig. 3.10 Maximum annual MAP values predicted by the 4 RCMs (1 panel for each RCM) in REF (black circles) and FUT (grey circles) period and GEV fit with maximum likelihhod, ML, method (black line for REF, dashed grey line for FUT). Each panel shows also OBS MAP values (plus) and GEV fit (thin black line).

Similar results were obtained estimating GEV parameters with the method of the probability weighted moments, PWM. Parameters are reported in table 3.6 while Fig. 3.11 shows max annual MAP values and fits as with the ML method.

	κ		σ		μ	
RCM	REF	FUT	REF	FUT	REF	FUT
ERC	0.009	-0.024	13.852	13.165	38.610	35.756
ERE	-0.019	-0.014	8.550	9.998	31.387	34.125
ERM	0.152	0.113	11.801	12.673	34.621	35.298
HRC	0.280	-0.016	10.891	17.474	33.524	35.928
OBS	0.211		9.495		27.241	

Table 3.6 Parameters of GEV fit with PWM method to maximum annual daily MAP values for each RCM in REF and FUT period and OBS data.

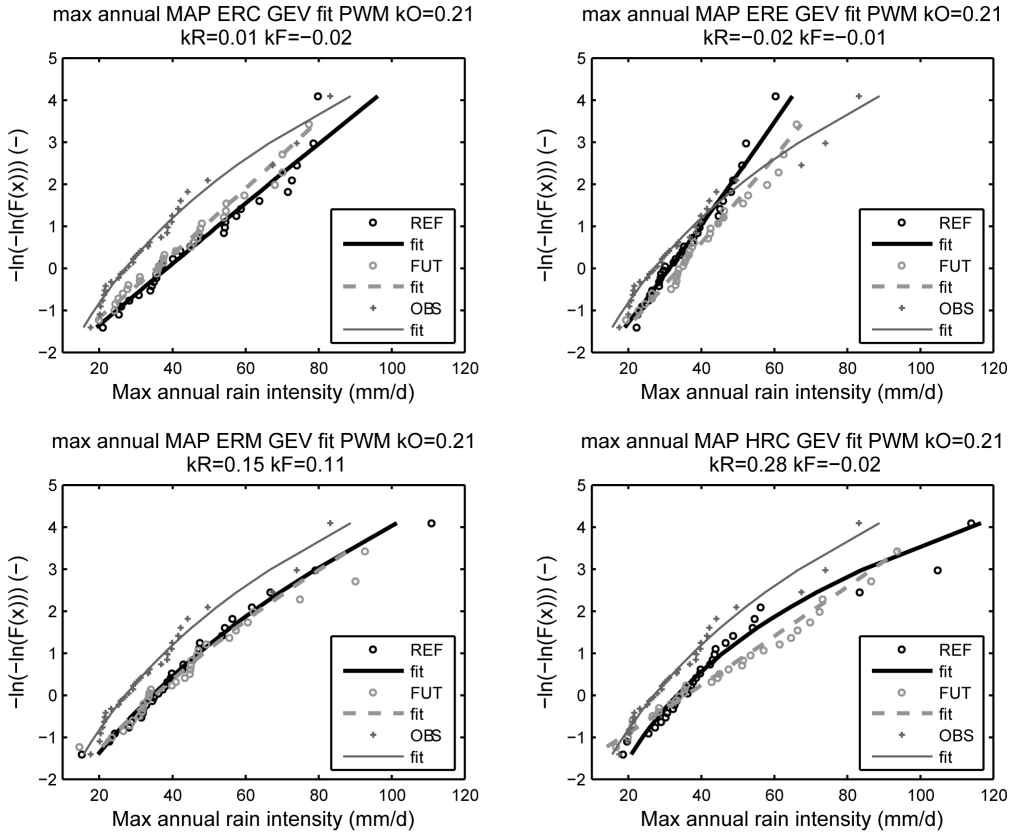

Fig. 3.11 Maximum annual MAP values predicted by the 4 RCMs (1 panel for each RCM) in REF (black circles) and FUT (grey circles) period and GEV fit with probability weighted moments, PWM, method (black line for REF, dashed grey line for FUT). Each panel shows also OBS MAP values (plus) and GEV fit (thin black line).

3.2 Impacts of climate change on hydrologic response

The tRIBS hydrologic model, set up and calibrated as discussed in the previous chapter, was forced with the outputs of the four RCMs to evaluate the effects of climate changes in the Rio Mannu basin. Meteorological input data were prepared adopting the same downscaling strategies for precipitation and reference evapotranspiration, as in the calibration validation period (section 2.5). To reduce computational time we re-aggregated the available precipitation and temperature grids (1 km resolution) to 5 km resolution (Fig. 3.12). Reference evapotranspiration values were obtained again starting from daily minimum and maximum temperatures and applying the specific downscaling procedure described in section 2.5.2. The DHM was run using the parallelized version (Vivoni et al., 2011) in a super computer (the Saguaro Cluster in Arizona State University) for the reference period (1971-2000) and the future period (2041-2070). In both cases simulations started two years before the beginning of the time slice in order to have a spin-up period to reach equilibrium conditions, as in the calibration-validation case (Mascaro et al., 2013b, chapter 2.6.2) and in Vivoni et al. (2005). A total of 256 years of simulations were performed (32 years x 2 periods x 4 RCMs forcing) with an additional simulation in REF period using observed meteorological data. Several hydro-climatic indexes were computed elaborating tRIBS time series and spatial maps in order to evaluate the RMB hydrologic response (river discharge, evaporation losses, soil water storage and groundwater recharge) to temperature and precipitation changes predicted by the 4 RCMs, previously described.

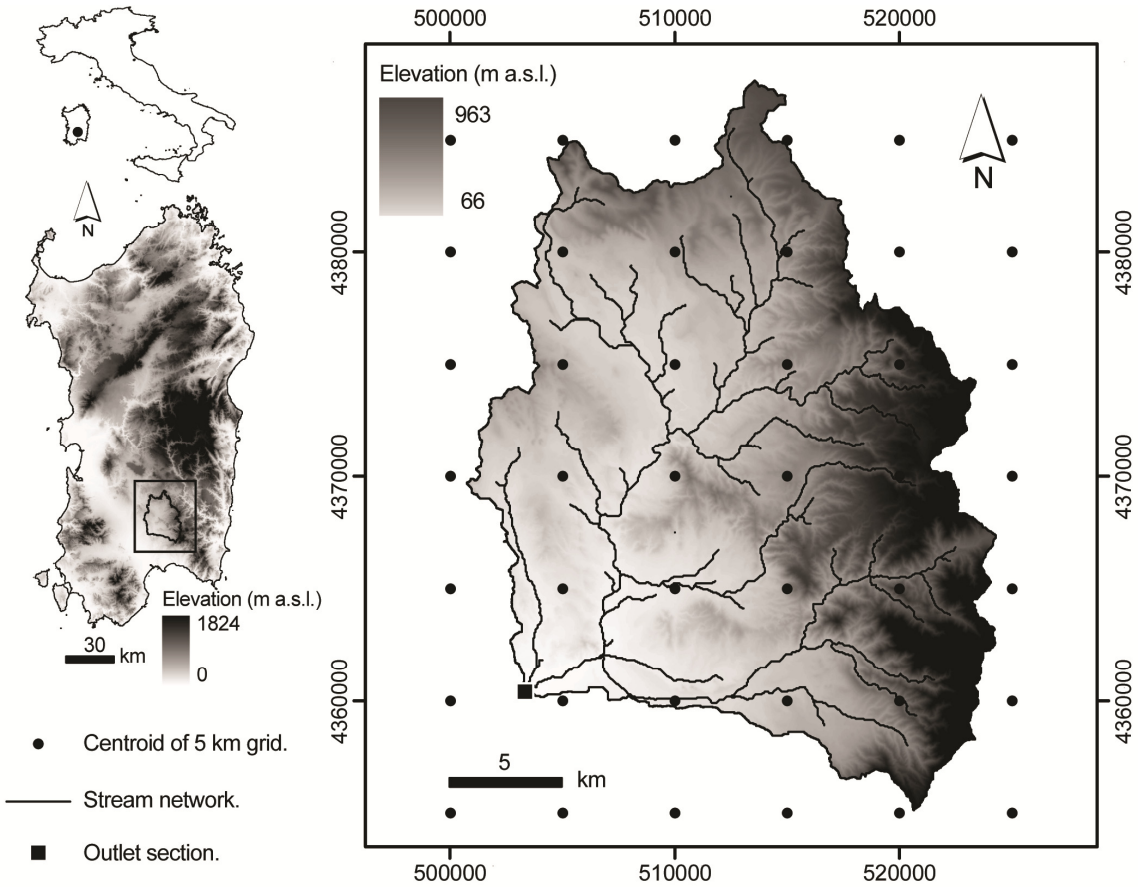

Fig. 3.12 Position of centroids of the downscaled RCMs grids at 5 km (dots) and position of the outlet section (square) in the Rio Mannu Basin.

3.2.1 River discharge

The hydrologic response in terms of streamflow was evaluated at the outlet section of RMB (square in Fig. 3.12). Fig. 3.13a shows the mean annual discharge simulated by tRIBS model forced with the 4 climate models in REF and FUT periods. All the simulations predicted a decrease in the future ranging from 17% (ERE) to 50% (HRC). This reduction confirmed what could be expected from precipitation and temperature annual anomalies (reduction and increase, respectively). While precipitation lowering and temperature rise predictions were quite similar according to the models ERC, ERE and ERM, models driven by the same GCM, the annual discharge loss in FUT period presented major differences showing the non linearity of the basin response. The simulation forced with observed meteorological data (OBS) presented a mean

annual streamflow slightly lower than that of RCMs simulations in agreement with the lesser mean annual MAP (dashed lines in Fig. 3.13a and 3.2, respectively). Seasonal behavior (Fig. 3.13b) was consistent in each simulation providing decreased monthly runoff with the exception of ERM in December and ERE in June even if MAP was expected to slightly increase during winter months (Fig. 3.3b). The simulation forced with HRC respected the expectation with the highest reduction values in all months.

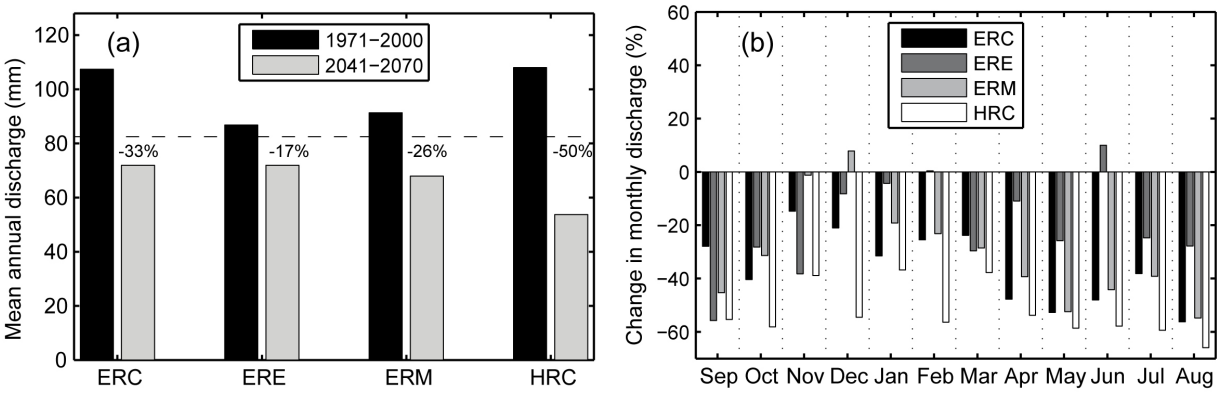

Fig. 3.13 (a) Mean annual discharge in the RMB simulated by tRIBS model forced with the 4 RCMs in REF (black bars) and FUT (gray bars) periods; horizontal dashed line represents mean annual discharge simulated using observed meteorological data in REF period (simulation OBS). (b) Relative change in mean monthly discharge between FUT and REF period.

The flow duration curves (FDCs) were computed based on daily discharge values and the relative results are displayed in Fig. 3.14. The FDCs (panel (a)) in REF period (all RCMs and OBS simulations) confirmed the typical streamflow regime of the basin characterized by low flows (less than 1 m^3/s) for the main part of the year (Mascaro et al., 2013b). The OBS FDC presented lower medium and high flow values with respect to RCMs curves due to lower precipitation amount. In the FUT period a downward shift in the FDCs was projected, implying a nearly uniform streamflow reduction over the entire range of exceedance probabilities. Again, the HRC predicted the largest deviation from the corresponding REF simulation with a significant reduction of water discharge in all the flow regimes.

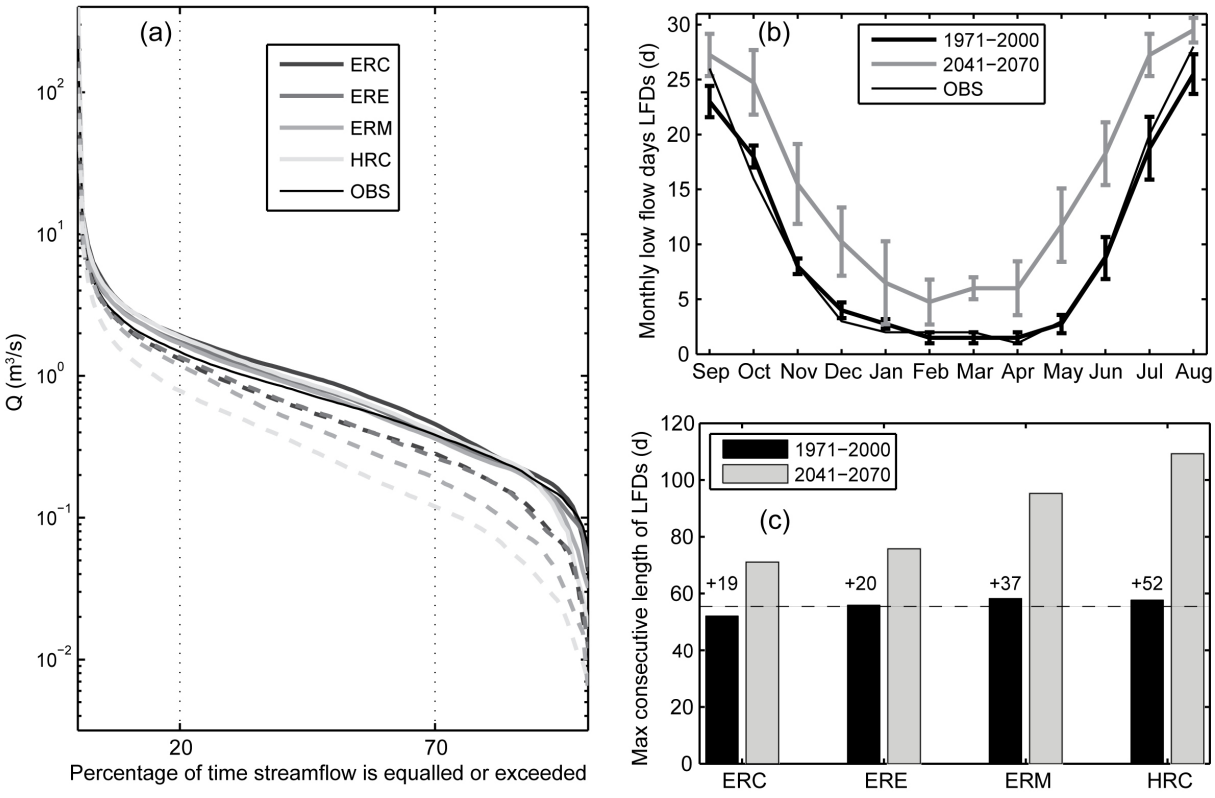

Fig. 3.14 (a) FDCs at RMB outlet section simulated by tRIBS model forced with the 4 RCMS in REF (continuous lines) and FUT (dashed lines) periods; thin continous line represents the FDC in simulation OBS. The vertical dot lines divide the curves into three portions corresponding to different flow magnitudes: high flows (0%–20%), medium flows (20%–70%), and low flows (70%–100%). The streamflows are plotted on a log scale which emphasizes differences in low flows. (b) Mean monthly low flow days (LFDs) plotted as mean ± standard deviation of the RCMs in the REF (black line) and FUT (gray line) periods; thin black line refers to simulation OBS. (c) Mean of annual maximum consecutive length of LFDs in REF (black bars) and FUT (gray bars) periods; thin dashed line represents results of simulation OBS.

The configurations ERC and ERE presented the lowest shift and a quite similar trend, as confirmed also by the mean annual discharge value (about 72 mm). Based on FDCs, we computed the mean monthly number of low flow days and the maximum consecutive length of low flow days during each hydrologic year (from September to August). Low flow days were defined as days during which the streamflow was lower than the averaged value of the 4 simulation in REF period corresponding to a 70% probability of exceedance (right vertical line in Fig. 3.14a). The monthly low flow days (Fig. 3.14b) were consistently expected to grow in each month. The OBS trend is quite similar to that of RCMs driven simulations except over August and September. Also the mean maximum consecutive length of low flow days in hydrologic

years, reported in Fig. 3.14c, tended to assume higher values in FUT period, especially according to HRC ensemble member (the mean consecutive length switched from 58 to 110 days, more than three months). These results depicted a basin with more days with almost no water in natural channels.

Further effects of climate change, in particular of precipitation trends, can be detected in the physical mechanism that governs runoff generation. Fig. 3.15a shows the percentages of the different runoff components in the reference period as simulated with RCMs and OBS data as forcing. In all simulations the main contribute was given by groundwater exfiltration (GE) ranging from 55% (HRC) to 61% (ERE) followed by saturation excess (SE) in RCMs driven simulations (about 22%) and by infiltration excess (IE) in OBS simulation (about 24%). Grouping the four mechanisms of runoff generation computed by tRIBS model in surface runoff (infiltration excess and saturation excess, IE + SE) and subsurface runoff (perched return flow and groundwater exfiltration, PR + GE), it could be seen that their occurrence was quite similar among the ensemble members. Future projected changes in precipitation (decreased precipitation amounts with a minor number of rainy days) created variations in the components, as reported in Fig. 3.15b. All RCMs simulations predicted an increased occurrence of infiltration excess (from 16% by ERM to 110% by HRC), a slight rise of perched return flow (from 4% by HRC to 20% by ERM) and a decrease in saturation excess (from -13% by ERE to -41% by HRC). Simulations ERE, ERM and HRC displayed also a decrease in groundwater exfiltration varying from -4% to -18%. Considering runoff subdivision in two main components, the HRC simulation was the only one which presented appreciable differences: the 10% decrease in subsurface runoff was compensated by the same raise in surface runoff. This variation was reduced to 4% in ERM simulation and 1% in the other two ensemble simulations.

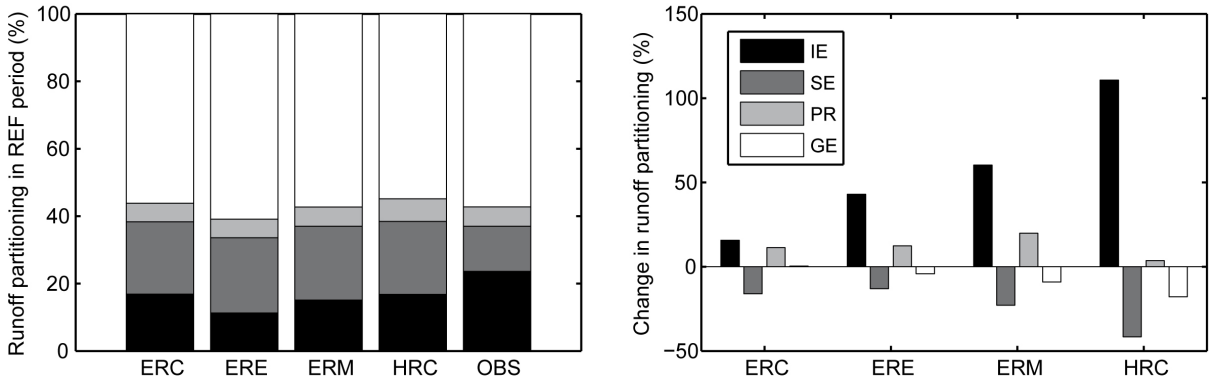

Fig. 3.15 (a) Runoff partitioning in the REF period predicted by RCMs simulations and OBS simulation: infiltration excess (IE), saturation excess (SE), perched return flow (PR), and groundwater exfiltration (GE) runoff components. (b) Relative change in runoff partitioning between FUT and REF period.

We investigated also the changes month by month computing the percentage of each component in the two periods and considering the difference (FUT - REF). Fig. 3.16 shows the plots for each RCM simulation: the IE and GE mechanisms presented the monthly highest degree of variability with positive and negative values compensating each other.

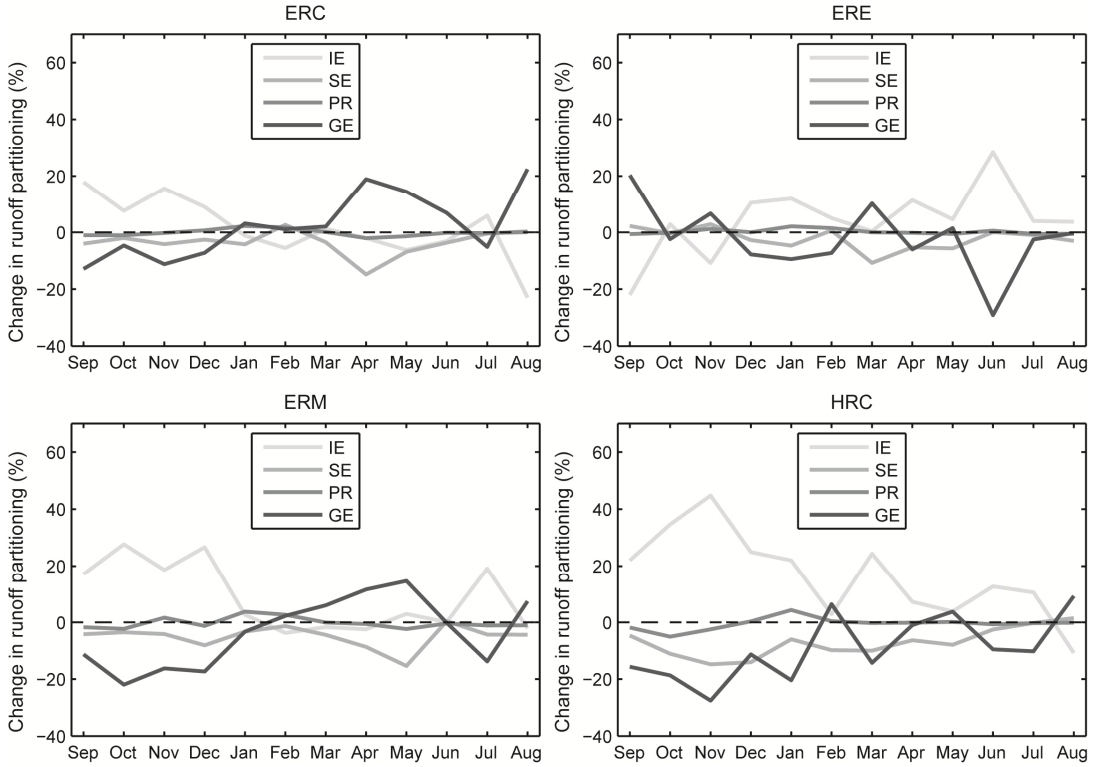

Fig. 3.16 Change in the percentages of monthly runoff partitioning (FUT - REF). Each panel refers to a RCM.

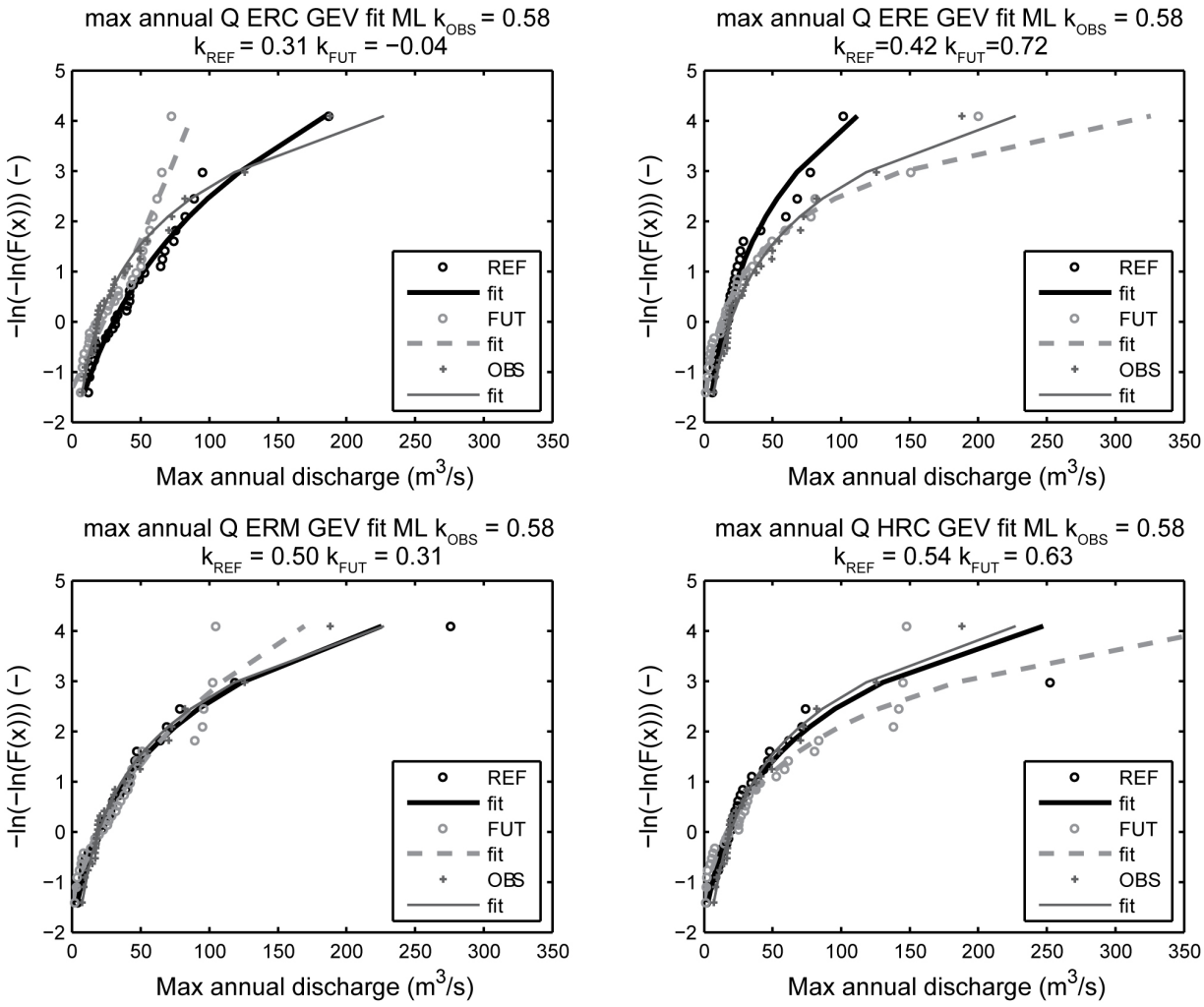

Fig. 3.17 GEV Maximum annual discharge values predicted by the simulations forced with the 4 RCMs (1 panel for each RCM) in REF (black circles) and FUT (grey circles) period and GEV fit with maximum likelihhod, ML, method (black line for REF, dashed grey line for FUT). Each panel shows also OBS maximum annual discharge values (plus) and GEV fit (thin black line).

We repeated the generalized extreme value (GEV) analyses to maximum annual daily discharge values, expressed in m^3/s. The results using the maximum likelyhood estimation method are shown in Fig. 3.17. The predicted changes in future precipitation (Fig. 3.10) were amplyfied considering annual discharge peaks.

3.2.2 Evaporation losses and soil water content

Hourly grids of potential evapotranspiration, ET_0, were used to force the hydrologic model tRIBS. They were computed starting from daily temperature grids provided by the 4 RCMs and applying the same downscaling procedure as in the calibration - validation period (Mascaro et al., 2013b, section 2.5.2). The mean potential evapotranspiration averaged on RMB (Fig. 3.18a) was projected to slightly increase in FUT period due to higher temperatures. As in the case of temperature, the differences in mean monthly values among the 4 RCMs were smoothed (small standard deviation bars in Fig. 3.5a and 3.18a). The apparent temperature rice, however, was slightly softened in potential evapotranspiration where the future change was lower.

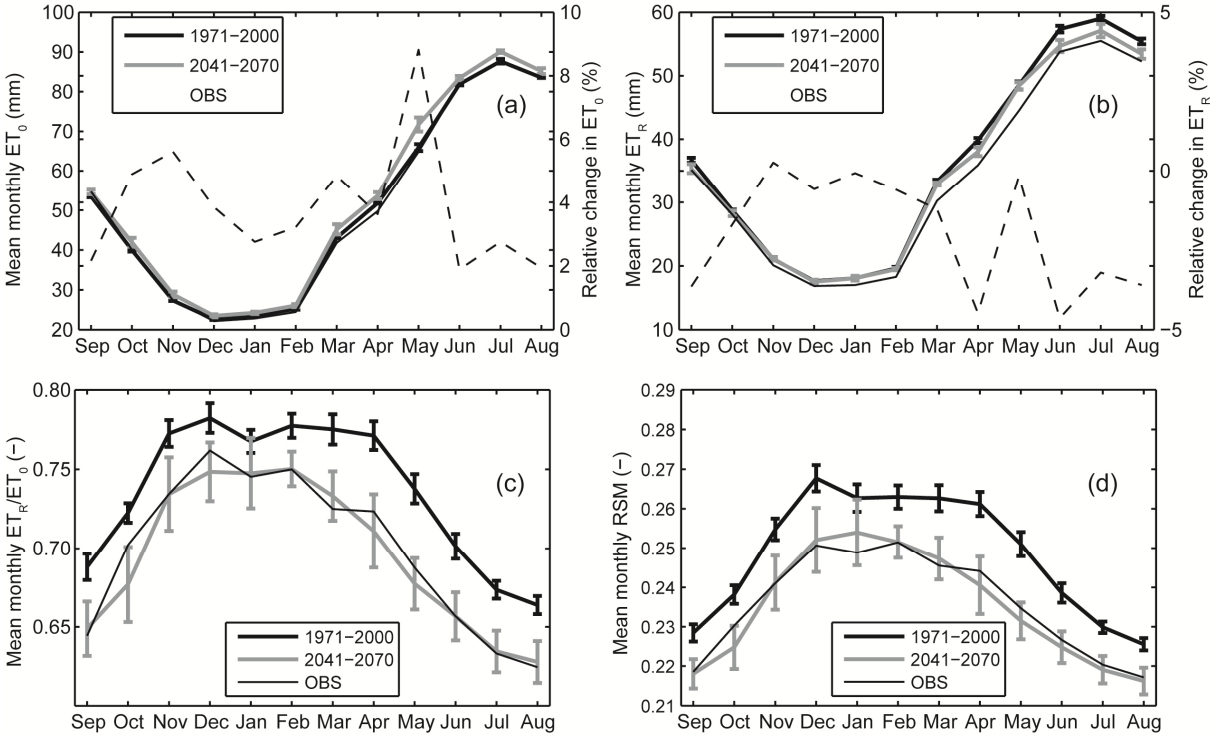

Fig. 3.18 a) Mean monthly potential evapotranspiration, ET_0, plotted as mean ± standard deviation of the RCMs in the REF (black line) and FUT (gray line) periods; thin black line refers to ET_0 computed with observed meteorological data; dashed line represents the percentages of ET_0 variation between FUT and REF periods. (b) Same as (a) but for real evapotranspiration, ET_R, provided by tRIBS model simulations. (c) Ratio of mean monthly ET_R and ET_0, plotted as in previous panels. (d) Mean monthly root soil moisture content, RSM, provided by tRIBS model simulations and plotted as in previous panels.

Our hydrologic model estimated the real evapotranspiration losses, ET_R, as a fraction of ET_0 based on the soil moisture available in the near surface soil layer, using a piecewise-linear equation (Mahfouf and Noilhan, 1991; Ivanov et al., 2004a). Real evapotranspiration (Fig. 3.18b), on the contrary of ET_0, was projected to decrease in FUT period as compared to REF period. Reduction in ET_R with higher ET_0 was most likely due to lower precipitation, which, in turn, led to drier soils. Fig. 3.18c shows the mean monthly ratio between actual and potential evapotranspiration which, as a consequence, presented smaller values in the future according to all the simulations. The relevant effect of soil humidity, and hence of precipitation amount, could also be inferred from the OBS simulations results: real evapotranspiration and ratio were more similar to that projected in the future period than in the reference one. The mean root zone soil moisture content (*RSM*, Fig. 3.18d) was expected to decrease in the FUT period according to all the ensemble members. Looking panels (c) and (d) of Fig. 3.18, it can be noticed the similar trend presented by the ratio of real and potential evapotranspiration and the soil moisture content. These results projected a basin condition of more water shortages with longer periods of dry soils despite having the same evaporation loss. In the future period, in fact, actual evapotranspiration presented similar or slightly lower values than in the reference period, even if potential evapotranspiration tended to a little rise, due to an increased emptying rate of the soil.

Soil humidity and evaporation losses are related to terrain characteristics and soil types (Ivanov et al. 2004b). The relationships can be seen plotting these hydrologic components as a function of the topographic index, λ, and considering the different soil texture classes. The topographic index (Vivoni et al., 2004), proposed by Beven and Kirby (1979) and O'Loughlin (1986), was computed as:

$$\lambda_i = \ln(A_i / \tan \beta_i) \qquad (3.1)$$

where λ_i was the topographic index, A_i was the contributing draining area and β_i the slope at the *i*-th voronoi polygon. This index, whose spatial pattern in RMB is displayed in Fig. 3.19, has the main objective to measure the tendency of the saturation excess runoff to occur in a TIN cell. Hence, it presents larger values in floodplain areas (the biggest is the draining area and the smallest is the local slope, the highest is the probability of saturated conditions, red areas in the figure) than in mountains areas (more yellow areas). Fig. 3.20 shows the variation in mean annual ET_R, surface soil humidity, *SSM*, root zone soil humidity, *RSM*, and depth of groundwater table, *Nwt*, as a function of the topographic index. Vertical bars from points in the plot represents standard deviations of the values computed for the corresponding bins. The magnitude of the standard deviation within a bin was also related to the terrain location and was relatively smaller or larger for certain ranges of the topographic index.

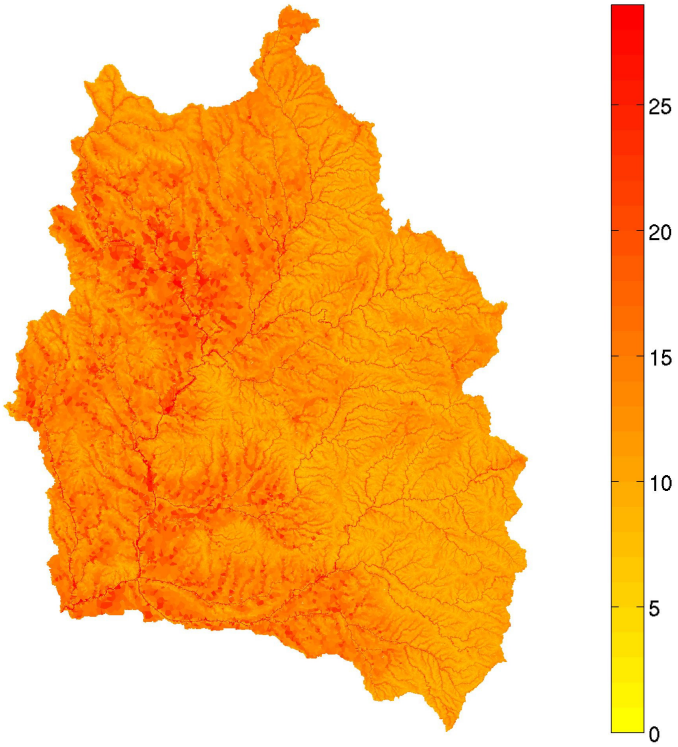

Fig. 3.19 Spatial distribution of topographic index, λ, ranging from 0 to 30.

The variation in mean annual ET_R (Fig. 3.20a) was characterized by slight increments in areas with low topographic index λ (mountain areas) and reductions that increased in areas with higher λ (from hillslopes to floodplains). The mean *SSM* (Fig. 3.20b) was expected to decrease, especially in areas with intermediate λ. Panel (c) of the figure shows that also the *RSM* was projected to reduce in particular in floodplain areas (from intermediate to high λ). All simulations predicted a drop in the groundwater table depth, *Nwt*, (Fig. 3.20d). The changes predicted with HRC forcing were the most extreme (highest decrease of ET_R, *RSM* and *Nwt*), due to lower precipitation and higher temperature in FUT (Fig. 3.2 and 3.4).

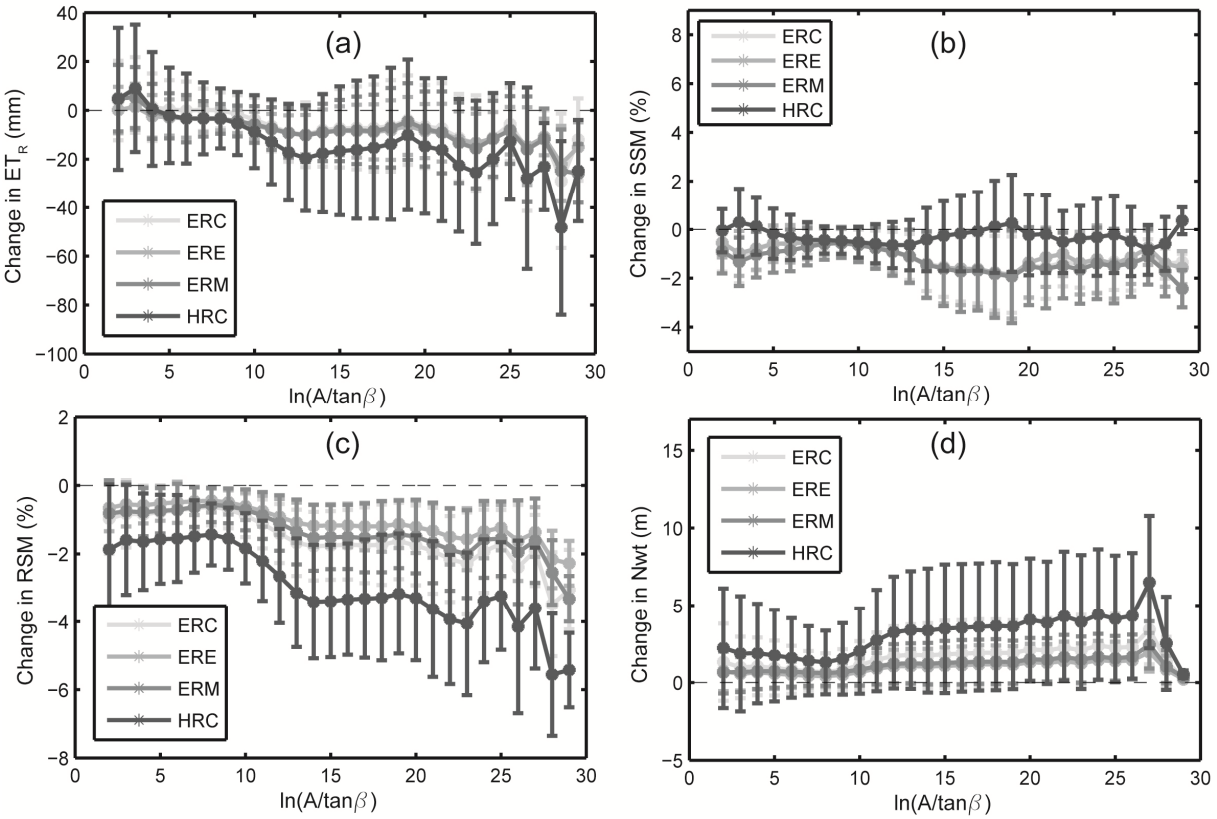

Fig. 3.20 Change in annual (a) real evapotranspiration, ET_R, (b) surface soil moisture, *SSM*, (c) root soil moisture, *RSM* and (d) groundwater table depth, *Nwt*, as a function of the topografic index, $\lambda = \ln(A/\tan\beta)$.

The infuence of topographic index and soil texture classes became even more evident considering seasonal variations plots for the main soil texture classes (sandy loam - sandy clay

loam, SL-SCL, clay loam - clay, CL-C, and sandy loam - loam, SL-L, Fig. 2.4b and table 2.4). Fig. 3.21 provides an example for the *RSM* change in the spring season predicted by the four simulations. The reduction was clearly more marked in areas with sandy soils and λ values from intermediate to high, while it was general smaller in loamy soils. Again, the HRC simulation presented the highest values of decrease.

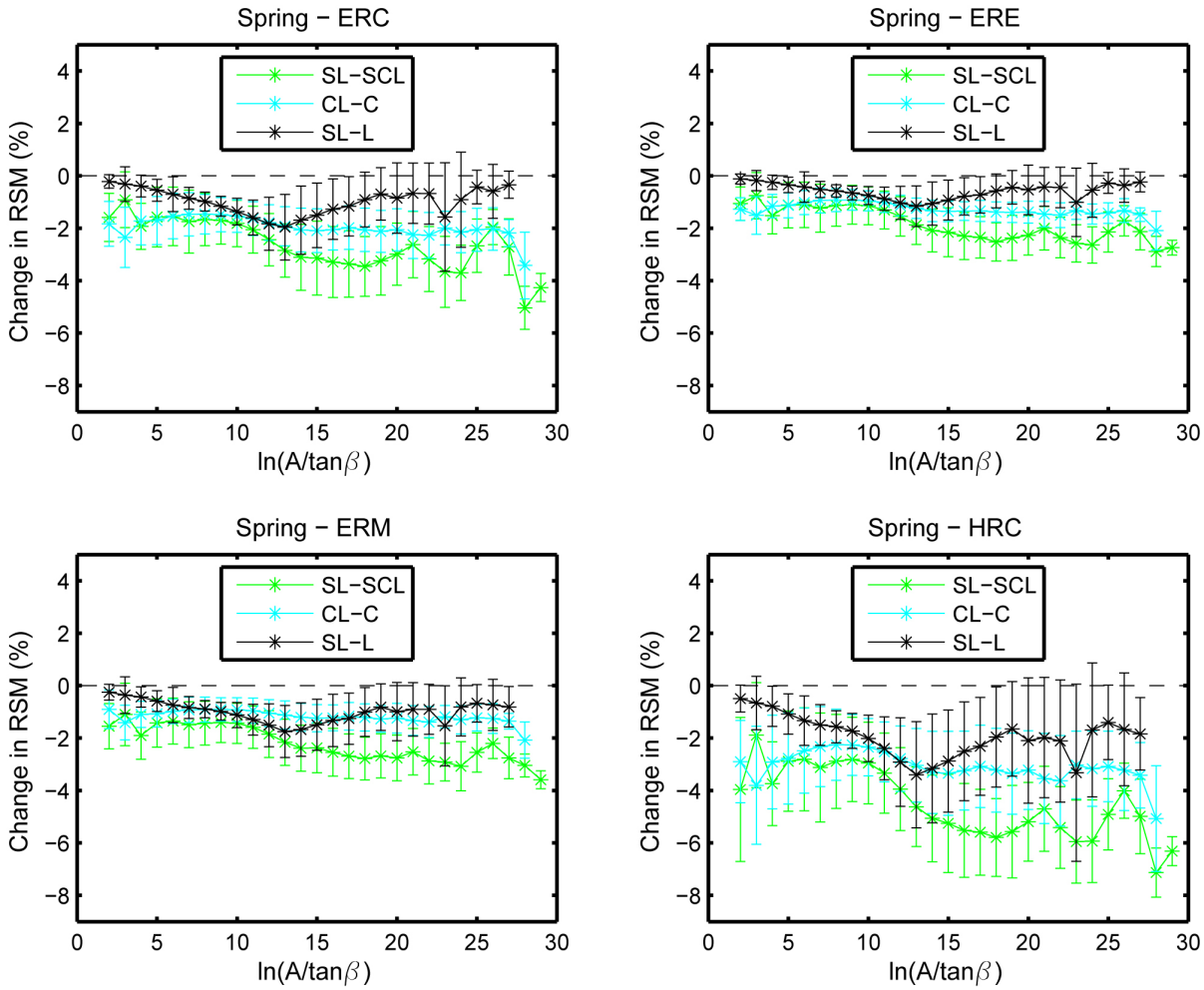

Fig. 3.21 Change in spring *RSM* for the main soil types (see text for the acronyms explanation) as a function of the topografic index, λ. Each panel refers to a RCM forced hydrologic simulation.

3.2.3 Spatial patterns of hydrologic variables changes

The distributed model tRIBS gives the possibility to show the spatial variation of several hydrologic variables providing spatial maps with instantaneous or integrated values at specified times. We set the model in order to have integrated values every month and computed seasonal variations (mean on FUT menus mean on REF) of soil moisture at different depths (*SSM* and *RSM*), real evapotranspiration losses (ET_R) and groundwater table depths (*Nwt*). The maps confirmed the influence of the spatial patterns of soil texture and terrain aspects on the hydrologic response of the basin, as it was inferred from the previous plots which related each variable to the topographic index. In addition, the maps, shown in figures 3.22-3.28, allowed seeing the effect of forcing grids. Each figure presents the variation (FUT - REF) of a component (*SSM*, *RSM*, ET_R or *Nwt*) during the four seasons according to two simulations. The *SSM* (top 10 cm of the soil, Fig. 3.22 and 3.23) variation, presented two main trends with similar values in winter and spring and in summer and autumn. In the first two seasons all the basin was affected by a slight decrease which was more marked in areas near the streamflow network (high λ) and corresponding to the sandy loam class (Fig. 2.4b). In the second period there were some areas of small rise (1%) in clay soils. ERE and HRC displayed also the influence of rainfall grids, with the latter evidencing the highest decrease in winter and a reversed trend near the stream network. The *RSM* (top 1 m, Fig. 3.24 and 3.25) again was affected by soil texture, topography and forcing grids with summer and autumn trends appearing similar. Simulations ERC and ERE manifested a general negative variation, except during winter in few areas of loamy soils. In this cold season also the ERM presented rises in the sandy loam-loam and clay loam-clay zones with major soil depths. Winter enhanced mean soil water content could be explained with the monthly precipitation rice (Fig. 3.3b). Again the HRC ensemble member showed the maximum reduction

values. The real evapotranspiration change (Fig. 3.26 and 3.27) was conditioned by the same factors as soil moisture. It presented positive values near the rivers (high topographic index), more pronounced in spring according to all the 4 simulations. This fact could be likely explained with the increase in spring potential evapotranspiration (average of 5.5%) which could be reached in areas with water availability. The topographic influence was less significant in autumn and winter. The change of this component showed the greatest variability among the ensemble members of this study, with the HRC manifesting the extreme values, as for the other variables.

Using the instantaneous values at the end of each month, we computed also the seasonal variation of groundwater table depths (m from soil surface) between future and reference period. In this case there were no meaningful differences among the seasons, hence only the variation, according to the four simulations, during autumn is displayed in Fig. 3.28 as an example. Every model presented an increase in groundwater table depths and hence a fall in the aquifer. The spatial pattern displayed the influence of soil texture, with higher drops of the water table in clay soils. Again, the HRC pointed out larger variation than the other members.

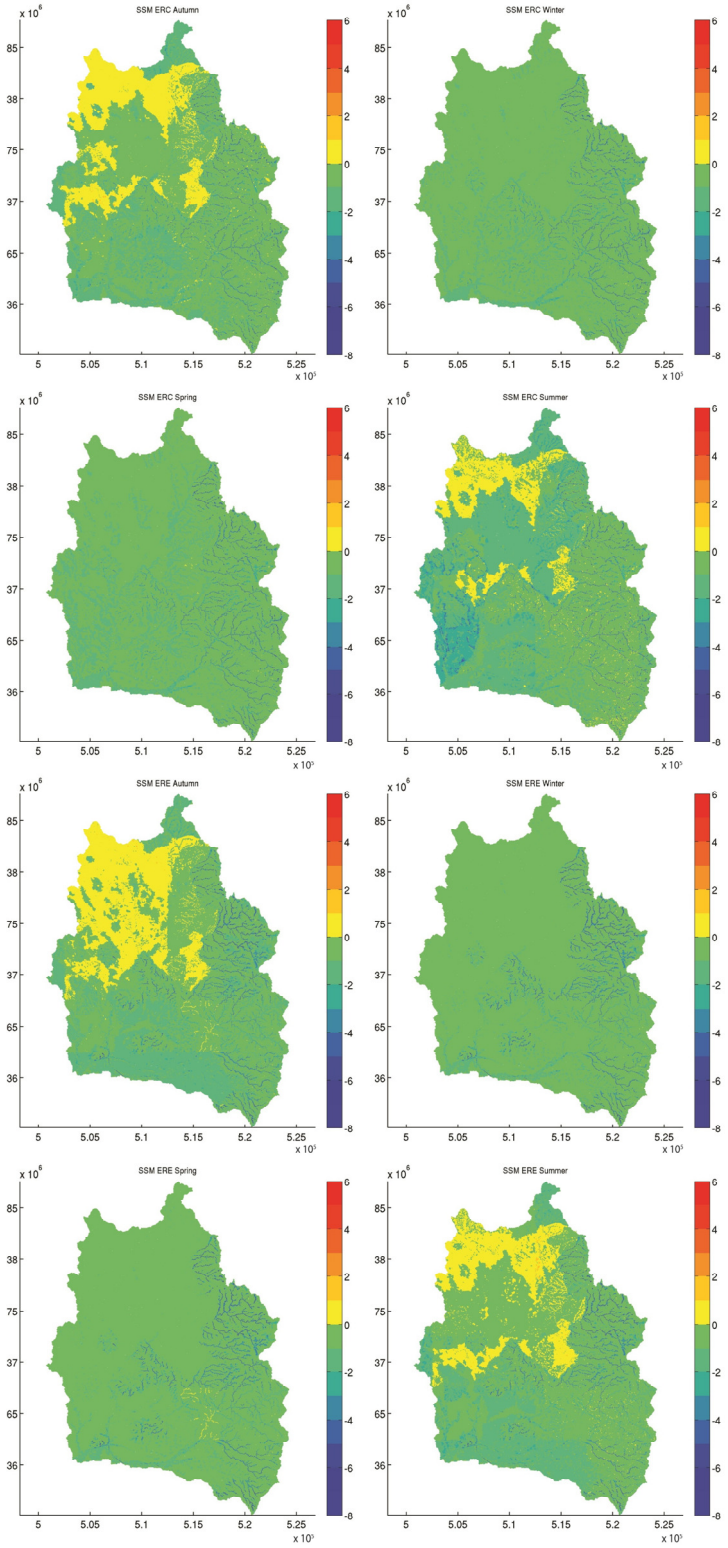

Fig. 3.22 Spatial maps of change in *SSM* during the four seasons as predicted by simulations forced with ERC (first four panels) and ERE (second group of four panels).

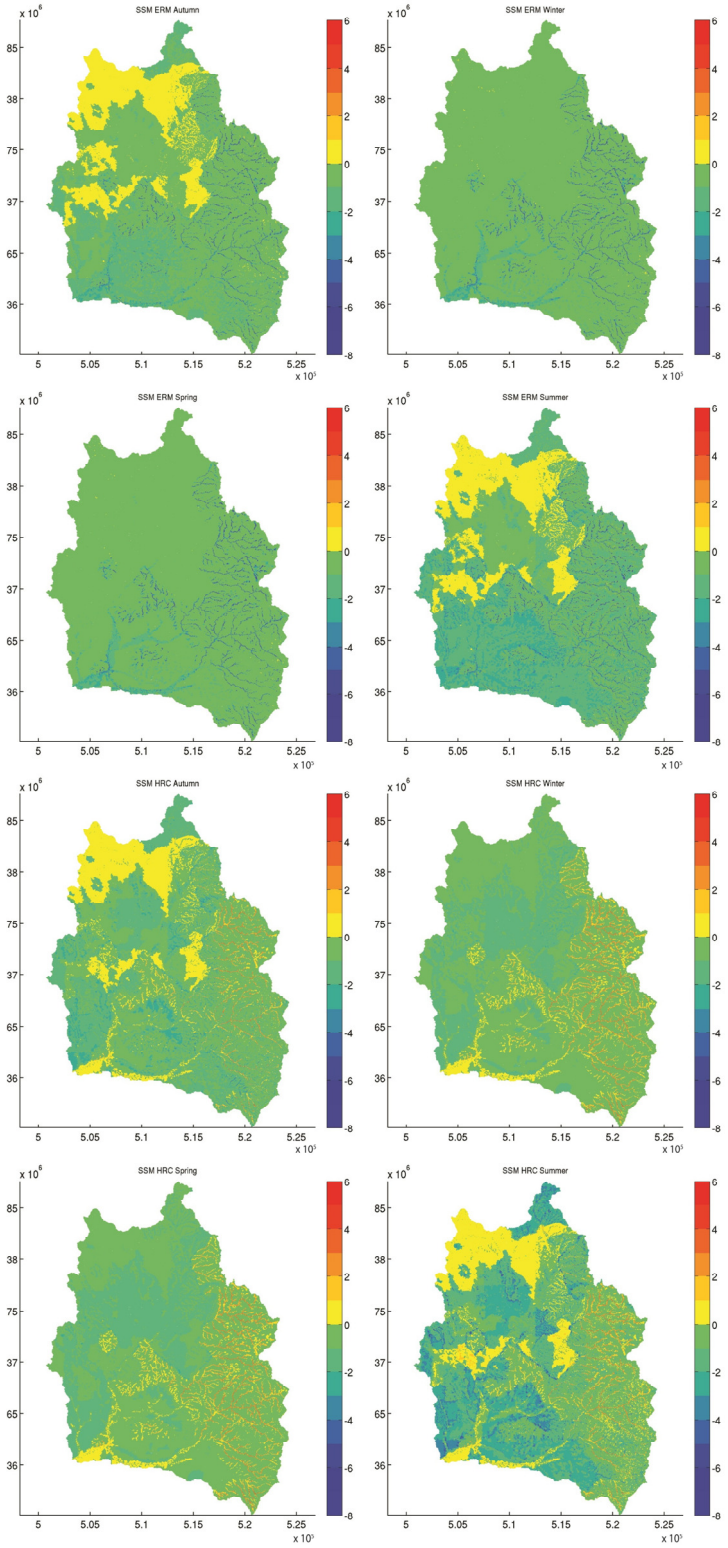

Fig. 3.23 Spatial maps of change in *SSM* during the four seasons as predicted by simulations forced with ERM (first four panels) and HRC (second group of four panels).

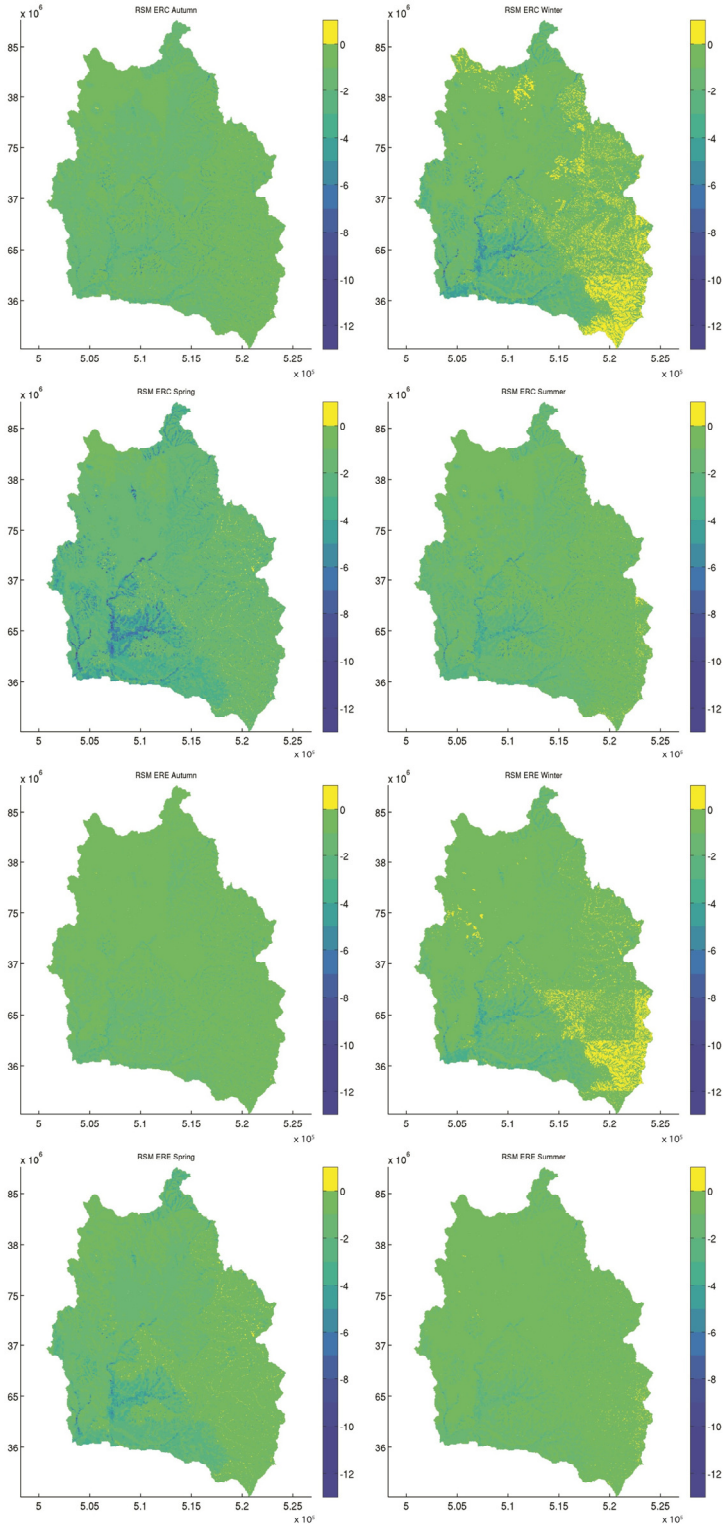

Fig. 3.24 Spatial maps of change in *RSM* during the four seasons as predicted by simulations forced with ERC (first four panels) and ERE (second group of four panels).

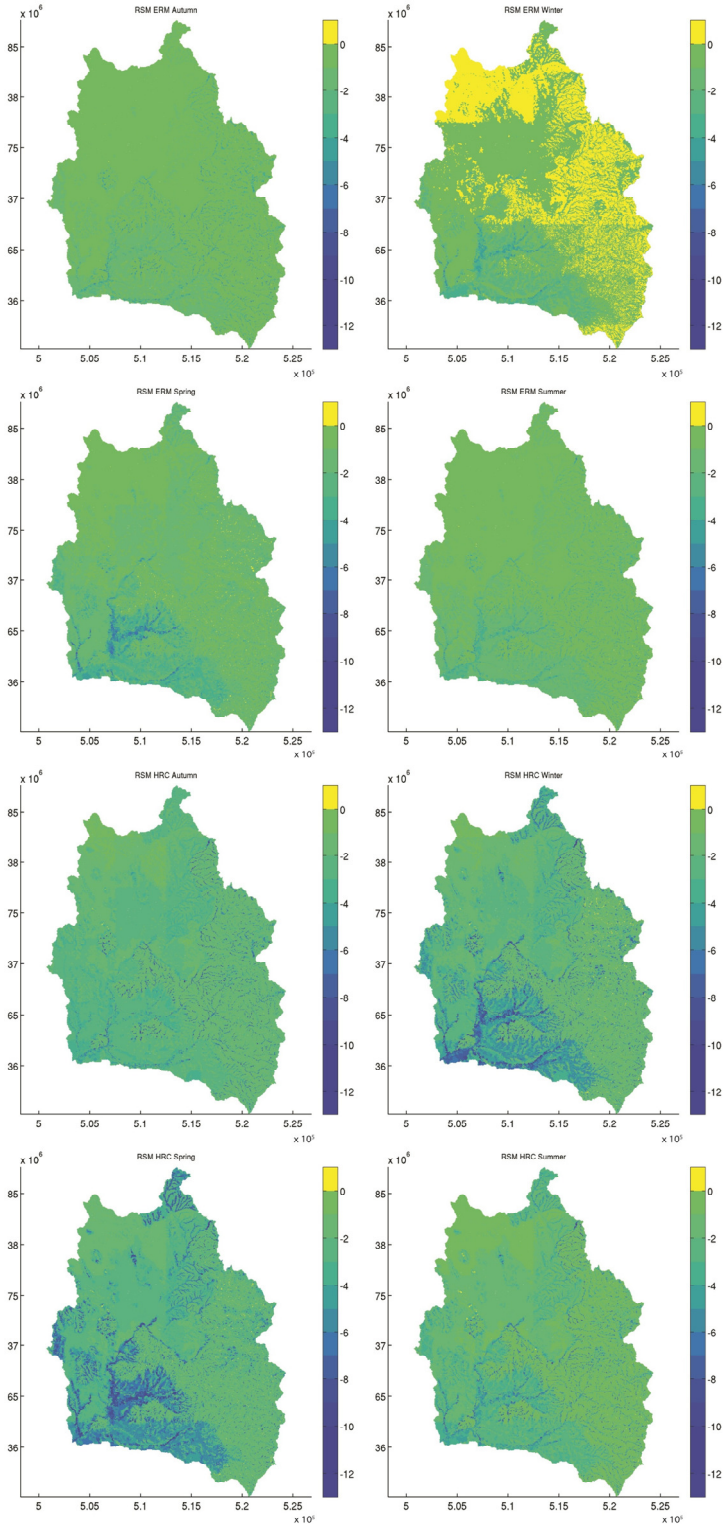

Fig. 3.25 Spatial maps of change in *RSM* during the four seasons as predicted by simulations forced with ERM (first four panels) and HRC (second group of four panels).

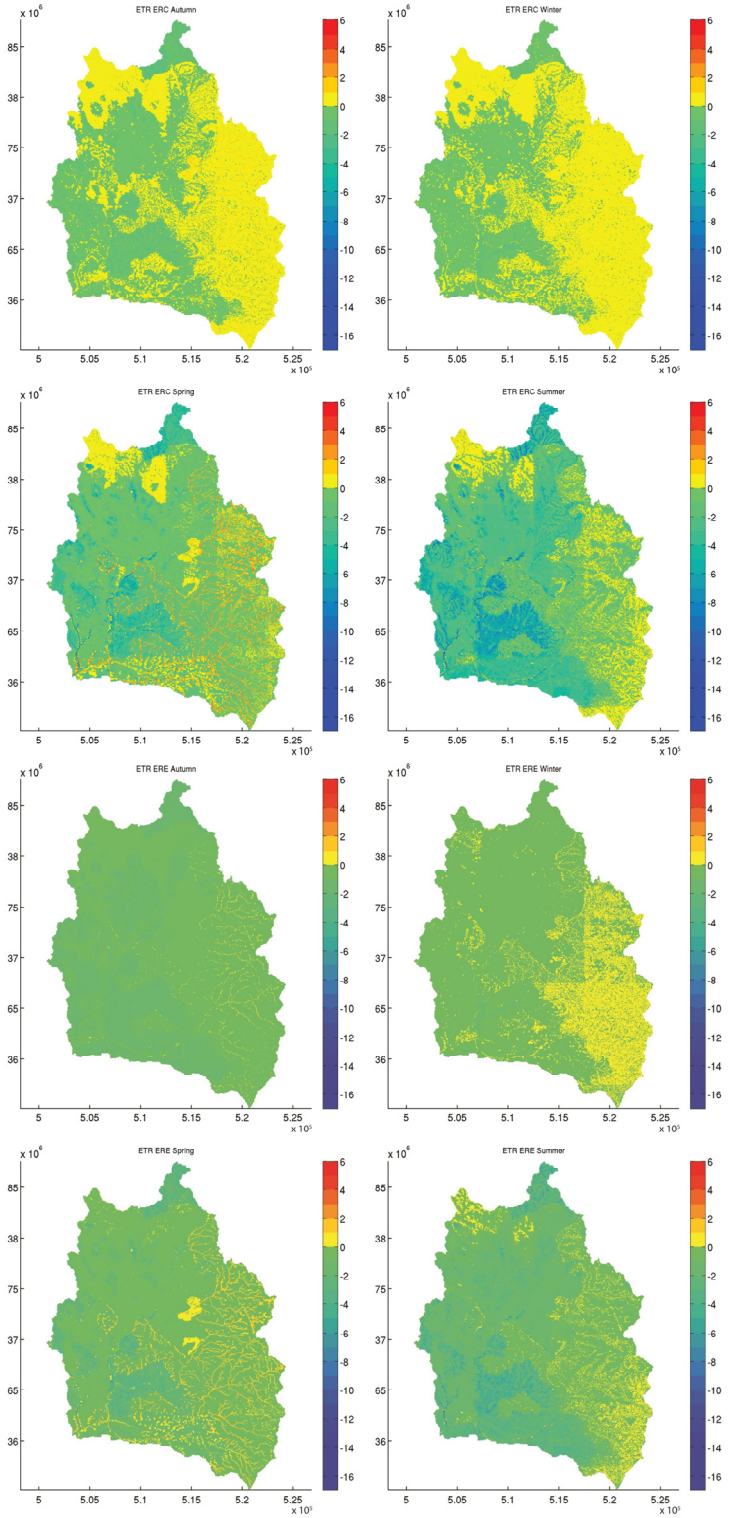

Fig. 3.26 Spatial maps of change in ET_R during the four seasons as predicted by simulations forced with ERC (first four panels) and ERE (second group of four panels).

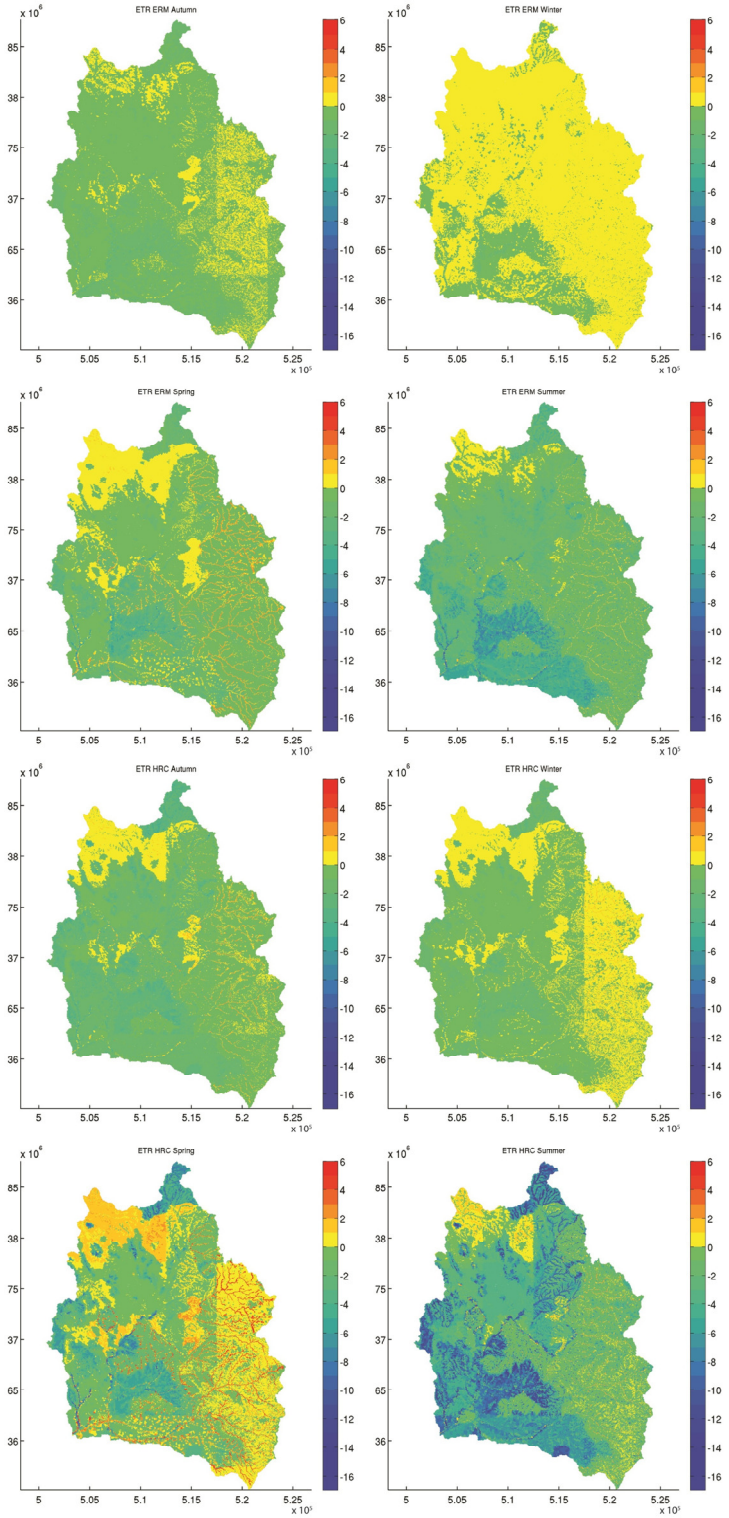

Fig. 3.27 Spatial maps of change in ET_R during the four seasons as predicted by simulations forced with ERM (first four panels) and HRC (second group of four panels).

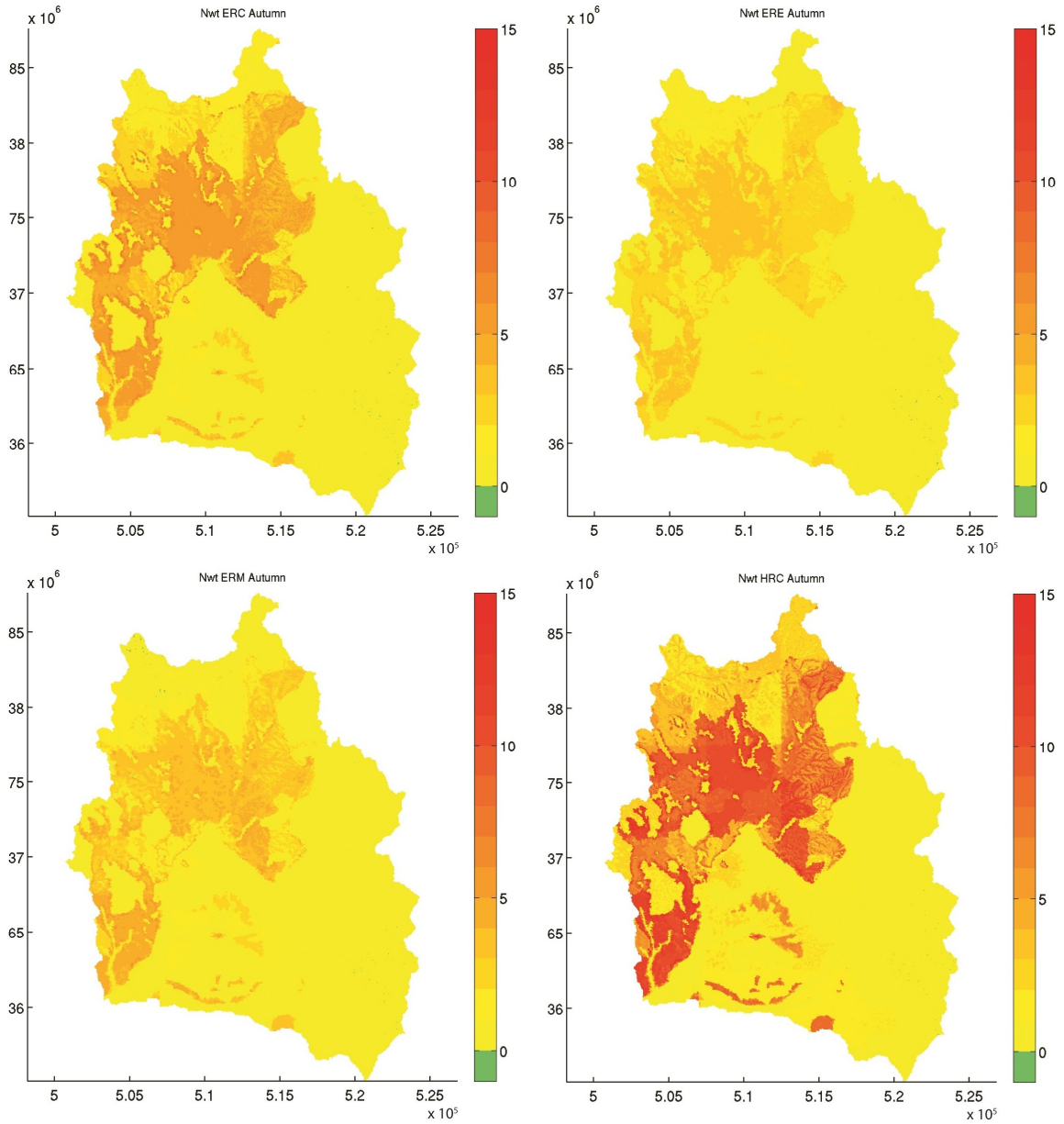

Fig. 3.28 Change in groundwater table depth, *Nwt*, during autumn as predicted by the simulataions forced with the 4 RCMS.

3.3 Discussion and conclusions

We used the physically-based distributed hydrologic model, tRIBS, to evaluate the effects of climate change in a medium-size Mediterranean watershed (area of 472.5 km^2). The basin is located in an agricultural area of Sardinia, Italy, which already suffered drought problems in the last decades. Climate projections were provided by four GCM-RCMs combinations among the ENSEMBLES models. They were selected as the best performing in this study site and in the other 6 watershed sparse in the Mediterranean area within the CLIMB project, ensuring to explore the uncertainty due to the driving GCM (two GCMs driving the same RCM) and to the RCM (two RCMs nested in the same GCM). Their outputs were validated and bias corrected using the E-OBS data set and downscaled in space to fit the scale of hydrologic models. The same time downscaling procedures which allowed a good calibration and validation of the tRIBS model (chapter 2) were applied to RCMs grids to create the required hourly input data. The basin response to projected changes in the climate signal (temperature and precipitation) was assessed in terms of river discharge, evaporation losses, soil water content and groundwater depths.

All RCMs predicted lower mean annual precipitation and higher mean temperatures in the future period 2041-2070 as compared to the period 1971-2000, confirming what is generally predict for Mediterranean areas. RCMs appeared to be more consistent in temperature than in precipitation projections. In fact, temperatures were projected to rise throughout the year while precipitation could increase in winter months. The main source of uncertainty appeared to be the driving GCM with the HRC model always displaying the highest variability and other models presenting more similar results.

Changes in climate forcing affected the different components of the basin hydrologic

response showing also its non linearity. The hydrologic simulations, indeed, indicated: (i) decreasing mean annual runoff, with modification of the generation mechanisms; (ii) lowering of mean real evapotranspiration, likely due to drier soil moisture conditions; (iii) reduced mean level of the groundwater table. In addition, while precipitation reduction and temperature rise predictions were quite similar according to the RCMs driven by the German ECHAM5 GCM, discharge loss in the future period presented larger differences among the simulations. Differences in the distribution of maximum annual values (GEV distribution) of mean areal precipitation were amplified when considering maximum annual discharge. The strong effect of soil water content on evaporation losses might suggest that the watershed behavior was more influenced by precipitation than by temperature. Hydrologic simulations projected basin conditions of more water shortages in future period with longer periods of dry soils despite having just the same evaporation loss as in reference period. The future changes in the mean values of the hydrologic variables were influenced by the spatial patterns of topography and soil texture.

4 Conclusions

The main contributions of this research work are presented in this final chapter. The primary outcome meets the main objective of this thesis, which is to develop a modeling approach to assess local hydrological impacts of climate change in a Mediterranean medium sized basin, located in an agricultural area of southern Sardinia, Italy, and affected by data sparseness. A process-based distributed hydrologic model (DHM), downscaling techniques and climate models are used in conjunction to reduce the uncertainty in the quantification of the local effects of climate change on water resources of a real case-study.

4.1 Summary

In this work, we used a DHM known as the TIN-based Real-time Integrated Basin Simulator (tRIBS, Ivanov et al., 2004a) to simulate the response of the Rio Mannu basin (RMB), a watershed of 472.5 km^2 located in southern Sardinia, Italy. This basin was one of the study areas of a multi-institutional and interdisciplinary project that aimed at analyzing ongoing and future climate-induced changes on hydrological budgets and extremes across the Mediterranean and neighboring regions (Ludwig et al., 2010). The RMB was selected as an emblematic study case in the island of Sardinia for conducting a multidisciplinary analysis of the local impacts of climate changes, ranging from the quantification of the future availability of water resources and occurrence of hydrologic extremes, to the evaluation of the corresponding social and economical vulnerability (last point being beyond the scope and contents of this research work).

As in most Mediterranean basins, the application of process-based hydrologic models, like tRIBS in the RMB, was prevented by the availability of hydrometeorological observations. In this thesis, we proposed an approach to circumvent this problem based on two statistical downscaling (or disaggregation) tools that allowed creating the high-resolution forcing

(precipitation and potential evapotranspiration) required to perform detailed hydrologic simulations at hourly time resolution (chapter 2). The downscaling tools were calibrated using data collected at different resolutions over diverse time periods. After demonstrating the reliability of each disaggregation algorithm, we used these tools to adequately calibrate and validate the hydrologic model based on streamflow observations available over a multi-year period (1930-1932), encompassing a wide range of flood and low flow conditions (Mascaro et al., 2013b).

The proposed downscaling routines were adopted to disaggregate outputs of different RCMs and create the high-resolution inputs (hourly in time, ~1 km in space) for the tRIBS model, with the goal of quantifying the impacts of a set of future climate scenarios on the water resources of the RMB (chapter 3). Among the different scenarios that had been generated within the International Panel on Climate Change (IPCC), only data for the most probable and accepted scenario, the A1B, was considered in this study. Climate models were audited and downscaled by a group of experts in a specific Work Package of the same CLIMB project. They compared outputs of 14 RCMs of the ENSEMBLES project with a gridded data set of observations (E-OBS) obtaining a classification of the models skills in each CLIMB study site. Based on this evaluation, 4 GCM-RCMs combinations were selected as the best performing and prepared to be used as input for hydrologic models (Deidda et al., 2013). Precipitations and temperatures were bias-corrected to better represent the seasonal statistics and downscaled to reach a spatial resolution more suitable for local scale hydrologic simulations. In this work they were further treated to be used as input for the tRIBS DHM during two simulation extents: a reference (1971-2000) and a future (2041-2070) period. Climate signals were evaluated comparing annual and seasonal means in the two periods. The hydrologic response of the RMB to projected changes

was evaluated post-processing time series and spatial maps provided by the hydrologic model. This allowed quantifying the changes on water resources availability and hydrologic extremes in the future climate scenario as compared to historical conditions.

4.2 Outcomes of this dissertation

Evaluate the hydrologic effects of climate change in Mediterranean basins is a difficult task because they are characterized by a strong seasonal behavior and complex surface - subsurface interactions and they could be affected by poor observed data availability to calibrate hydrologic models. We focused on the Rio Mannu basin in Sardinia, an emblematic study site of such Mediterranean issues. We overcame the challenges through the following steps:

- We proposed two strategies to disaggregate daily precipitation and potential evapotranspiration data at hourly scale. In order to develop, calibrate and validate these procedures we exploited high resolution meteorological data available in the last decades. For precipitation the multifractal downscaling model known as Space Time RAINfall (STRAIN) model was adopted (Deidda et al., 1999; Deidda, 2000 and Badas et al., 2006). The model had been demonstrated to well reproduce the rainfall statistical variability in time over a large range of standardized rainfall intensities and to capture the small-scale spatiotemporal precipitation distribution with reasonable accuracy. Second, an empirical procedure to disaggregate potential evapotranspiration from daily to hourly scale was designed, using the hourly dataset of meteorological variables available in recent years (1995-2010), the Penman - Monteith and the Hargreaves formulas.
- We showed how the downscaling strategies could be used to calibrate, with reasonable accuracy, the distributed hydrologic model, tRIBS. In particular, we

chose three consecutive years during which discharge data uncertainty appeared to be minor: the wettest for calibration and the other two for validation. Among the several tRIBS parameters, two parameters related to water infiltration in the soil were found as the most influencing ones, as in Ivanov et al. (2004a). Those parameters were manually changed until a good estimation of the observed monthly streamflow volumes was reached. The Nash-Sutcliffe coefficients at different aggregation scales were used as a metric to evaluate the hydrologic model performances. Overall, we concluded that the conjunct use of the downscaling tools and the tRIBS model allowed satisfactorily reproducing the hydrologic response of the Rio Mannu during the three years selected for calibration and validation.

- We applied the downscaling strategies to disaggregate outputs of 4 RCMs in the reference (1971-2000) and future (2041-2070) periods and evaluated climatic trends in the study area comparing meteorological data in the two time slices. The 4 RCMs were the best performing GCM-RCM combinations with the property of maintaining at least two RCMs nested in the same GCM, and two different GCMs forcing the same RCM. In the reference period, we compared also statistical properties of mean areal precipitation in RMB predicted by the RCMs with observed ones.
- We forced the tRIBS hydrologic model with the disaggregated outputs of the four RCMs for the REF and FUT periods. Time series and spatial maps simulated by the DHM were post-processed to analyse the different components of the Rio Mannu hydrologic response: mean annual and monthly discharge at the outlet section, FDCs, runoff partitioning, mean actual evapotranspiration, surface and root zone

soil moisture and depths to groundwater table.

The study allowed to provide a scenario of possible future changes in the local climatology. Mean annual precipitation was predicted to decrease while mean annual temperature to increase according to all the RCMs. Precipitation was projected to slightly increase in winter months and decrease in the other seasons while temperature was expected to increase throughout the year. This could have important effects on the water availability of the RMB because they affected seasons characterized by irrigation activities. The use of a multi-model ensemble of four RCMs allowed to consider uncertainties coming from numerical schemes and parameterization used by different climate model. The small number of RCMs, nevertheless, and the use of only two GCMs to provide boundary conditions for the future climate scenarios, should not be considered as a representative sample of the complete range of possible future climate on the basin. However, such group of high resolution RCMs were the best available data we had at the moment and one of the first attempts in this direction in the study case. In this work extreme projected changes were given by climate scenarios driven by the two different GCMs. This proved that a better assessment of the full range of likely changes in climate could be provided using climate scenarios driven by different GCMs. The statistical analyses of precipitation values put on evidence the absence of coherence among the RCMs and during the two periods and the distance from observed data both as values and as type of distribution. By no way it should be thought that the range of future climate changes presented in this thesis will certainly realize in the Rio Mannu basin. Uncertainties coming from the emission scenario, skill of GCM-RCM combinations to realistic reproduce the climate under emission forcing that have been never observed before should also be taken into account. We explored some possible scenarios of future climate with the best information we had at the moment and

the results correspond to the best projections we could make based on our imperfect knowledge of a complex and non linear phenomena.

The hydrologic simulations under the provided range of future climate forcing indicated reduced water resources availability. Mean annual runoff was predicted to decrease according to all the simulations. This was confirmed by a downward shift of the FDCs over the entire range of exceedance probabilities. As a result, the number of low flow days was projected to rise in all months as their maximum consecutive length per hydrologic year. The runoff generation mechanism was predicted to be influenced by changes in precipitation distribution. Mean real evapotranspiration was predicted to decrease due to drier soil moisture conditions. All simulation projected a drop in the groundwater table level. The changes predicted with the Hadley HadCM3-RCA, HRC, model forcing were the most extreme (highest decrease of discharge, evapotranspiration and groundwater table) in agreement with the lower precipitation and higher temperature provided by this model in the future period. The high resolution spatial information (e.g. soil moisture and actual evapotranspiration maps), which could be used to support water management, showed the influence of spatial patterns of topography and soil texture. By no means it should be thought that the hydrological impacts of climate changes expected in the RMB will certainly lie between the ranges provided by this work. Further uncertainties coming from input data used to force the hydrologic model, its calibration-validation procedure (e.g. the selection of a single set of parameters), limited number of GCM-RCMs combination, performance of the downscaling techniques, unconsidered changes in land use and soil properties, add complexity to the *cascade of uncertainties* involved in the impact assessment. Again it can be claimed that we explore some possible scenarios of future climate, with the best information available at the moment, and that the predicted hydrological effects correspond to the best projections we could make based on our imperfect knowledge of this challenging topic.

4.3 Open issues and further research

Calibration and validation of complex hydrologic models in basins affected by data sparseness still remain a difficult task. In this thesis we proposed an *ad hoc solution* but we underline that further research should focus on this topic. Streamflow measurements in nested catchments could help in this direction. The possibility to calibrate the DHM using also alternative observed data with respect to discharge data should be explored. Requiring even a hypothetical perfect model good input data, it is fundamental to collect and check data quality.

GCMs and RCMs usually have spatial resolutions which differ from medium size catchment scale resolution, hence coupling climate and hydrologic models is not so immediate. Downscaling techniques are used to overcome the problem but the procedure is not yet standardized. Model climate variables usually differ from measured values requiring bias correction in order to at least match the corresponding reference distribution. Different methods can be adopted for the correction but the solution seems not to be unique.

The use of ensemble of climate models is fundamental when trying to probabilistic evaluate the likely effects of climate change. Notwithstanding the combinations used in this study allowed to explore the uncertainty related to model parameterization and numerical schemes used by different climate models, the consideration of only one emission scenario and a small number of GCMs only provides a limited sample of the possible future climate.

This thesis only analyzes expected change in water resources of the Rio Mannu basin. Variability of water demand for agricultural and civil requests in the future should be incorporated in integrated studies to be useful for assessing the final real effect of mitigation policies, being one of the aims of CLIMB project.

References

Abbaspour, K. C., Faramarzi, M., Ghasemi, S. S., and Yang, H.: Assessing the impact of climate change on water resources in Iran, Water Resour. Res., 45, W10434, doi:10.1029/2008WR007615, 2009.

Allen, R. G., Jensen, M. E., Wright, J. L., and Burman, R.D.: Operational estimates of reference evapotranspiration, Agron. J., 81, 650–662, 1989.

Allen, R. G., et al.: A recommendation on standardized surface resistance for hourly calculation of reference ET_0 by the FAO56 Penman-Monteith method, Agr.Water Manage., 81, 1–22, doi:10.1016/j.agwat.2005.03.007, 2006.

Aru A, et al.: Carta dei suoli della Sardegna 1:250,000. Regione Autonoma della Sardegna, Assessorato Programmazione, Bilancio ed Assetto del Territorio, 1992.

Badas, M. G., Deidda, R., and Piga, E.: Modulation of homogeneous space-time rainfall cascades to account for orographic influences, Nat. Hazard Earth Sys. Sci., 6, 427–437, 2006.

Bardossy, A., and Pegram, G.: Downscaling precipitation using regional climate models and circulations patterns toward hydrology, Water Resour. Res., 47, W04505, 1-18, 2011.

Barnes, S. L., 1964: A technique for maximizing details in numerical weather map analysis. J. Appl. Meteor., 3, 396–409.

Barnes, S. L., 1973: Mesoscale objective analysis using weighted time-series observations. NOAA Tech. Memo. ERL NSSL-62, National Severe Storms Laboratory, Norman, OK, 60 pp.

Beven, K.: Runoff generation in semi-arid areas, in: Dryland Rivers, Bull LJ, Kirkby MJ (eds). J. Wiley & Sons; 57–105, 2002.

Beven, K., and Kirkby, M. J.: A physically-based variable contributing area model of basin hydrology, Hydrol. Sci. Bull., 24, 43-69, 1979.

Cabral, M. C., Garrote, L., Bras, R. L., and Entekhabi, D.: A kinematic model of infiltration and runoff generation in layered and sloped soils, Adv. Water Resour., 15, 311–324, 1992.

Camporese, M., Paniconi, C., Putti, M., and Orlandini, S.: Surface-subsurface flow modeling with path-based runoff routing, boundary condition-based coupling, and assimilation of multisource observation data, Water Resour. Res., 46, W02512, doi:10.1029/2008WR007536,2010.

Cayan, D. R., Dasa, T., Piercea, D. W., Barnetta, T. P., Tyreea, M., and Gershunova, A.: Future dryness in the southwest US and the hydrology of the early 21st century drought, P. Natl. Acad. Sci. USA, 107, 21271-21276. doi:10.1073/pnas.0912391107, 2010.

Chessa, P. A., Cesari, D., and Delitala, A. M. S.:Mesoscale precipitation and temperature regimes in Sardinia (Italy) and their related synoptic circulation, Theor. Appl. Climatol., 63, 195– 221, 1999.

Chessa, P. A., Ficca, G., Marrocu, M., and Buizza, R.: Application of a limited-area short-range ensemble forecast system to a case of heavy rainfall in the Mediterranean region, Weather Forecast., 19, 566–581, 2004.

Cudennec, C., Leduc, C., and Koutsoyiannis, D.: Dryland hydrology in Mediterranean regions – a review. Hydrolog. Sci. J., 52, 1077-1087, 2007.

Deidda, R: Multifractal analysis and simulation of rainfall fields in space. Phys.Chem. Earth, 24(1–2), 73–78, 1999.

Deidda R.: Rainfall downscaling in a space-time multifractal framework, Water Resour. Res., 36(7), 1779–1784, 2000.

Deidda, R.: A multiple threshold method for fitting the generalized Pareto distribution to rainfall time series, Hydrol. and Earth Syst. Sci., 14, 2559-2575, doi:10.5194/hess-14-2559-2010, 2010.

Deidda, R., Benzi, R., and Siccardi, F.:Multifractal modeling of anomalous scaling laws in rainfall, Water Resour. Res., 35, 1853–1867, 1999.

Deidda, R., Badas, M. G., and Piga, E.: Space-time scaling in high-intensity Tropical Ocean Global Atmosphere Coupled Ocean-Atmosphere Response Experiment TOGA-COARE storms, Water Resour. Res., 40, W02506,doi:10.1029/2003WR002574, 2004.

Deidda, R., Badas M.G., and Piga E.: Space-time Multifractality of Remotely Sensed Rainfall Fields, J. Hydrol., 322, 2-13, 2006

Deidda, R., Marroccu, M., Caroletti, G., Pusceddu, G., Langousis, A., Lucarini, V., Puliga, M., and Speranza, A.: Climate model validation and selection for hydrological applications in representative Mediterranean catchments, Hydrol. Earth Syst. Sci., 17, 5041-5059, doi:10.5194/hess-17-2013, 2013.

Delrieu, G., et al.: The catastrophic flash-flood event of 8–9 September 2002 in the Gard region, France: a first case study for the Cévennes–Vivarais Mediterranean hydrometeorological observatory,J. of Hydrometeorol., 6, 34–52, 2005.

Forman, B. A., Vivoni, E. R., and Margulis, S. A.: Evaluation of ensemble-based distributed hydrologic model response with disaggregated precipitation products, Water Resour. Res., 44, 1–18, doi:10.1029/2008WR006827, 2008.

Frei, C., Schöll, R., Fukutome, S., Schmidli, J., and Vidale, P.L.: Future change of precipitation extremes in Europe: intercomparison of scenarios from regional climate models, J. of Geophys. Res., 111, D06105, DOI: 10.1029/2005JD005965, 2006.

Gallart F, Llorens P, Latron J, Regüés D.: Hydrological processes and their seasonal controls in a small Mediterranean mountain catchment in the Pyrenees, Hydrol, Earth Syst. Sci.,6(3), 527–537, 2002.

Giandotti, M.,: Previsione delle piene e delle magre dei corsi d'acqua. Ministero LL.PP., Memorie e studi idrografici, Vol. 8, Rep. No. 2, Servizio Idrografico Italiano, Rome (in Italian), 1934.

Giorgi, F.: Climate change hot-spots, Geophys. Res. Lett., 33, L08707, doi:10.1029/2006GL025734, 2006.

Hargreaves, G. H.: Defining and using reference evapotranspiration, J.Irrig.Drain.E.-ASCE, 120(6), 1132–1139,1994.

Hargreaves, G. H., and Allen, R. G.: History and evaluation of Hargreaves Evapotraspiration equation,J.Irrig.Drain.E.-ASCE, 129(1), 53–63, 2003.

IPCC (Intergovernmental Panel on Climate Change), Climate change 2007: impacts, adaptation and vulnerability. Contribution of Working Group II to the Fourth Assessment Report of the Intergovernmental Panel on Climate Change,Cambridge University Press, Cambridge, UK, 976, 2007.

IPCC (Intergovernmental Panel on Climate Change), Climate Change and Water, Technical Paper of the Intergovernmental Panel on Climate Change, IPCC Secretariat, Geneva, 210, 2008.

Ivanov, V.Y., Vivoni, E. R., Bras, R. L., and Entekhabi, D.: Catchment hydrologic response with a fully-distributed triangulated irregular network model, Water Resour. Res., 40 (11), doi:10.1029/2004WR003218, 1–23, 2004a.

Ivanov, V. Y., Vivoni, E. R., Bras, R. L., and Entekhabi, D.: Preserving high-resolution surface and rainfall data in operational-scale basin hydrology: A fully-distributed physically-based approach, J. Hydrol., 298, 80–111, doi:10.1016/j.jhydrol.2004.03.041, 2004b.

Klemes, V.: "Operational testing of hydrological simulation models, Hydrol. Sci. J., 31, 13-24, 1986.

Liston, G. E., and Elder, K.: A Meteorological Distribution System for High-Resolution Terrestrial Modeling (MicroMet). J. Hydrometeor., 7, 217-234, 2006.

Liuzzo, L., Noto, L. V., Vivoni, E. R., and La Loggia, G.: Basin-scale water resources assessment in Oklahoma under synthetic climate change scenarios using a fully distributed hydrological model, J. Hydrol. Eng., 15(2), 107–122, doi:10.1061/ASCEHE.1943-5584.0000166, 2010.

Ludwig, R., et al.: Climate-induced changes on the hydrology of Mediterranean basins - A research concept to reduce uncertainty and quantify risk, Fresen. Environ. Bull., 19 (10 A), 2379–2384, 2010.

Mahfouf, J. F., and Noilhan, J.: Comparative study of various formulations from bare soil using in situ data,J. Appl. Meteorol., 30, 1354–1365, 1991.

Mascaro, G., Vivoni, E. R., and Deidda, R.: Implications of ensemble quantitative precipitation forecast errors on distributed streamflow forecasting, J. Hydrometeorol., 11(1), 69–86, doi:10.1175/2009JHM1144.1, 2010.

Mascaro, G., Deidda, R., and Hellies, M.: On the nature of rainfall intermittency as revealed by different metrics and sampling approaches,Hydrol, Earth Syst. Sci., 17, 355–369, doi:10.5194/hess-17-355-2013, 2013a.

Mascaro, G., Piras, M., Deidda, R., and Vivoni, E. R.: Distributed hydrologic modeling of a sparsely monitored basin in Sardinia, Italy, through hydrometeorological downscaling, Hydrol, Earth Syst. Sci., 17, 4143–4158, doi:10.5194/hess-17-4143-2013 , 2013b.

Maurer, E. P. and Hidalgo, H. G.: Utility of daily vs. monthly large-scale climate data: an intercomparison of two statistical downscaling methods, Hydrol. Earth Syst. Sci., 12, 551–563, doi: 10.5194/hess-12-551-2008, 2008.

Mearns, l. o., Hulme, M., Carter, T. R., and Whetton, P.: Climate Scenario Development, in Climate Change 2001: The scientific Basis, Chapter 13, Contribution of Working Group III to the Third Assessment Report of the Intergovernmental Panel on Climate Change (IPCC), edited by J. T. Houghton, K. Maskell, X. Dai, P. j. van der Linden, C. A. Johnson, Y. Ding, D. j: Griggs, and M. Noguer, pp. 739-768, Cambridge University Press, Cambridge, UK. 3, 52, 88.

Montaldo, N., Albertson, J. D., and Mancini, M.: Vegetation dynamics and soil water balance in a water-limited Mediterranean ecosystem on Sardinia, Italy, Hydrol, Earth Syst. Sci.,12, 1257–1271, 2008.

Monteith, J. L.:Evaporation and environment, Sym. Soc. Exp. Biol., 19, 205–234, 1965.

Montenegro, S., and Ragab, R.,: Impact of possible climate and land use changes in the semi arid regions: a case study from North Eastern Brazil, J. Hydrol., 434-435, 55–68, doi:10.1016/j.jhydrol.2012.02.036, 2012.

Moussa, R., Chahinian, N., and Bocquillon, C.: Distributed hydrological modeling of a Mediterranean mountainous catchment – model construction and multi-site validation. J. Hydrol., 337, 35–51,doi:10.1016/j.jhydrol.2007.01.028, 2007.

Nakićeović, N., Alcamo J, Davis G, de Vries HJM, Fenhann J, Gaffin S, Gregory K, Grubler A, Jung TY, Kram T, La Rovere EL, Michaelis L, Mori S, Morita T, Papper W, Pitcher H, Price L, Riahi K, Roehrl A, Rogner H-H, Sankovski A, Schlesinger M, Shukla P, Smith S, Swart R, van

Rooijen S, Victor N, Dadi Z. 2000. *Emissions Scenarios. A Special Report of Working Group III of the Intergovernmental Panel on Climate Change*. Cambridge University Press: Cambridge; 559.

Nash, J. E., and Sutcliffe, J. V.: River flow forecasting through conceptual models part I—A discussion of principles, J. Hydrol., 10(3), 282–290, 1970.

Nikolopoulus, E.I., Anagnostou, E.N., Borga, M., Vivoni, E.R., and Papadopoulus, A.: Sensitivity of a mountain basin flash flood to initial wetness condition and rainfall variability, J. Hydrol., 402, 165–178, doi:10.1016/j.jhydrol.2010.12.020, 2011.

Noto, L. V., Ivanov, V. Y., Bras, R. L., and Vivoni, E. R.: Effects of initialization on response of a fully-distributed hydrologic model, J. Hydrol., 352(1-2), 107–125, doi:10.1016/j.jhydrol.2007.12.031, 2008.

O'Loughlin, E. M.: Prediction of surface saturation zones in natural catchments by topographic analysis, Comput. Vis. Graph. Image Process., 28, 323-344, 1986.

Olesen, J.E., and Bindi, M.: Consequences of climate change for European agricultural productivity, land use and policy, Eur. J. of Agron., 16 (4), 239–262, 2002.

Penman, H. L.: Natural evaporation from open water, bare soil and grass, P. R. Soc. London, Ser-A, 193, 120–145, 1948.

Piñol, J. Beven, K., and Freer, J.: Modelling the hydrological response of Mediterranean catchments, Prades, Catalonia. The use of distributed models as aids to hypothesis formulation, Hydrol. Process., 11, 1287–1306, 1997.

Prudhomme, C., and Davies, H.: Assessing uncertainties in climate change impact analyses on the river flow regimes in the UK. Part 1: baseline climate, Climatic Change, 93(1-2), 177–195, doi:10.1007/s10584-008-9464-3. 3, 88, 2009a.

Prudhomme, C., and Davies, H.: Assessing uncertainties in climate change impact analyses on the river flow regimes in the UK. Part 2: future climate, Climatic Change, 93(1-2), 197–222, doi:10.1007/s10584-008-9461-6. 3, 2009b.

Rawls, W. J., Brakensiek, D. L., and Saxton, K. E.:Estimation of soil properties, T. ASAE, 1316–1328, 1982.

Robles-Morua, A., Vivoni, E.R., and Mayer, A.S.: Distributed hydrologic modeling in Northwest Mexico reveals the links between runoff mechanisms and evapotranspiration, J. Hydrometeor., 13, 785–807,doi:10.1175/JHM-D-11-0112.1,2012.

Schröter, D., et al.: Ecosystem service supply and vulnerability to global change in Europe, Science, 310(5752), 1333–1337, 2005.

Silvestro, F., Gabellani, S., Giannoni, F., Parodi, A., Rebora, N., Rudari, R., and Siccardi, F.: A hydrological analysis of the 4 November 2011 event in Genoa,Nat. Hazard Earth Sys. Sci., 12, 2743–2752, 2012.

Sulis, M., Paniconi, C., Rivard, C., Harvey, R., and Chaumont, D.: Assessment of climate change impacts at the catchment scale with a detailed hydrological model of surface-subsurface interactions and comparison with a land surface model, Water Resour. Res., 47, W01513, doi:10.1029/2010WR009167, 2011.

Sulis, M., Paniconi, C., Marroccu, M., Huard, D., and Chaumont, D.: Hydrologic response to multimodel climate output using a physically based model of groundwater/surface water interactions. Water Resour. Res., 48, W12510, doi:10.1029/2012WR012304, 2012.

Todd, M. C., Taylor, R. G., Osborn, T. J., Kingston, D. G., Arnell, N. W., Gosling, S. N.: Uncertainty in climate change impacts on basin-scale freshwater resources – preface to the special issue: the QUEST-GSI methodology and synthesis of results. Hydrol, Earth Syst. Sci., 15, 1035-1046, 2011.

Van der Kwaak, J. E., and Loague, K.: Hydrologic-response simulations for the R-5 catchment with a comprehensive physics-based model, Water Resour. Res., 37(4), 999–1013, 2001.

Vivoni, E. R., Ivanov, V. Y., Bras, R. L, and Entekhabi, D.: Generation of triangulated irregular networks based on hydrological similarity, J. Hydrol. Eng., 9(4), 288–302,doi:10.1061/ASCE1084-0699(2004)9:4(288), 2004.

Vivoni, E. R., Ivanov, V. Y., Bras, R. L., and Entekhabi, D.: On the effects of triangulated terrain resolution on distributed hydrologic model response, Hydrol. Process., 19(11), 2101–2122, doi:10.1002/hyp.5671, 2005.

Vivoni, E. R., Entekhabi, D., Bras, R. L., Ivanov, V. Y, Van Horne, M. P, Grassotti, C., and Hoffman, R.N.: Extending the predictability of hydrometeorological flood events using radar rainfall nowcasting, J. Hydrometeorol., 7(4), 660–677, 2006.

Vivoni, E. R., Entekhabi, D., Bras, R. L, and Ivanov, V. Y.: Controls on runoff generation and scale-dependence in a distributed hydrologic model, Hydrol, Earth Syst. Sci., 11(5), 1683–1701, 2007.

Vivoni, E. R., Tai, K., and Gochis, D.J.: Effects of initial soil moisture on rainfall generation and subsequent hydrologic response during the North American monsoon, J. Hydrom., 10(3), 644–664, doi:10.1175/2008JHM1069.1, 2009.

Vivoni, E. R., Rodriguez, J. C., and Watts, C. J.: On the spatiotemporal variability of soil moisture and evapotranspiration in a mountainous basin within the North American monsoon region, Water Resour. Res., 46, W02509, 1-18, doi:10.1029/2009WR008240, 2010.

Vivoni, E.R., Mascaro, G., Mniszewski, S., Fasel, P., Springer, E.P., Ivanov, V.Y. and Bras, R.L.: Real-world hydrologic assessment of a fully-distributed hydrological model in a parallel computing environment, J. Hydrol., 409, 483–496, doi:10.1016/j.jhydrol.2011.08.053, 2011.

Wilby, R. L.: Uncertainty in water resources model parameters used for climate change impact assessment, Hydrol. Process., 19, 3201-3219, doi:10.1002/hyp.5819, 2005.

Wilby, R.L., and Wigley, T. M. L.: Downscaling general circulation model output: A review of methods and limitations, Prog. Phys. Geogr., 21, 530–548, 1997.

Wilby, R. L., Hay, L. E., Gutowski, W. J., Arritt, R. A., Takle, E. S., Pan, Z., Levesley, G. H., Clark, M.: Hydrological responses to dynamically and statistically downscaled climate model output. Geophysical Research Letters 27, 1199-1202, 2000.

Wood, A. W., Leung, L. R., Sridhar, V., and Lettenmaier, D. P.: Hydrologic implications of dynamical and statistical approaches to downscaling climate model outputs, Climatic Change, 62(1-3), 189–216, 2004.

Xu, C., Widen, E., and Halldin, S.: Modelling hydrological consequences of climate change – Progress and challenges, Adv. Atmos. Sci. 22, 789-797, 2005.